UNIVERSITY OF SOUTHAMPTON

FACULTY OF ENGINEERING AND PHYSICAL SCIENCES

Mechatronics Research Group

A Linear to Rotary Magnetic Gear

By

Thang Van Lang

Thesis for the degree of Doctor of Philosophy

November 2020

UNIVERSITY OF SOUTHAMPTON

ABSTRACT

FACULTY OF ENGINEERING AND PHYSICAL SCIENCES

Mechatronics Research Group

Doctor of Philosophy

A Linear to Rotary Magnetic Gear

By Thang Van Lang

Although magnetic gears are more expensive and larger than mechanical gears for a given power rating, they are more efficient. They also offer the advantage of physical separation between the driving and driven shafts which can be in different environments, e.g., in water and in air. Recent research has focused on rotary magnetic gears, with limited work on linear to rotary and vice versa motion conversions, which is desirable in many applications such as wave energy harvesting.

This thesis focuses on the development of the theory and design optimisation of a novel linear-rotary magnetic gear derived from a variable reluctance permanent magnet (transverse-flux) rotational machine topology. The configuration of a linear to rotary magnetic gear is developed and discussed. A design optimisation methodology is implemented based on finite element analysis. Using this methodology, optimal proportions and dimensions of a linear to rotary magnetic gear demonstrator are determined. It is shown that increasing the magnet thickness results in the increase transmitted torque, but with diminishing returns. The optimal results showed that the maximum torque density obtained about 11.3 kNm/m^3. The proposed design methodology is successfully applied to the design of a two-pole (on the rotor) magnetic gear. A demonstrator is built and successfully tested, and theoretical predictions are validated.

Based on the demonstrator in this study, the use of a linear-rotary magnetic gear for applications such as wave energy harvesting looks promising.

Table of Contents

List of Figures

List of Tables

Declaration of authorship

I, **Thang Van Lang** declare that this thesis and the work presented in it are my own and has been generated by me as the result of my own original research.

A Linear to Rotary Magnetic Gear

I confirm that:

1. This work was done wholly or mainly while in candidature for a research degree at this University;
2. Where any part of this thesis has previously been submitted for a degree or any other qualification at this University or any other institution, this has been clearly stated;
3. Where I have consulted the published work of others, this is always clearly attributed;
4. Where I have quoted from the work of others, the source is always given. With the exception of such quotations, this thesis is entirely my own work;
5. I have acknowledged all main sources of help;
6. Where the thesis is based on work done by myself jointly with others, I have made clear exactly what was done by others and what I have contributed myself;
7. Parts of this work have been published as:

   T. V. Lang, S. M. Sharkh, J. R. Anglada, M. Hendijanizadeh and M. Moshrefi-Torbati, A low cost rotary to linear magnetic gear, *ICEM2020*, 20-26 August 2020, Gothenburg, Sweden.

Signed: .....

Date: .....

Acknowledgements

First and foremost, I would like to express my sincere gratitude to my supervisors, Dr. Mohamed Moshrefi-Torbati and Professor Suleiman Sharkh, for their guidance, support, and encouragement throughout my studies. Without their kindness and invaluable advice, it would have been impossible for me to come this far. They are always willing to share their experience and I have learned innumerable lessons and insights on research and other academic issues from them. Being their student is among the best things of this journey.

I feel deeply grateful to my examiner, Professor Andrew Cruden and Professor Kais Atallah, for giving me valuable feedback and supporting me as a PhD candidate and an early career researcher.

I would like to express my appreciation to Dr. Mehdi Hendijanizadeh and Dr. Jaime Renedo Anglada for generous support and sharing their knowledge during my PhD at University of Southampton.

I want to thank all students and staffs at Mechatronics Research Group who have contributed with their friendship and support to complete this journey.

My journey would not have been this amazing without my friends in Southampton. I am especially indebted to those who have shared all these PhD ups and downs with me and being such amazing friends. I also appreciate all the help from my colleagues and friends in Vietnam.

Finally, this work would impossible without the vital support and constant encouragement of my beloved family menbers which I am deeply grateful. I am especially pleased send this honour work to my defunct mommy who never be forgotten in my mine.

Symbols

μ_0	Permeability of free space
H	Magnetic field intensity
B	Magnetic flux density
B_s	The magnetic field produced in a slotless geometry at the middle of the air gap
J	Current density
K_B	Flux factor
D	Effective rotor's diameter
$\mathscr{F}$	Magnetomotive force
F	Magnetomotive force (MMF) produces by the winding
F_t	Translator force
T_r	Rotor torque
F_m	Magnetomotive force of the permanent magnets
n_s	Number of pole pieces
p_i	Number of pole pairs of inner rotor
p_o	Number of pole pairs of outer rotor
g	Air gap
G	Gear ratio
h	I-cores height
l	I-cores length
t	I-cores thickness
h_c	Core-back thickness
h_t	Ferromagnetic pole-pieces thickness
d	Magnet thickness
L_T	Translator's active length
M	Magnetisation field of the magnet
n	Revolutions speed of the rotor
N_{cores}	Number of C-cores
P	Number of poles of proposed magnetic gear

P_i	Number of pole-pairs on inner rotor
P_o	Number of pole-pairs on outer rotor
q_m	Number of modulator segments
V	Voltage
V_T	Translator linear speed
λ	Pole pitch
ω	Angular speed of the rotor
ω_i	Angular speed of the inner rotor
ω_o	Angular speed of the outer rotor
w	Magnet width
V_{ac}	Active volume
r_{ii}	Core-back outer radius of rotor
r_{io}	Outer radius of rotor magnet
T_m	Pull out torque
J_M	Moment of inertia
z	Displacement of the translator
θ	Angle of the rotor
T_L	Load torque
F_L	Load force
m	Seismic mass
T_i	Electrical torque of the generator
C_{bg}	Overall damping
R_i	Internal resistance
R_l	Load resistance
k	Spring stiffness

Chapter 1 Introduction

1.1 Motivation and problem statement

Technologies have been developed over the years to harvest energy from renewable energy resources to deal with climate change and global warming. The UK government released a renewable energy target in accordance with the EU Renewable Energy Directive 2018 [1] to deliver at least 32% of total energy demand from renewable sources by 2030. This was supposed to come mainly from bioenergy, onshore and offshore wind, solar, hydropower plant, and wave and tidal energy. In the UK, both onshore and offshore wind showed the largest increased in electrical generation while wave and tide contribute a smaller share so far; The Renewable Statistics in 2019 [2] has shown that renewable electricity generation represented 37.1% of total renewable electrical energy, in which wind electricity generation increased rapidly (22.9% offshore and 28.3 % onshore) and captured more than 50% of total renewable electricity. Wave and tidal energy represented a small amount of about 1% of the total electricity generation supplying in the UK.

Wave is one of the main energy source in the marine environment. In some energy harvesting systems, an intermediate mechanism is utilised to convert the linear low-frequency motion of waves to a high-frequency rotational motion to reduce the size and cost of the device [3]. Obviously, the low frequency of wave means a directly coupled linear generator will be large and expensive. Ball screw has been exploited to convert linear to rotary motion in wave energy harvesting systems. This is helpful in transforming slow linear motion into high frequency of rotary motion. Hendijanizadeh [4] used a ball screw for the development of an electromagnetic harvester at the University of Southampton.

Initially, this PhD work focused on developing a hybrid wave energy harvester by adding a linear generator to Hendijanizadeh's electromagnetic harvester and a conference paper [5] was published. It was shown that the generated power increased significantly without changing any of the parameters in the original system. A case study with four different linear generators was presented where it was shown that the output harvested power

could increase between 18% and 50%. Obviously, the trade-off for this power increase is the additional weight and space of the linear generator that must be considered in the calculations of the power density. However, linear generators can potentially be large and expensive. In addition, the friction contact between screw and nut of the ball screw is the main source of non-linear behaviour. It further causes problems such as high maintenance cost, noise and vibration. But, as a common solution, ball screws is inefficient. On the other hand, a magnetic gear provides a better solution in term of multi-media applications, efficiency, energy density, maintenance, and service life.

In recent years, the development of magnetic gears has provided a viable alternative solution for the replacement of mechanical gears. The main advantage of the magnetic gear is physical separation between the driving and driven shafts so that they avoid some drawbacks of traditional mechanical gears. For example, they are lubrication free; have lower maintenance cost; improved reliability; inherent anti-jamming transmission property and possess very low acoustic noise and vibration characteristics. Conversely, some drawbacks that restrict their widespread applications in industry include the high cost of permanent magnet, larger size for given transfer torque in comparison with the mechanical gears.

While there has been a vast amount of research on rotary magnetic gears, little has been done on linear to rotary gears. In fact, there have been only two linear to rotary magnetic gear developments that are derived from conventional mechanical gears, namely, the rack and pinion magnetic gear [6] and the helical magnetic gear which is similar to a nut and screw mechanism [7,8]. Recently, Anglada's PhD thesis [9] has introduced a basic concept of a linear to rotary magnetic gear that is derived from a transverse-flux machine. Anglada has provided the working principles of the concept without developing any theory or analyses. This thesis carries out fundamental research into this novel device in order to develop the underlying theories and analyses.

1.2 Magnetic gears

1.2.1. State of the art of magnetic gears.

Gears are mechanisms that transfer torque and speed from one shaft to another shaft by the use of meshing teeth or permanent magnets. Some magnetic gears are similar to mechanical gears in their structures, for instance, magnetic spur and planetary gears. Magnets on the gearing wheels transfer torque, as a result of which, there will be a fictive torsion spring effect between gear wheels. The torsion spring effect can be explained by imaging one wheel being fixed while the other wheel is rotated an angle. Therefore, there will be a certain torque application between the gear wheels which depends on the angle of displacement of the second wheel.

A magnetic gear will have a torque limitation $T_{max}(Nm)$, also referred to as the pull-out torque, where the gear will reach its maximal torque. If the applied torque is increased further than T_{max}, then the gear wheels will slip. Therefore, a magnetic gear should be operated under its torque limit. The torque spring for a magnetic gear will not be constant because it is the rate of change in torque divided by the angle change.

Torque density is an important criterion for assessing the performance of the magnetic gears. Torque density can be calculation as torque per unit rotor volume or torque per total unit volume. Using computer aided design, rotor volume can be determined accurately. A gear with magnets has a certain amount of rotor volume and this volume versus the maximum transferred torque is here defined as the active torque density ρ_A.

$$\rho_A = \frac{T_{max}}{V_A}\left(\frac{Nm}{m^3}\right) \tag{1.1}$$

To compare the torque density for magnetic gears with mechanical gears, a total torque density can be measured for the magnetic gears, given the total outer gear volume V_T.

$$\rho_R = \frac{T_{max}}{V_T}\left(\frac{Nm}{m^3}\right) \tag{1.2}$$

Mechanical gears have a corresponding torque density factor, ρ_F, which is calculated from the rated torque, T_N.

$$\rho_F = \frac{T_N}{V_T} \tag{1.3}$$

The efficiency of magnetic and mechanical gears is defined as the ratio of the power at the output shaft divided by the power at the input shaft.

$$\eta = \frac{P_{out}}{P_{in}} \times 100\% \tag{1.4}$$

The torque density of various magnetic gears is compared with those of mechanical gears in Table 1.1. Some magnetic gear that are mimic mechanical gears [10, 11, 12, 13, 16, 18, and 33] have torque density less than 12kNm/m^3, which is far less than that provided by the mechanical spur gear (from 100 to 200 Nm [10]).

1.2.2. Overview of magnetic gear topologies

The first magnetic gear (MG) was designed by Armstrong [11] in 1901. The idea of this MG is similar to a mechanical spur gear, but the transmission by contact tooth meshing was replaced by the contactless magnetic interactions. In 1941, Faus [12] proposed a magnetic worm gear with a structure based on a mechanical worm gear. However, this design received little attention due to its low torque density (nearly 5% of mechanical spur gears [10]). This was due to the poor performance of permanent magnet (PM) materials available at that time (namely SmCo5) [13-14]. In the 1980s, the development of rare earth permanent magnet materials (NdFeB) brought magnetic gear into potential industrial applications [15].

The development of new PM materials attracted more research funding, but the MG's topologies were still mainly based on mechanical gears and they are so-called converted MGs. This early development of magnetic gears mainly focused on worm type [16-18] and spur type [19-33] topologies. Although a large number of magnetic poles can increase torque capacity, the limitation of these MGs is their relatively low torque density due to the single pole-pair interaction between two shafts. In addition, planetary MGs also received attention

[34-37] because they offered advantages such as high gearing ratios and high torque density. Magnetic gears based on bevel gears [38-39] have also been developed. It is shown that these developments of converted MGs have low torque densities, i.e., far less than their mechanical gear counterparts and hence, they have received little attention in industrial applications.

Table 1: Torque density of different gears [10].

Gear type	Transm-ission ratio	Operating principle	Torque density [kNm/m^3]	Compl-exity	Utilizat-ion of PMs
Involute MG [11]	3:1	Magnetic meshing	1-7	Yes	Low
Magnetic worm gear [12]	33:1		0.74		
Magnetic skew gear [13]	1.7:1		0.15		
Multi-element MG [16]	24:1	Variable reluctance	3.96		
Parallel-axis MG [18]	4:1	Magnetic meshing	11.6	No	High
Perpendicular-axis MG [33]	1:1		3		
Magnetic torque coupler [26]	1:1		230		
Magnetic planetary gear [28]	3:1		100	Yes	Low
Concentric magnetic gear [36]	1.7-100	Variable reluctance	70-150		High

In recent years, a different MG topology has been developed by using ferromagnetic pole-pieces to modulate the magnetic field produced by both outer and inner rotors [40-44], which is called a field-modulated magnetic gear. These MGs have a relatively higher torque density due to the contribution of all PMs to torque transmission. Therefore, they have been recommended for applications such as wind energy [45-51] and electric vehicles [52-59].

Moreover, a different topology of MGs has been investigated in the form of transmission from linear to linear, rotary to linear motion and vice versa [60-64]. These MGs offer some advantages in comparison with mechanical gears such as low friction, low maintenance and overload protection. This type of MG can offer significant merits for applications in wave energy and railway traction [13-15].

However, MGs have disadvantages such as the maximum torque capability may not be sufficient for some applications, they are more expensive and typically heavier than conventional gears. Several topologies have so far been studied, but further research is needed for their implementation and more practical validation is desired to ascertain their advantages. Obviously, most topologies of MGs present a low torque density (10-80% of the mechanical spur gears) together with complex structures (more assemble parts). Thus, we should apply a new methodology and principle to improve the limitations of MGs in order to be able to attract more attention for their applications.

1.2.3. Converted magnetic gears

As mentioned above, this section describes the development of the converted MGs that include operational principle, topologies, and general characteristics.

Figure 1.1 shows involuted magnetic gears that were proposed by Tsurumoto and Kikuchi [16] in 1987. By using SmCo5 for the permanent magnet, this magnetic gear has a gear ratio of 1:3 with the maximum transmitted torque of 5.5 Nm at the driven magnetic gear. In 1993, the authors also designed a magnetic worm gear [17] that is illustrated in figure 1.2. One year later, this worm gear was developed with a trial construction of a magnetic skew gear [18]. Generally, these MGs have not only a complicated arrangement, but also a low torque density (from around 5% to 10% of mechanical spur gears).

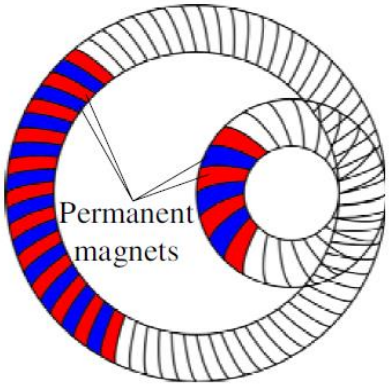

Figure 1. 1 Involute magnetic gears [16]

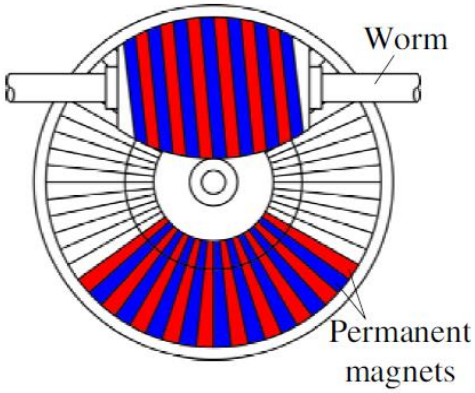

Figure 1. 2. Magnetic worm gears [17]

An intensive development of the converted MGs has focused on studying parallel-axis MGs, such as spur type. The first typical spur MG was proposed and patented in the US, in 1970, by Rand [19]. In 1974, a very similar structure was developed by Hetzel [20]. Although these suggestions have potential applications, they lack detailed analysis to investigate their working capabilities. In 1980, Hesmondhalgh *et al.* [21] developed a theoretical basis of its operation and built a demonstrator to conduct experiments. Analytical calculations, developed by Ikuta *et al* [22] and Yao *et al* [23], investigated the external and internal spur MGs (shown in Figure 1.3), were also accompanied with a finite element analysis (FEA). Moreover, Jorgensen *et al.* [24] and Fulani [25] developed two-dimensional analytical calculations that produced a similar result to the FEA approach. Although these analyses helped to improve the characteristics of spur MGs, they are still limited in applications due to their poor torque density.

A similar mechanism to spur MGs is magnetic couplers, which can be used to transmit torque between two coupling halves at the same speed [26, 27]. The couplers can be divided into two types, axial and coaxial couplers, as shown in Figure 1.4. The parameters of axial couplers, that can be found in the research work of Fulani [28, 29], were analysed by using both FEA and torque formula methods. In addition, Yao *et al* [30] compared these methods on torque calculations, both theoretically and experimentally. This research has shown that the torque of the couplers can be increased by increasing the number of poles for magnetic coupling between magnetic rings with short gaps between them (air gap). Coaxial couplers have been studied by Wu *et al.* [31]. In his research, by using 2D and 3D FEA, design optimisation was carried out to minimise the volume of the magnetic materials. Moreover, Elies [32] implemented a study of the coaxial coupler in 1999 wherein the radial stiffness of cylindrical-air gap magnetic couplings was computed analytically in order to determine the force exerted between two magnets. It is shown that this stiffness becomes zero for some axial shift regardless of what the amount of angular shift and the torque to be transmitted.

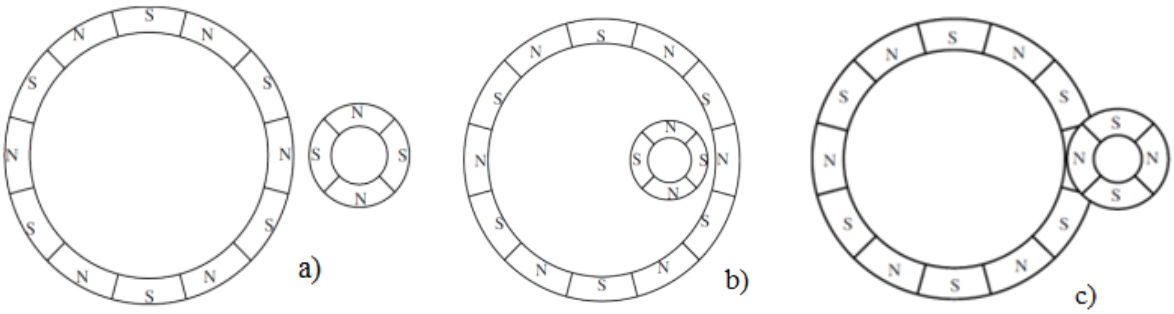

Figure 1. 3. Radial parallel-axes spur MGs: a) External type b) Internal type c) axial type [23]

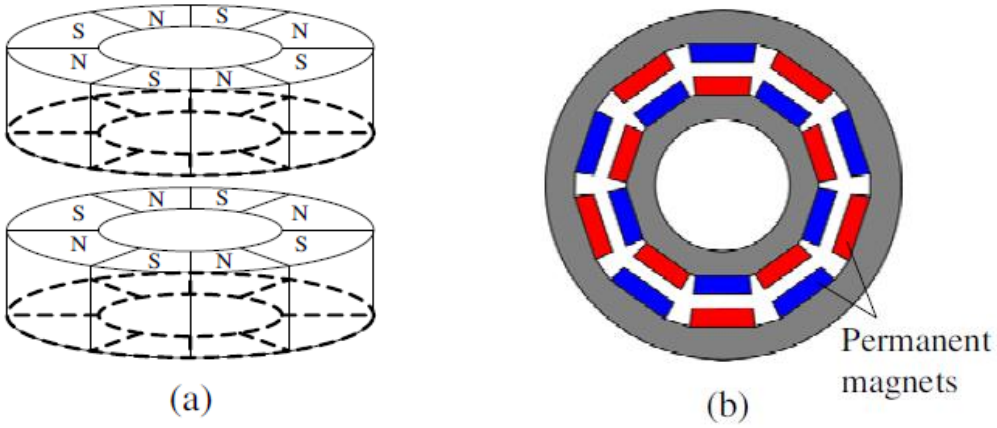

Figure 1. 4. Magnetic torque couplers: a) Axial coupler; b) Coaxial coupler [28]

Obviously, these types of couplers have a higher torque transmission capability than the previous one; therefore, they can be used in some specific applications (e.g., chemical industry) where the driving and driven parts need to be separated.

Another development of a magnetic gear, with reference to the mechanical gear equivalent, was a magnetic planetary gear that was proposed by Huang [33] in 1996, as shown in Figure 1.5. The later developments by the author in 2008 [34] and 2011 [35] pointed out that the transmitted torque was dependent on the number of the magnetic planet gears. By using the FEA method, the magnetic planetary gear can be derived to achieve approximately 100 kNm/m^3 with six magnetic planetary gears. In addition, a FEA optimisation was carried out by Kong *et al* [36] for the reduction of cogging torque and torque ripple, so that the transmitted efficiency can be greatly improved. Moreover, a comparison

between mechanical and magnetic planetary gears was made by Li *et al.* [37], in 2011. They showed that the MG can have comparable or better performances than its mechanical counterpart with the obvious benefits of avoiding mechanical drawbacks. Therefore, as the study has suggested, a magnetic planetary gear can replace a mechanical gear in applications such as hybrid vehicles, airplanes, and medical applications.

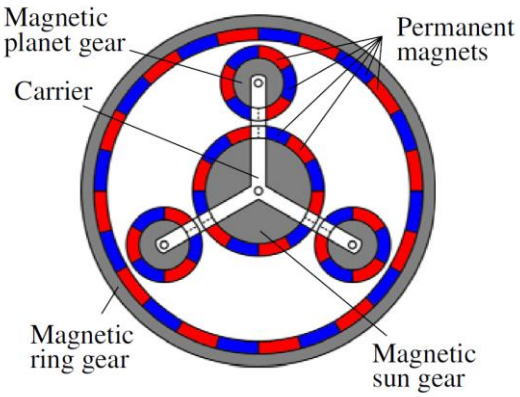

Figure 1. 5. Magnetic planetary gear [37]

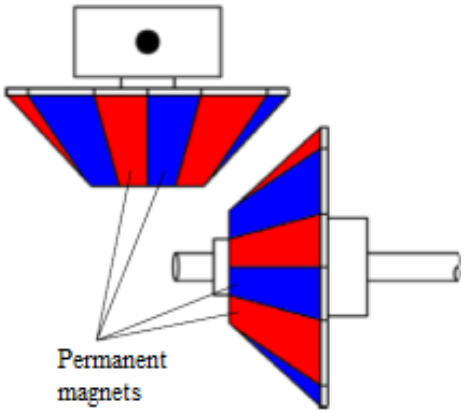

Figure 1.6. Perpendicular-axis MG [38]

A perpendicular-axis coupler shown in Figure 1.6 was studied by Yao *et al.* [38] in 1996 and developed by Muruganandam *et al.* [39] in 2012. The analysis has presented that the transmitted torque is highly dependent on the number of poles and the size of air gap. Similar to magnetic spur gears, the single pole pair interaction between two shafts of magnetic bevel gear also gives a relatively poor torque density.

1.2.4. Field modulated magnetic gears

In 2001, a concentric magnetic gear was proposed by Atallah and Howe [40]. The basic operational principle of the MG relied on the use of ferromagnetic pole-pieces that interposed between the inner and the outer rotors to modulate the magnetic fields, as shown in Figure 1.7. This MG has been analysed in [41] where it is shown that it has a high torque density (i.e., 50-150 kNm/m^3) due to the contribution of all PMs to torque transmission.

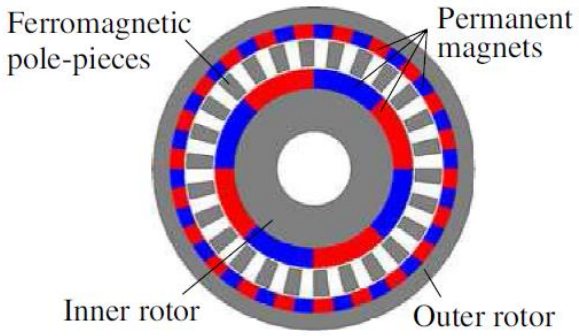

Figure 1.7. A coaxial magnetic gear with ferromagnetic pole-pieces in between two rotors [40]

As shown in Figure 1.7, the outer rotor has a higher number of pole-pairs than that of the inner rotor, resulting in the inner rotor having a higher speed than the outer rotor. The number of pole-pairs on the inner and outer rotors, p_i and p_o, and the number of modulator segments, q_m are related by [40]:

$$q_m = p_o + p_i \tag{1.5}$$

with a stationary modulator, the gear ratio G is given by

$$G = \frac{p_o}{p_i} = \frac{q_m - p_i}{p_i} = \frac{q_m}{p_i} - 1 = -\frac{\omega_i}{\omega_o} \tag{1.6}$$

where ω_i and ω_o are the angular speeds of the inner and outer rotors respectively. When the outer rotor is held stationary, the gear ratio between the inner rotor and the rotating modulator is [40]:

$$G = \frac{q_m}{p_i} = \frac{\omega_i}{\omega_m} = 1 - \frac{\omega_i}{\omega_o} \tag{1.7}$$

where ω_m is the angular speed of the modulator.

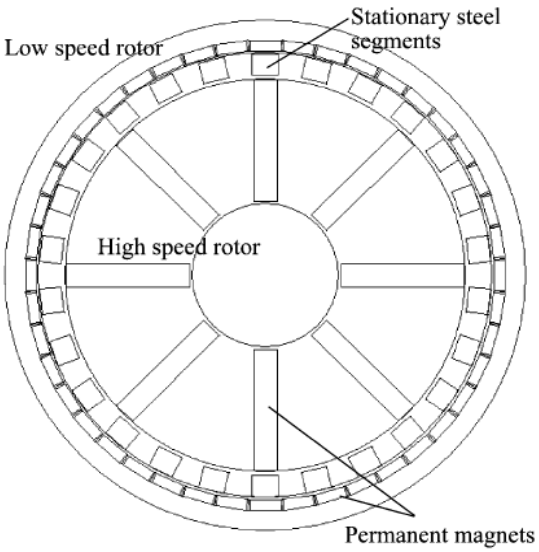

Figure 1. 8. A coaxial magnetic gear proposed by Rasmussen *et al.* [42]

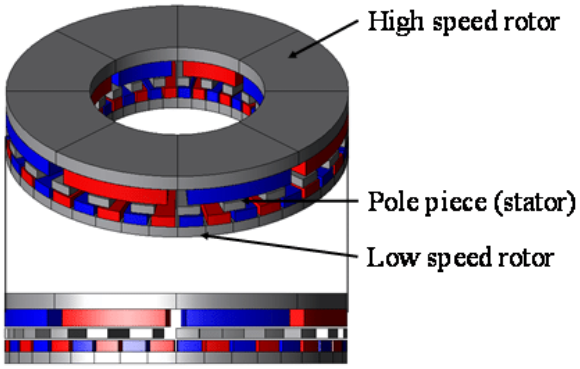

Figure 1. 9. Axial-field magnetic gear [43]

The work of Atallah and Howe has inspired many researchers to investigate this topology. Rasmussen *et al.* [42] proposed a different structure to decrease the end-effect caused by the short stack of the PMs, as shown in Figure 1.8. By using the FEA method, the analysis showed that a better efficiency of magnetic gear than the mechanical gear estimated at 96% can be achieved. A prototype was built to conduct experiments which showed that the actual efficiency of the fabricated prototype was only 86%. The report pointed out that the lower efficiency than analytical was mainly caused by the magnetic field interference in an extra installed bearing and manufacturing problems.

A disc type concentric magnetic gear was also proposed in [43], as depicted in Figure 1.9. The research reported that a torque density over 70 kNm/m^3 can be obtained with this axial field MG, and that the axial forces exerted on the two rotors and the ferromagnetic pole pieces are relatively low.

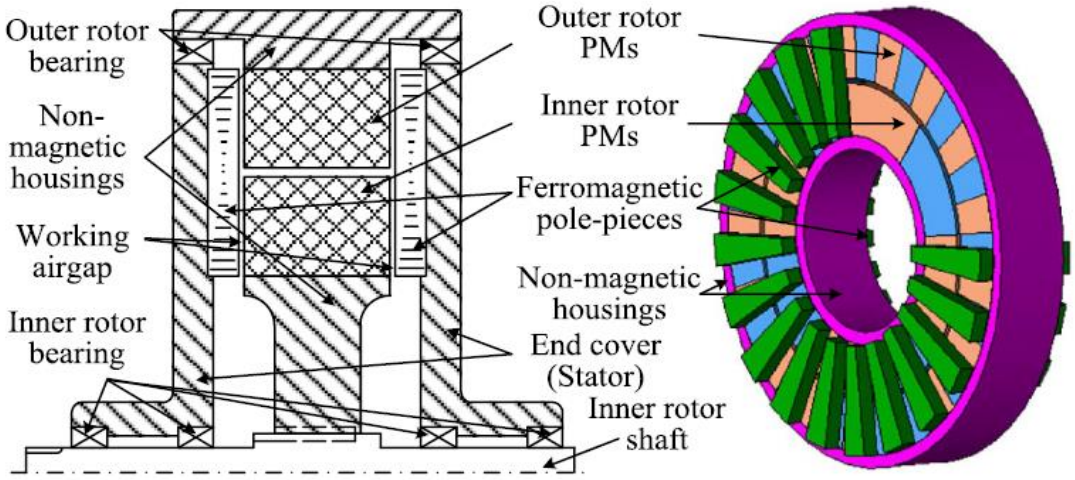

Figure 1. 10. An axial-field flux-modulated magnetic gear [44]

Further research on field modulated magnetic gear was developed, i.e., axial-field flux-modulated magnetic gear, that was proposed by Zhu *et al.* [44] in 2016, as shown in Figure 1.10. Instead of putting the ferromagnetic pole pieces between the outer and inner rotors to produce the coaxial field distribution, two stationary modulation rings were arranged on the two end-faces of the PMs on two rotors to achieve the axial-flux configuration. This proposed design offered a simpler mechanical structure and decreased the gap length between two rotors. By using FEA and an optimisation process, a torque density exceeding 77 kNm/m^3 can be achieved.

Due to its high performance, this type of MGs has been investigated for some applications such as wind generators [45-46] and electric vehicles [47-49]. However, further research is needed to validate its merits and bring its readiness to the industrial world.

1.2.5. Associated linear topologies of MGs

In the previous section, MGs were summarised in term of rotational transmission, but this section will introduce different types of transmission such as linear to linear, rotary to linear motion and vice versa.

In 2005, Atallah *et al.* [50] proposed a linear MG, which transmits linear movement, as shown in Figure 1.11. The principle of operation is similar to the field modulated MGs, which was described in section 1.2.3. Using FEA method, it has been shown that the linear MG can transmit a force density in excess of 1.7 kNm/m^3 with NdFeB magnets. Thus, by increasing the speed of the linear translator, it can combine with a linear generator to increase the power captured in wave power generation [51], as shown in Figure 1.12. This configuration has been also analysed and tested by Holehouse *et al.* [52] to meet the performance requirement of an aerospace application.

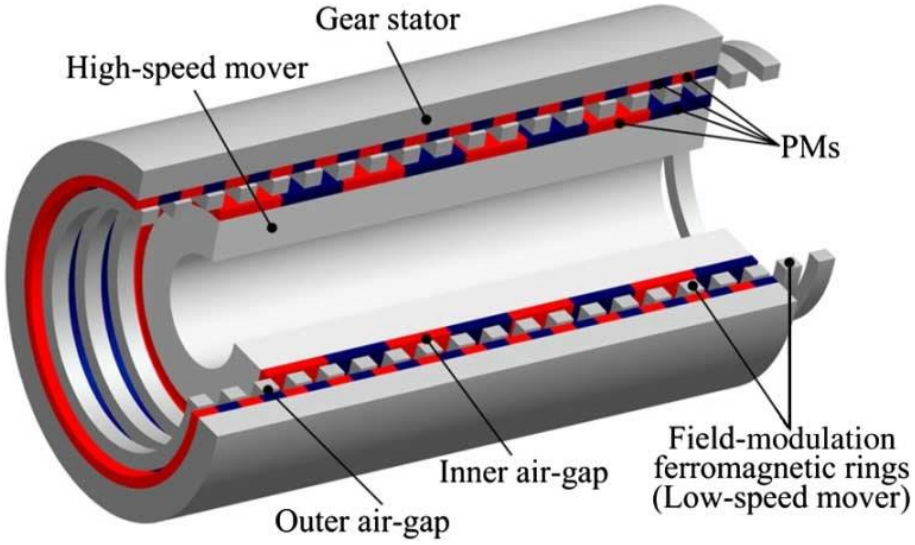

Figure 1. 11. A schematic of a linear magnetic gear [50]

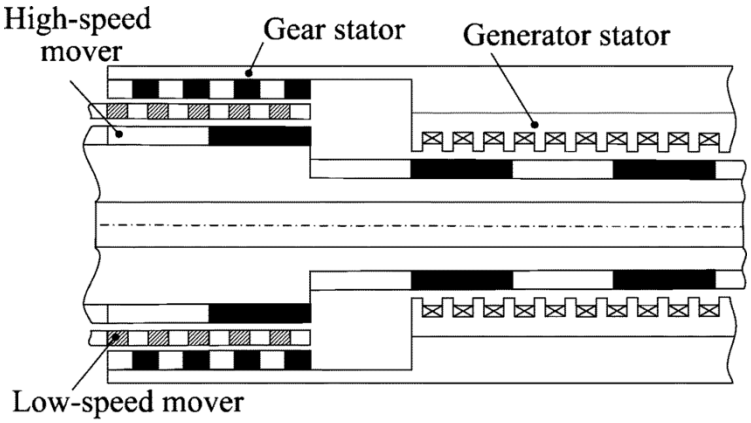

Figure 1. 12. Configuration of wave generator using a linear magnetic gear [50]

For transmission from linear to rotary motion or vice versa, some MGs have also been proposed. Andrews [53] introduced a magnetic gear in 1925, with a similar principle of operation to a screw and nut mechanism. The configuration of a helical MG structure of was designed by Pakdelian [54] in 1978, as shown in Figure 1.13, together with the analyses of torque transmission and experimental work to validate the analytical model. In addition, the helical structure was analysed and optimised analytically and by using 2D and 3D FEA models in [55-56] and was shown that a torque density of more than 15 kNm/m^3 can be achieved.

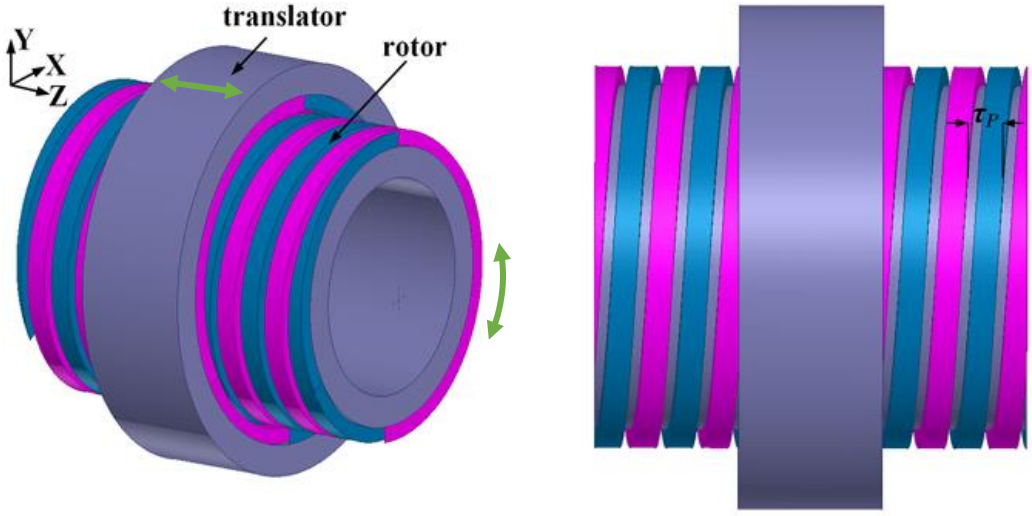

Figure 1. 13**.** A helical structure of linear-rotary magnetic gear [54]

In 2016, a rotary-linear motion MG was presented by Hua *et al.* [57], based on the design principle of a reluctance motor. Figure 1.14 shows the configuration of such MG. By using 2D and 3D FEA models, the rotary-linear reluctance MG has been analysed and optimised with three magnetic pole pair arrangements. However, the authors have not yet produced torque equation and its characteristics.

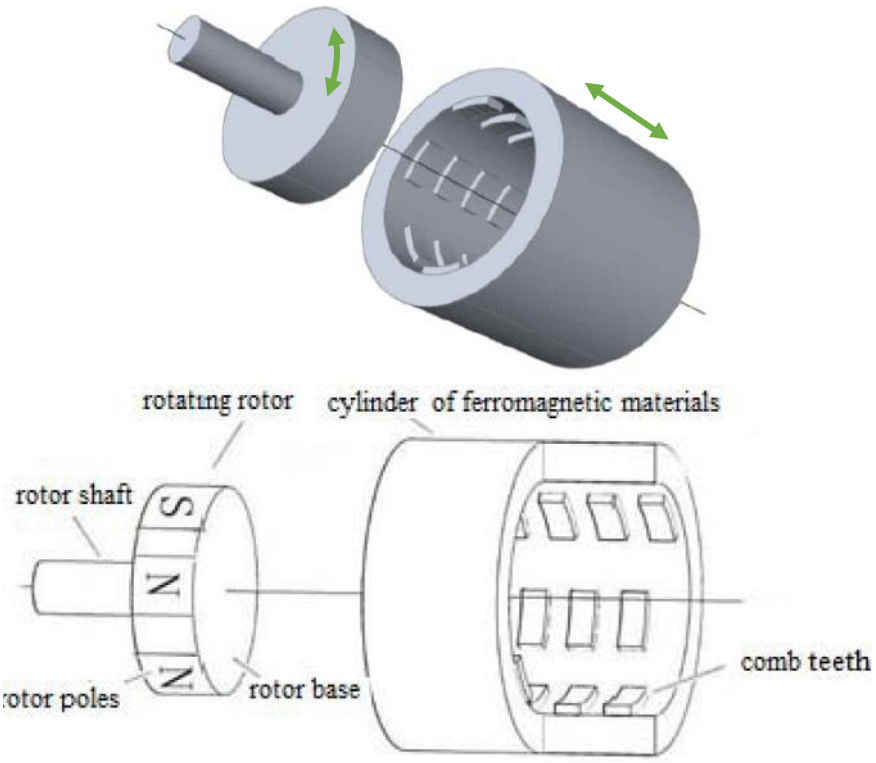

Figure 1. 14. Reluctance Rotary-linear magnetic gear [57]

Kouhshahi and Bird et al. [58,59] presented an alternative linear to rotary magnetic gear that combines the principles of a magnetic screw, with a helical magnet on the rotor, with that of a gear incorporating a layer of skewed ferromagnetic pieces to modulate the flux. On the outer cylinder, a flux concentrating structure is used comprising ferromagnetic rings sandwiched between ring magnets. The flux-modulating translating ferromagnetic pieces between the rotor and the outer cylinder layers are also skewed.

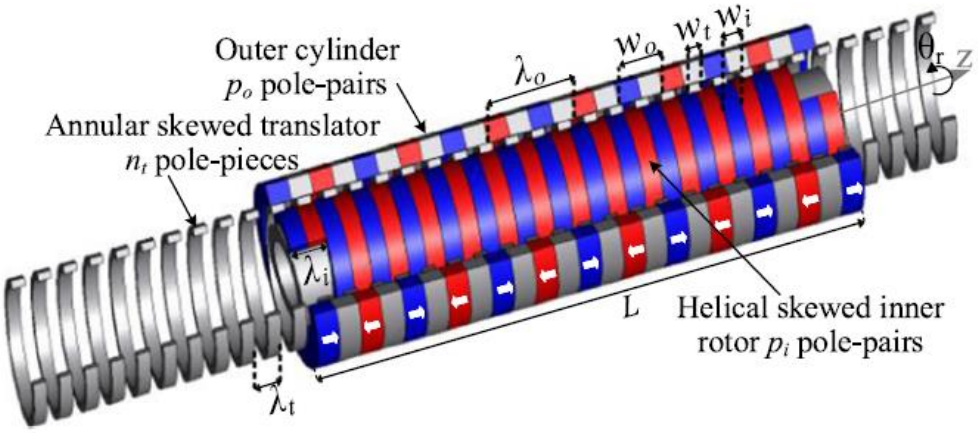

Figure 1. 15. A magnetically geared lead screw [59]

It is noted from aforementioned works that the structures of the MGs are complex together with the low torque density so that it is difficult to bring them into real applications. Furthermore, these topologies still require further studying and testing to validate their merits and weaknesses. Thus, further investigations into these topologies are needed, and meanwhile, it is necessary to seek alternative, effective methods and principles for the development of MGs.

1.3 A linear to rotary magnetic gear based on transverse-flux machine

In this section, the idea of a linear to rotary magnetic gear is presented. In the transverse-flux machine, the winding in the stator produces a magnetic flux and affects the magnets on the rotor through the C-cores which have the function of modulating the magnetic flux. When the current in the winding changes direction, the rotor rotates.

Figure 1.16 shows a front view of the transverse-flux machine built at the University of Southampton [70]. In the stator hub, there are two rows of C-cores mounted with a coil in each row. The C-cores are pieces of magnetic materials in the shape of a ‘C’ that help to modulate the magnetic field.

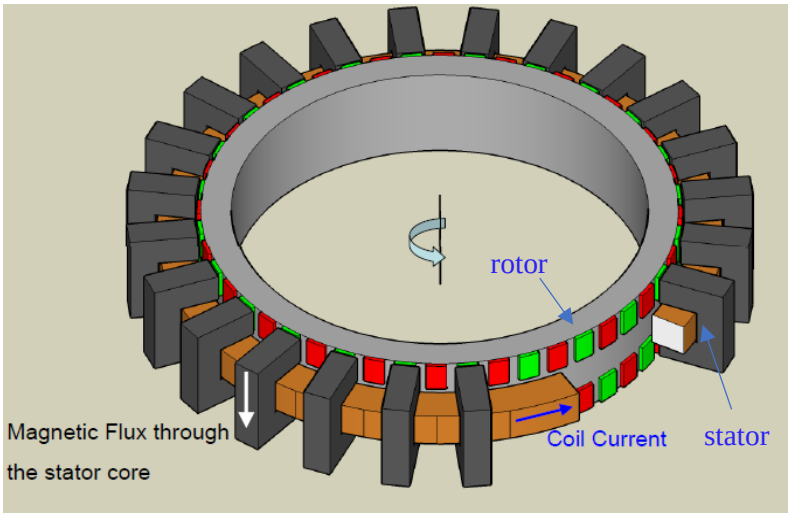

Figure 1. 16. A phase of the transverse-flux machine including the rotor and stator

The principle of operation is based on the variation of the reluctance with position because of the orientation of the magnets. Figure 1.17 shows schematically the path of the magnetic field in two different positions. If there is a current that goes out of the paper (dot in the figure) because of the *right-hand rule* the magnetic field will be anti-clockwise and there will be an electromagnetic force that will try to move the rotor towards the magnets that create a magnetic field in the same direction.

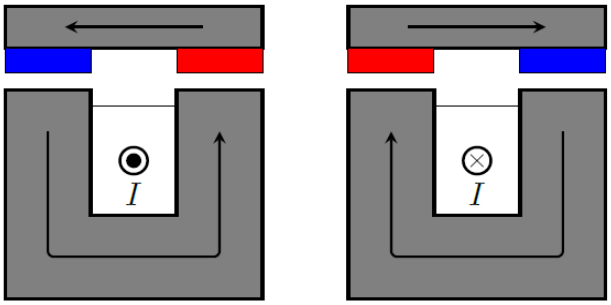

Figure 1. 17**.** Path of the magnetic field depending on the current [9]

When the current goes into the paper, the magnetic field produced will be clockwise and the electromagnetic force will try to align with the magnets in the opposite way to the previous case. Figure 1.18 illustrates the magnetisation of a magnet with the equivalent current loops [9]. The total flux through the equivalent current loop can be calculated directly

by integrating along the magnet thickness the differential flux in through each of the different current where M is the magnetisation of the magnet.

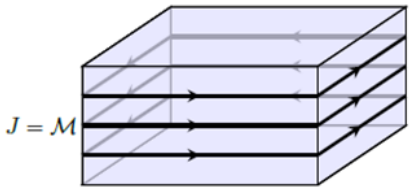

M	the magnetisation of the magnet
J	the current density

Figure 1. 18. A rectangular magnet with the equivalent current loops [9]

Figure 1.19 shows magnetic flux in a C-core of the transverse-flux machine. With the appropriate current waveform with more than one phase, this machine can produce a net positive torque. The machine built in Southampton has two phases with 90 electric degrees difference and 20 C-cores per phase, in each phase, there are two rows of 40 magnets with alternating polarity. Figure 1.20 shows the developed model of the airgap of the transverse-flux machine with the magnets in an arbitrary position. In aligned position, the rotor torque is equal to zero due to the equivalent force of the magnets at the top of the C-cores. In contrast, the unaligned position makes the rotor start rotating because of repelling forces of the magnets and flux from C-cores, and the torque is maximum at the half-misaligned position.

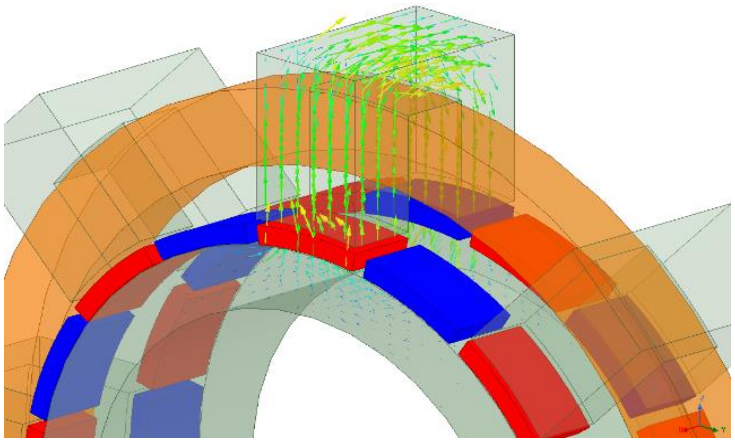

Figure 1. 19. Magnetic flux in a C-core for a single-phase transverse-flux machine

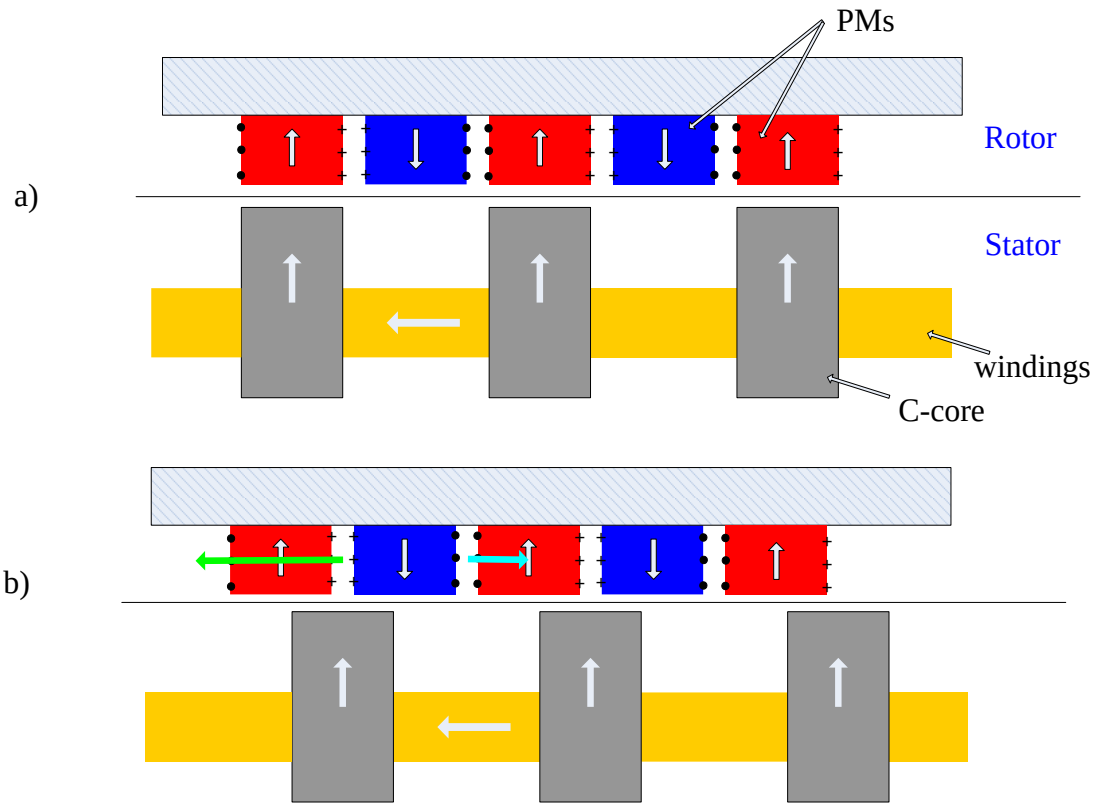

Figure 1. 20. Position of the rotor with the C-cores a) aligned, b) unaligned

The electromagnetic interaction described is very different from the one of a typical generator; this is why employing an analytical method to estimate the torque produced in this machine represents a great challenge. In torque calculations, the most important parameter is flux factor, K_B, which is the coefficient that will indicate which part of the total magnetic field produced by the windings is effectively producing torque.

In a progress report [9], Anglada proposed a magnetic gear whose principle of operation was directly derived from the original transverse flux machine. A schematic cross-section and a 3D view of the magnetic gear are shown in Figure 1.21; the 3D view does not show the upper coreback for clarity. The configuration of the magnetic gear consists of a rotor, T-cores and four rows of magnets that are embedded on the surface of two outer corebacks. The T-cores modulates the magnetic field experienced by the four rows of rectangular magnets. However, this structure of this configuration that was proposed by Anglada is complicated

and will be difficult to manufacture. In addition, the T-core has a relatively high reluctance due to the length of the magnetic path, which together with significant leakage flux reduce magnet utilisation.

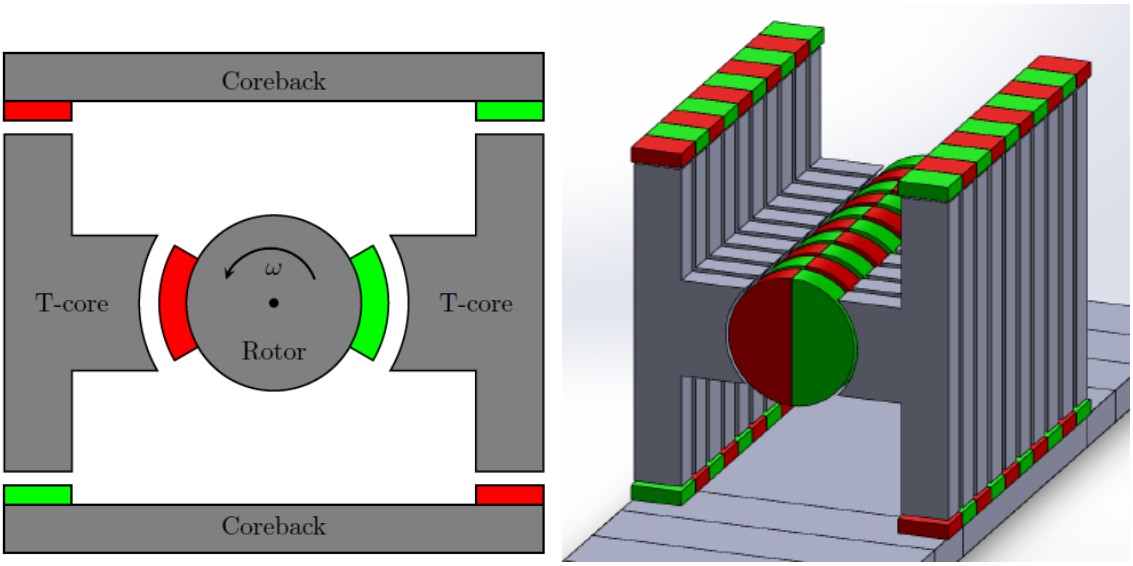

Figure 1. 21. A schematic and 3D view of a magnetic gear suggested by Anglada [9]

Figure 1.22 shows a configuration of the transverse-flux machine replacing the winding by a stack of magnets. It is noted that the C-cores are cut out to become two I-cores (ferromagnetic pole-pieces). To change magnetic flux direction in the I-cores, the magnetic stack will be translated. Thus, the magnets on the top of the I-cores will be changed from the North Pole to the South Pole. When the stack of the magnets moves, the rotor rotates. This is the same situation in which the direction of the current changes in the winding. Therefore, by using a transverse-flux machine mechanism combined with a stack of magnets, the translation of the stack of magnets can be converted into the rotation of the rotor. It is also noted that the I-cores are held stationary.

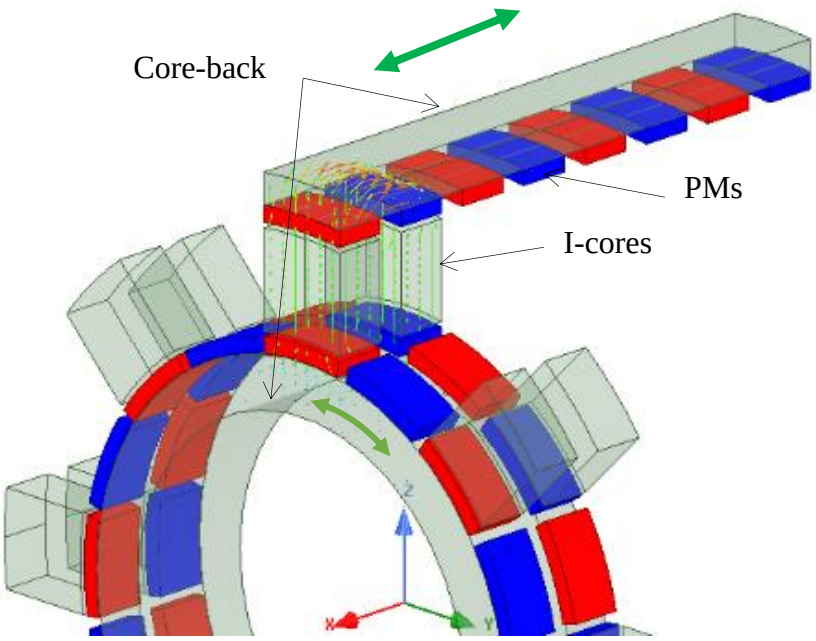

Figure 1. 22. Transverse-flux machine with replacing the windings by a magnet stack

The transverse-flux machine's characteristics are low speed and high torque. This is due to a large number of poles on the rotor. However, in an energy conversion system, particularly in wave energy devices, the purpose is to convert low linear movement of the waves into a high rotary speed to have a higher level of efficiency. Therefore, in the magnetic gear, the number of poles on the rotor should be minimised to obtain the highest speed.

Figure 1.23 represents the structure of a proposed magnetic gear. The system consists of three main parts; a rotor, translators and I-cores (ferromagnetic pole-pieces), and these parts are isolated by an air gap in between. Two poles are so-called phase 1 with magnets aligned with magnets on rotor, two more stacks are added to the translator (acting as a second phase) but they are place at half a pitch in comparison with the first phase. The translators move along the Z-axis and the rotor rotates about the same axis.

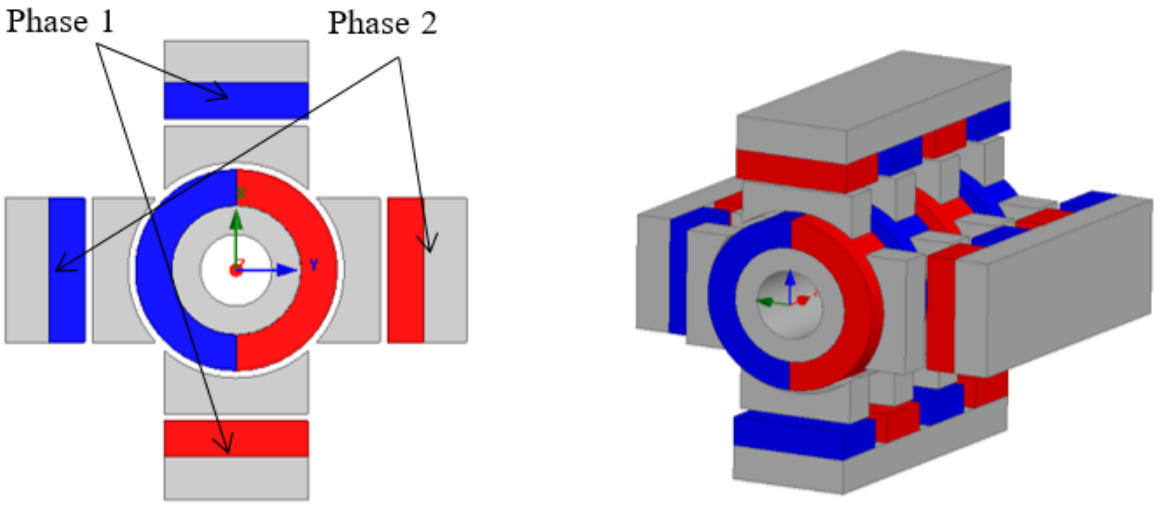

(a) (b)

Figure 1. 23. Structure of the magnetic gear a) front view, b) isometric view

1.4 Aims and objectives

The aim of this study is to develop the theory and analysis for investigating the performance of a novel magnetic gear. Design parameters of the proposed magnetic gear will be considered and 2D and 3D model finite element analysis (FEA) will be exploited to determine the torque and force of the device. A linear to rotary magnetic gear has several fields of applications such as linear actuators for medical and chemical devices, wave harvesting devices, aerospace systems, etc. Therefore, such magnetic gear needs to be studied in detail to better understand its positive and negative aspects. The objectives of this thesis can be summarised as:

1. A proposed magnetic gear is introduced based on the operation principles of a transverse-flux machine. In order to understand the working principles of the proposed magnetic gear, 2D and 3D models are developed by using the finite element analysis method to predict the flux density distribution in the air gap and the ferromagnetic pole-pieces. Then transmitted torque characteristics are determined.
2. Design optimisation studies are undertaken in order to determine the effects of the permanent magnets' key parameters, the sizes of pole-pieces and the air gap length

on the performance of the magnetic gear. Consequently, optimal dimensions of a linear to rotary magnetic gear demonstrator are determined.

3. Constructing and testing a magnetic gear prototype to validate the analytical and finite element analysis.
4. Future work will provide the dynamic behaviour of the proposed magnetic gear and it is examined in terms of oscillation of the rotor. Then, the magnetic gear is modelled in a driven train system with an input force on the translator and a load on the magnetic rotor shaft. Also, the proposed magnetic gear is considered for constrained applications, such as in wave energy harvesting.

Chapter 2 Magnetic Field Theory

2.1 Introduction

In this chapter, basic theories and methods to calculate the magnetic field in the airgap are reviewed. It is essential to have accurate models to calculate the magnetic flux-density distribution in the airgap of a magnetic machine in order to determine the performance characteristics such as torque and force. In solving field problems, three types of techniques are mainly used: experimental, analytical and numerical. Experimental methods need to setup a laboratory equipment so that it is expensive and time consuming. Analytical methods are widely used in order to provide exact solution and give a better insight, but they become hard to use for flexible and complicated models. Numerical methods are commonly used since the development of the computing capacities even though they are calculated by using approximate solutions but giving sufficient accuracy for engineering purposes [61]. The numerical methods also provide tools for swept parametric analysis with parameter variation. Therefore this method can be used to validate for analytical methods and an efficient solution for the final design.

2.2 Basic magnetic field theory

In this section, basic concepts in magnetic circuit theory will be presented. A simple magnetic circuit will provide a fundamental relationship between the key parameters.

2.2.1 Biot-Savart law

Applying electrical current through a conductor produces a magnetic field which is presented either by magnetic field intensity, $\vec{H}$, or magnetic flux density vector, $\vec{B}$. These two vectors are related by the material of conductor, i.e.,

$$\vec{B} = \mu\vec{H} = \mu_0\mu_r\vec{H} \text{ (T)} \tag{2.1}$$

Where $\mu_0 = 4\pi \times 10^{-7} \frac{H}{m}$ the permeability of free space, and μ_r is the relative permeability of a material compared to the permeability of free space. For example, the value of μ_r is 1 for air or could be several thousands in case of ferromagnetic materials.

The Biot-Savart law is fundamental in nature and is used to calculate $\overrightarrow{dB}$ or $\overrightarrow{dH}$ at a given point with the position vector r, due to an elemental current $i\vec{dl}$ and is given by:

$$\overrightarrow{dB} = \frac{\mu_0 \mu_r}{4\pi} \frac{i\overrightarrow{dl} \times \vec{r}}{r^3} \tag{2.2}$$

If the dimensions and shape of the conductor carrying current are known then the field at a given point can be calculated by integrating the right hand rule in the above equation.

$$\vec{B} = \frac{\mu_0 \mu_r}{4\pi} \int_{length} \frac{i\overrightarrow{dl} \times \vec{r}}{r^3} \tag{2.3}$$

where, length indicates that the integration is to be carried out over the length of the conductor.

2.2.2 Ampere's circuital law

This law states that line integral of the vector $\vec{H}$ along any arbitrary closed path is equal to the current enclosed by the path. Mathematically:

$$\oint \vec{H}\, \overrightarrow{dl} = I \tag{2.4}$$

where *H* is the magnetic field intensity produced by the current *I*, and *dl* is a differential element of length along the path of integration. For certain problems, particularly in magnetic circuit problems, Ampere's circuital law is used to calculate field instead of the more fundamental Biot Savart law for reasons going to be explained below. Consider an infinite straight conductor carrying current *i* and we wish to calculate the field at a point situated at a distance *d* from the conductor. Now, take the closed path to be a circle of radius *d*. At any point on the circle the magnitude of field strength will be constant and its direction will be tangential. Thus, the above equation simply becomes H × 2π*d*. So the field strength is

$$H = I/2\pi d \ (A/m) \tag{2.5}$$

It should be noted that in arriving at the final result no integration is required and it is obtained rather quickly. However, one has to choose a suitable path looking at the distribution of the current and arguing that the magnitude of the field remains constant throughout the path before applying this law advantageously.

2.2.3 The magnetic circuits

The basic law governing the production of a magnetic field by a current is Ampere's law in Eq. (2.4). To better understand the meaning of this equation, it is helpful to apply it to the simple example in Figure 2.1 which shows a rectangular core with a winding of *N* turns of wire wrapped around one leg of the core.

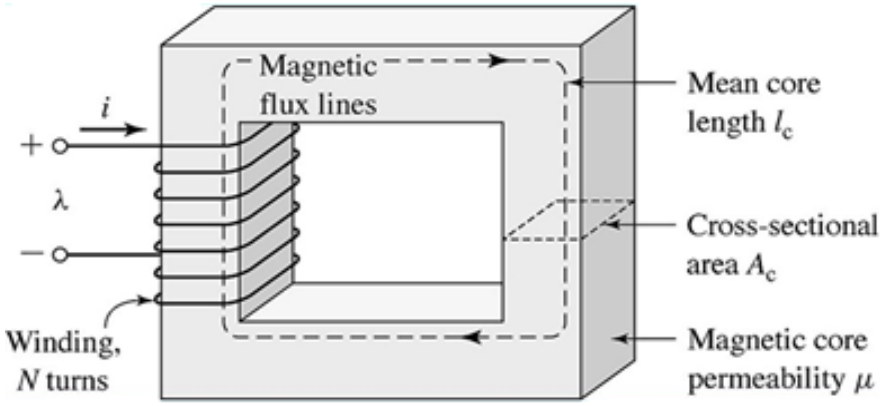

Figure 2. 1. Schematic view of a magnetic circuit [9]

If the core is a ferromagnetic material, all the magnetic field produced by the current will be confined inside the core, thus the integration path in Ampere's law is the mean path length of the core l_c. The current passing within the path of integration I is the product of *Ni*, since the coil of wire cuts the path of integration *N* times while carrying current *i*. Ampere's law thus becomes

$$Hl_c = Ni \tag{2.6}$$

Thus, Eq. (2.1) becomes

$$\vec{B} = \mu\vec{H} = \frac{\mu Ni}{l_c} \tag{2.7}$$

Now, the total flux in a given area is given by

$$\phi = \oint_A \vec{B} d\vec{A} \text{ (Wb)} \tag{2.8}$$

where *dA* is the differential unit of area. If the flux density vector is perpendicular to the plane of area A, and if the flux density is constant throughout the area, then this equation reduces to

$$\phi = BA = \frac{\mu N i A}{l_c}, \tag{2.9}$$

where A (m^2) is the cross-sectional area of the core.

In a simple electric circuit, a voltage source V drives a current I around the circuit through a resistance R. The relationship between these quantities is given by Ohm's law:

$$V = IR \tag{2.10}$$

By analogy, the corresponding quantity in a magnetic circuit is called the magnetomotive force ($\mathscr{F}$) which is equal to the effective current flow applied to the core, or

$$\mathscr{F} = Ni \tag{2.11}$$

where $\mathscr{F}$ is measured in ampere-turns (At). In an electric circuit, the applied voltage causes a current I to flow and, similarly in a magnetic circuit, the applied magnetomotive force causes flux to flow. The relationship between voltage and current in an electric circuit is given by the Ohm's law. The relationship between magnetomotive force and flux is

$$\mathscr{F} = \phi \mathscr{R} \tag{2.12}$$

Where $\mathscr{R}$ is reluctance of the circuit.

The reluctance of a magnetic circuit is the counterpart of electrical resistance, and its units are ampere-turns per weber (At/Wb).

There is also a magnetic analogous of conductance. Just as the conductance of an electric circuit is the reciprocal of its resistance, the permeance of a magnetic circuit is the reciprocal of its reluctance:

$$\mathcal{P} = \frac{1}{\mathscr{R}} \ (At/Wb) \tag{2.13}$$

The relationship between magnetomotive force and flux can thus be expressed as

$$\phi = \mathcal{F}\mathcal{P} \tag{2.14}$$

The resulting flux in the core is given by Eq. (2.9)

$$\phi = B \times A = \frac{\mu N i A}{l_c} = Ni\frac{\mu A}{l_c} = \mathcal{F}\frac{\mu A}{l_c} \tag{2.15}$$

By comparing Eq. (2.11) with Eq. (2.14), we can see that the reluctance of the core is

$$\mathcal{R} = \frac{l_c}{\mu A} \tag{2.16}$$

Reluctances in a magnetic circuit obey the same rules as resistances in an electric circuit. The equivalent reluctance of several reluctances in series is

$$\mathcal{R}_{eq} = \mathcal{R}_1 + \mathcal{R}_2 + \mathcal{R}_3 + \cdots \tag{2.17}$$

and in parallel is

$$\frac{1}{\mathcal{R}_{eq}} = \frac{1}{\mathcal{R}_1} + \frac{1}{\mathcal{R}_2} + \frac{1}{\mathcal{R}_3} + \cdots \tag{2.18}$$

Now, we can apply the same idea for a complicated geometry, such as the one shown in Figure 2.2, that is similar to the previous case but with an air gap within the core.

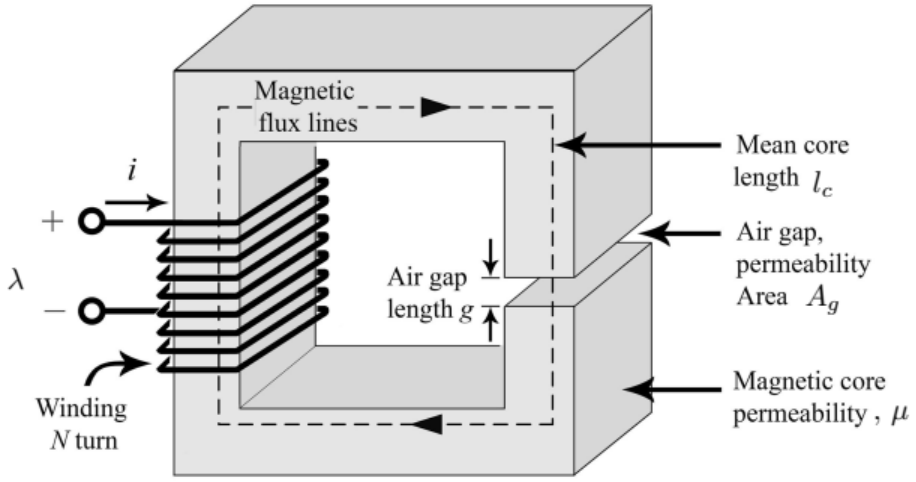

Figure 2. 2. Schematic view of a magnetic circuit with an airgap [9]

The magnetic circuit in this case has two reluctances, one for the core $\mathcal{R}_c$, and one for the air gap $\mathcal{R}_g$

$$\mathscr{R}_c = \frac{l_c}{\mu A_c} \tag{2.19}$$

$$\mathscr{R}_g = \frac{g}{\mu_0 A_g} \tag{2.20}$$

and the total flux is

$$\phi = \frac{\mathcal{F}}{\mathcal{R}_{total}} = \frac{\mathcal{F}}{\mathcal{R}_c + \mathcal{R}_g} = \frac{\mathcal{F}}{\frac{l_c}{\mu A_c} + \frac{g}{\mu_0 A_g}} \tag{2.21}$$

2.2.4 Leakage and fringing effect

In practice, all the flux produced by the *mmf* will not be formed in the core. There will be some flux lines which will complete their paths largely through the air gap, as depicted in Figure 2.3. Since the reluctance of air is higher compared to the reluctance of the core, the leakage flux produced is rather small.

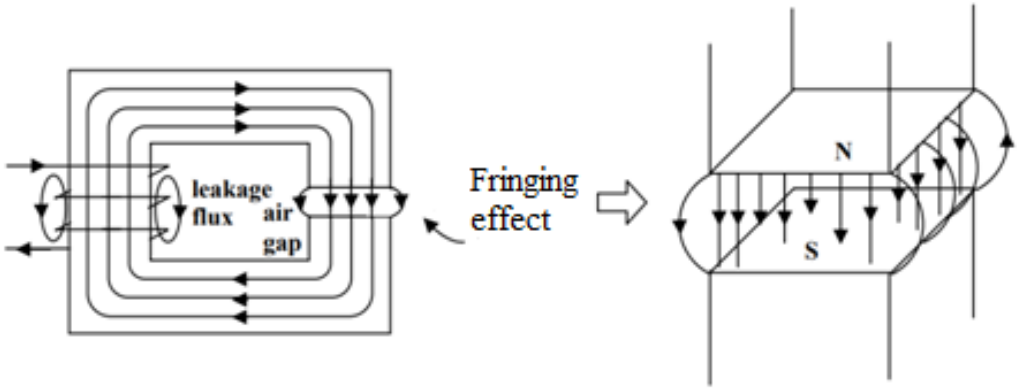

Figure 2. 3. Magnetic flux in core and fringing effect

For an exciting current, the flux lines produced are shown. These flux lines cross the air gap from the top surface to the bottom surface of the core. So, the upper surface behaves like a north pole and the bottom surface like a south pole. Thus, all the flux lines will not be vertical and confined to the core face area alone. Some lines of force in fact will reach the

bottom surface via the bulged out curved paths outside the face area of the core. The flux which follows these curved paths is called fringing flux and the phenomenon is called fringing effect. Obviously, the effect of fringing will be small if the air gap is small and conversely, it will be appreciable if the air gap length is large. In short, the effect of fringing is to make flux density in the air gap a bit less than in the core as in the air the same amount of flux is spread over an area which is greater than the core sectional area.

2.3 Magnetic field analysis

2.3.1 Reluctance network

Reluctance network is based on an equivalent magnetic circuit and used to solve magnetic flux problems. This method provides a simple formulation, even if the results are approximated; it provides an intuition to understand and significant insight into the system. For this reason, several researchers have tried to generalise this methodology to make it suitable for applications that require a better accuracy.

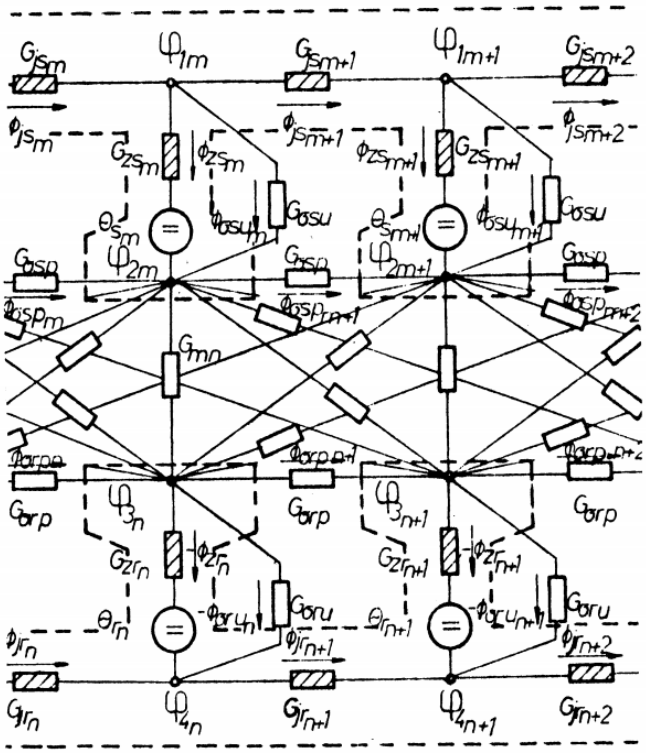

Figure 2. 4. Magnetic equivalent circuit of an induction motor [61].

Ostovic published some papers [61-63] to estimate different flux paths by equivalent magnetic circuit in the airgap to take into account fringing, inter-polar flux and leakage; then the problem is formulated as a system of matrix equations. Figure 2.4 illustrates the magnetic equivalent circuit of the airgap of an induction machine to show the complexity of this approach. The increased complexity of these reluctance networks provides more accurate results but on the other hand it makes the physical interpretation more difficult and therefore the insight provided into the system less straightforward.

Amrhein and Krein [64] developed this method into a general framework that can be used for 3D geometrical calculation with the idea of connecting component of the magnetic circuit by using nodes. Figure 2.5 shows an arbitrary 3D node with six branch reluctances. Obviously, the work by Amrhein and Krein brought several advantages of increasing computational accurate, but the high number of nodes offered a massive matrix that requires high computation in comparison with traditional analytical method.

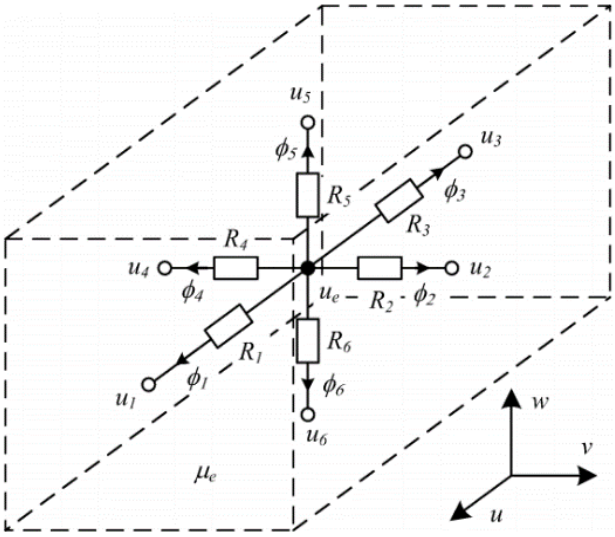

Figure 2. 5. A node with the reluctance branches and fluxes [63]

2.3.2 Finite element analysis

Finite Element Analysis (FEA) is a numerical method for solving problems of engineering and mathematical physics and it is useful for problems with complicated geometries, loadings, and material properties where analytical solutions cannot be obtained. Figure 2.6 shows the general process of finite element analysis [65].

This method was first presented in the 1970s by Chari and Silvester [66], since then it has become the most widely used computational method for electromagnetic field analysis for electric machines [67]. Due to the compatibility with the computational implementation several commercial software (like Ansys and Opera for example) and open-source software (like OpenFOAM and FEM) have been developed. This software uses very refined algorithms for the meshing and solving, and they are compatible with other CAD software for the design process making FEA a very powerful tool for both industry and academia.

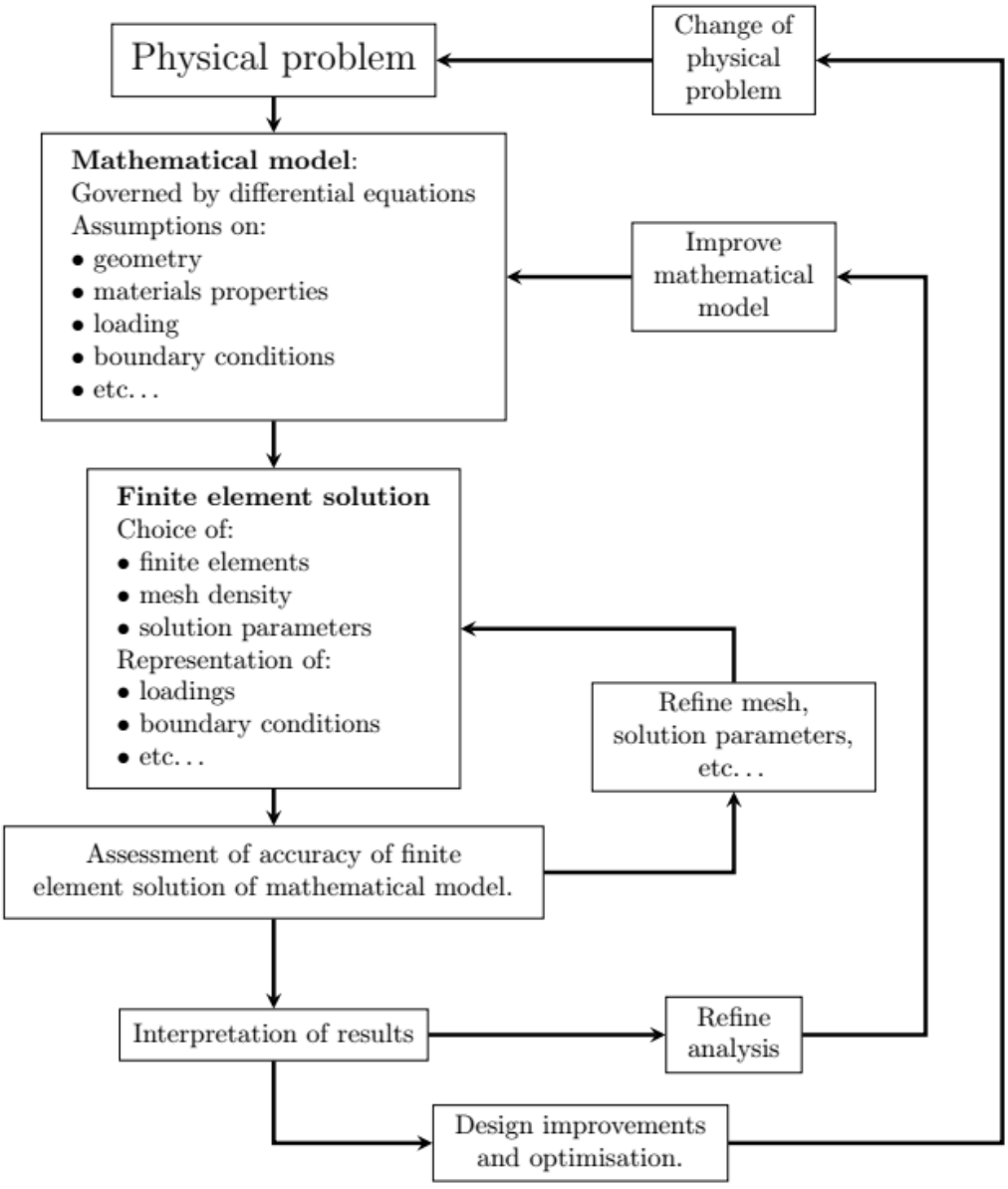

Figure 2. 6. The process of finite element analysis [65]

2.3.3 Calculation of the torque with FEA

Based on the magnetic field distribution in the airgap, the characteristics of a machine can be calculated under study like torque this is one of the most importance objective of the design process. Almost every FEA software uses the Maxwell Stress Tensor (MST) to calculate the torque (or force) in the electromagnetic analysis. It is very useful to derive the stress tensor by using expression of Kirtley [67].

The traction, τ, can be calculated as the cross product of the current (as a vector in 3D) and the flux density at any point. But there is other component of the traction that comes from the variation of the permeability. An empirical expression for the flux density using this idea according to Kirtley is as follows:

$$\vec{f} = \vec{J} \times \vec{B} - \frac{1}{2}(\vec{H} \cdot \vec{H})\nabla\mu \tag{2.22}$$

where $\vec{H}$ is the magnetic field intensity and μ is the permeability of the material at each point. As the current density is the curl of the magnetic field intensity so Eq. (2.22) can be rewritten as:

$$\vec{f} = (\nabla \times \vec{H}) \times \mu\vec{H} - \frac{1}{2}(\vec{H} \cdot \vec{H})\nabla\mu$$

$$\vec{f} = \mu(\nabla \times \vec{H}) \times \vec{H} - \frac{1}{2}(\vec{H} \cdot \vec{H})\nabla\mu$$

since

$$(\nabla \times \vec{H}) \times \vec{H} = (\vec{H} \cdot \nabla)\vec{H} - \frac{1}{2}(\vec{H} \cdot \vec{H})\nabla\mu$$

Then the force density can be written as:

$$\vec{f} = \mu(\nabla \times \vec{H})\vec{H} - \nabla\left(\frac{1}{2}\mu(\vec{H} \cdot \vec{H})\right) \tag{2.23}$$

If Eq. (2.23) applies for *k*'th component of the force density, is obtained as

$$\vec{f_k} = \frac{\partial}{\partial x_i}\mu H_i H_k - \frac{\mu}{2}\delta_{ik}\sum_k H_n^2 \tag{2.24}$$

where δ_{ik} is Kroneker's delta that is $\delta_{ik} = 1$ if $i = k$ and 0 otherwise. Instead of working with sums, the tensor *T* and density can be defined as the divergence of the tensor as

$$f_k = \frac{\partial}{\partial x_i} T_{ik}$$

For the three components we can use the vector operator:

$$\vec{f_k} = \nabla \cdot T \tag{2.25}$$

This deduction is valid for the context of a low frequency electromagnetic and it is based on Kirtley's analysis [67]. For a complete formulation it is necessary to include the Poynting vector, for more detailed analysis see reference [68].

Now let us apply this to the particular case we are interested in, an electric machine, in a Cartesian coordinate system. The coordinate system x, y and z, for an arbitrary point r = (x; y; z) at the instant of time *t* the MST, *T*, is the following:

$$T(\vec{r}, t) = \begin{bmatrix} T_{xx} & T_{xy} & T_{xz} \\ T_{yx} & T_{yy} & T_{yz} \\ T_{zx} & T_{zy} & T_{zz} \end{bmatrix} =$$

$$\begin{bmatrix} \frac{\mu_0}{2}\left(H_x^2 - H_y^2 - H_z^2\right) & \mu_0 H_x H_y & \mu_0 H_x H_z \\ \mu_0 H_y H_x & \frac{\mu_0}{2}\left(H_y^2 - H_x^2 - H_z^2\right) & \mu_0 H_y H_z \\ \mu_0 H_z H_x & \mu_0 H_z H_y & \frac{\mu_0}{2}\left(H_z^2 - H_x^2 - H_y^2\right) \end{bmatrix} \tag{2.26}$$

For example, if we want to calculate the force density in the *x* component:

$$f_x(\vec{r}, t) = \frac{\partial T_{xx}(\vec{r}, t)}{\partial x} + \frac{\partial T_{xy}(\vec{r}, t)}{\partial y} + \frac{\partial T_{xz}(\vec{r}, t)}{\partial z} \tag{2.27}$$

To obtain the total force for a solid object we can integrate this expression over a volume V:

$$\vec{F} = \iiint_V \vec{f} \cdot dv = \iiint_V \nabla \cdot T dv \tag{2.28}$$

If *S* is a closed surface that surrounds *V*, then Eq. (2.28) can apply the divergence theorem as following:

$$\vec{F} = \iiint_V \vec{f} \cdot dv = \oiint_S T \cdot d\vec{a} \tag{2.29}$$

It is important to recognise in Eq. (2.29) is that the total force that a body is induction that do not need to calculate the force density in all volume, but it is only necessary to know the MST, or what is the same: the field intensity, over a surface that surround this body.

If the method applies to a two-dimensional model of a rotating electric machine in order to calculate the torque produced using the MST. The traction in the tangential direction $\boldsymbol{\tau}_\theta$ is obtained as follows:

$$\tau_\theta = \mu_0 H_r H_\theta$$

If the length of the machine is *L* and *Γ* is a closed path in the air-gap, then the total tangential force is the following:

$$F_\theta = \oint_\Gamma \tau_\theta \, L d\ell = \oint_\Gamma \mu_0 H_r H_\theta d\ell$$

so the torque:

$$T = F_\theta \cdot r = Lr \oint_\Gamma \mu_0 H_r H_\theta d\ell \tag{2.30}$$

Observing throughout this section has been proved that FEA provides a powerful tool to investigate the electromagnetic behaviour of electric machines. Also, it has increased the accuracy solution by applying refined algorithms for meshing. The combination of FEA with MST provides an immediate result in calculating the torques and forces. The actual trend in the design of magnetic machines is dominated by FEA. The typical procedure is: idea of a concept machine, parametrisation of the geometry, FEA calculation of the field and optimisation. For this reason, the aim of this project is to work with FEA that investigates the proposed magnetic gear that is mentioned in chapter 1.

2.4 Magnetic materials

A magnetic material is identified and characterised by its B – H characteristic. A typical hysteresis loop of a magnetic material is presented in Figure 2.7. When a high magnetising force occurs, a point is reached where further increase in H, does not cause useful increase in, B. This point is known as the saturation point of that material. The saturation flux density, B_s, and the required magnetising force, H_s, to saturate the core are shown with dashed lines.

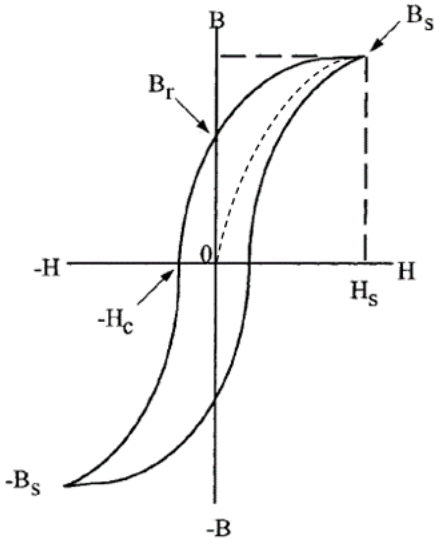

Figure 2. 7. Typical B-H or Hysteresis loop of a soft magnetic material [69].

In free space or in air the relationship between B and H is linear and the constant of proportionality is the permeability μ_0. However, the relationship between B and H is not linear, as shown in the hysteresis loop in Figure 2.7. The permeability of a magnetic material is a measure of the ease in magnetising the material. Permeability, μ, is the ratio of the flux density, B, to the magnetising force, H. It is evident that the ratio, B/H, (permeability), also varies. The variation of permeability with flux density, B, is shown in Figure 2.8. Also, it shows the flux density at which the permeability is at a maximum.

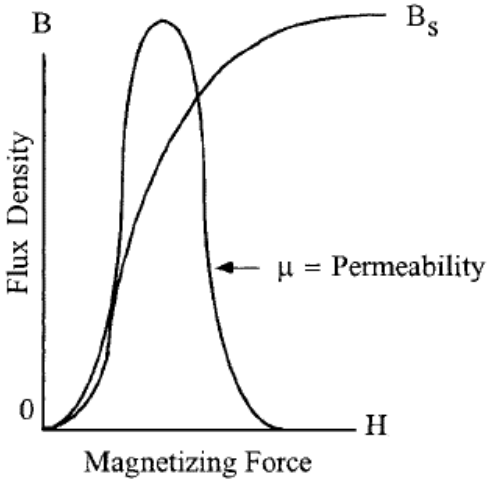

Figure 2. 8. Variation in permeability μ with B and H [69].

The enclosed area within the hysteresis, shown in Figure 2.7, is a measure of the energy lost in the core material during that cycle. This loss is made up in two components: (1) the hysteresis loss and (2) eddy current loss. The hysteresis loss is the energy loss when the magnetic material is going through a cycling state. The eddy current loss is caused when the lines of flux pass through the core, inducing electrical currents in it. These currents are called eddy currents and produce heat in the core. If the electrical resistance of the core is high, the current will be low; therefore, a feature of low-loss material is high electrical resistance. In the norm, when designing magnetic components, the core loss is a major design factor. Core loss can be controlled by selecting the right material and thickness. Selecting the correct material, and operating within its limits, will prevent overheating that could result in damage to the wire insulation and/or the potting compound.

2.5 Summary

In this chapter, basic magnetic field theory and the different methods of magnetic field analysis are reviewed. Basically, analytical methods are intensively used for general purpose to provide an insight and exact solution, but it is extremely difficult to apply in the complicated models. In contrast, FEA method is very accurate and easily implemented in the design process due to the capacity of current numerical software. Therefore, the main work on this thesis will apply FEA throughout to investigate the proposed magnetic gear that was introduced in previous chapter.

Chapter 3 A linear to rotary magnetic gear

This chapter presents a novel magnetic gear whose principle of operation is derived from that of the transverse-flux machine. Practical configurations are developed and discussed and finite element analysis (FEA) is used to obtain the characteristics of a magnetic gear. Furthermore, components structure of the proposed magnetic gear such as the outer core-back and ferromagnetic pole pieces are examined and discussed. Also, a comparative design between the proposed magnetic gear and a helical magnetic gear, with similar geometric parameters is carried out. In addition, a magnetic gear with different pole arrangement is derived from the proposed magnetic gear's structure to compare with a different screw magnetic gear. Finally, a summary is presented to highlight key points of the chapter.

3.1 Structure of a magnetic gear

3.1.1 Topology development

As described earlier in the introduction (chapter 1), the idea of a magnetic gear can be achieved by traversing from a transverse flux machine. Figure 3.1 shows an illustration of the construction of an inner rotor version of a two-phase transverse flux machine as reported in [70-72]. The housing is removed and not all the C-cores are shown. The rotor has four rows of heteropolar magnets. Each stator phase coil is enclosed within an array of laminated C-cores; the number of C-cores per phase equals half the number of rotor PM poles. In this version of the machine, the magnets of the two phases are aligned, but their respective C-cores are shifted by 90 electrical degrees. This means that when vector control is used in the maximum torque per ampere mode, the current in phase two will be maximum and the current in phase one will be zero [73].

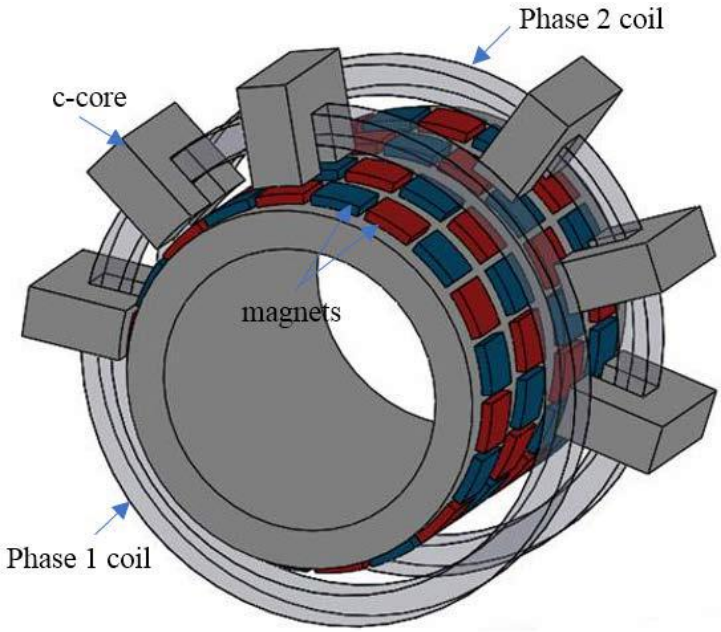

Figure 3. 1. An illustration of a two-phase outer rotor VRPM machine showing a partial number of C-cores for clarity. The stator housing that holds the C-cores is not shown.

In order to better understand how the transverse flux machine can be transferred to a magnetic gear, a two-pole version of the machine is depicted in Figure 3.2. This in fact shows a poor utilisation of magnet material, which can be improved by increasing the number of poles. It must be remembered that the current of each phase will be shifted by 90 electrical degrees with respect to another. The alternating current in the coils generates an alternating magnetic field in the air-gap opposite the C-cores, which has maximum strength when the C-cores are unaligned with rotor's magnets.

Now imagine that the C-cores are cut to become I-cores and the coils are replaced by arrays of hetero-polar magnets (the so-called translators) moving over the outer end of the I-cores, as shown in Figure 3.3. As the magnets move in the axial direction, alternating flux will travel through the corresponding airgaps. Once the arrangement of phase 1 magnet array corresponding to the I-core and phase 2 are shifted spatially by 90 electrical degrees in axial direction, then the flux pattern will be immediately the same as that produced by the two-phase coils. Consequently, rotor movement will be achieved by the linear movement of the array's magnets, i.e., the so-called linear-to-rotary magnetic gear [74].

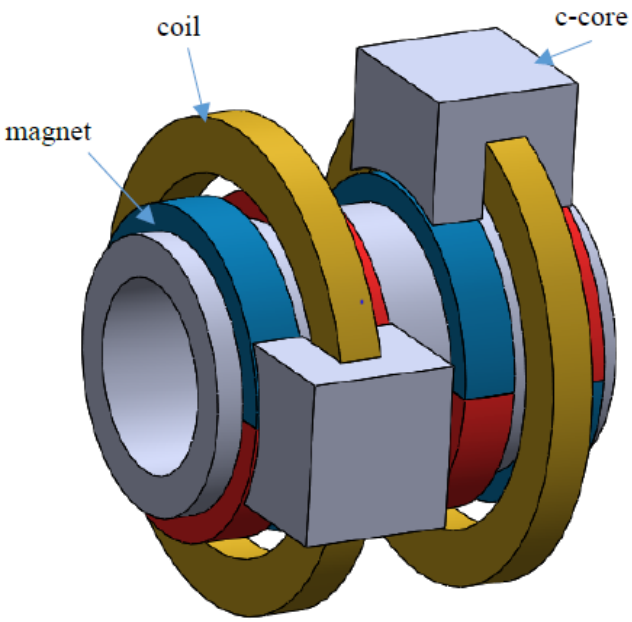

Figure 3. 2. A 2-pole variant of the transverse flux machine.

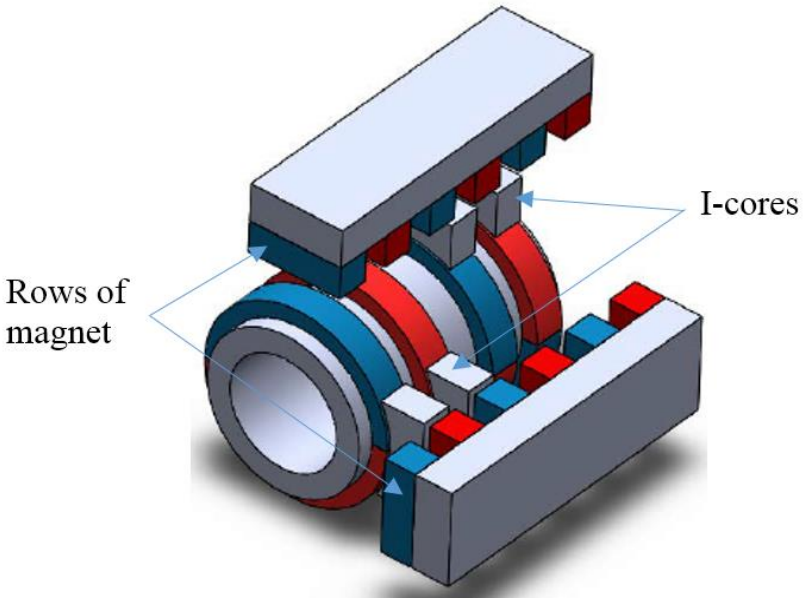

Figure 3. 3. A linear-to-rotary magnetic gear derived from the 2-pole transverse flux machine.

As well known, the coils in the transverse flux machine, generate a homo-polar flux in all C-cores surrounding them, however, the magnets generate flux in each set of I-cores

independently. From this viewpoint, another set of I-cores can be added on the opposite side of each phase with their flux provided by an array of magnets that are shifted by 180 electrical degrees. It must be remembered that the I-cores of both phases are put in the same plane and interacted with the same rotor, as depicted in Figure 3.4. Consequently, we can duplicate the structure in the axial direction as much as required of the torque that the rotor would produce. However, increasing the number of I-cores essentially increases the cogging torque and reduces stiffness.

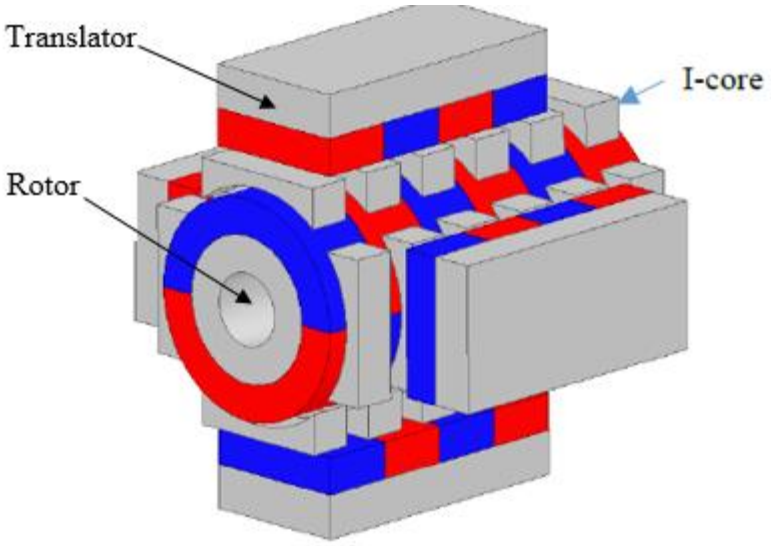

Figure 3. 4. The final topology of the linear-to-rotary magnetic gear derived from a 2-pole VRPM machine.

Considering the interaction between the magnets in Figure 3.5, it becomes evident that the I-cores are not actually essential to the operation of this configuration. They can be advantageously removed to eliminate the associate core loss and replace the two gaps with one, which increases the flux, force and torque. However, as using the bar magnets on the arrays, the I-cores are needed to interface the rectangular geometry of the translators to the cylindrical rotor. One can also envisage a cylindrical version of the machine as also shown in Figure 3.5, although the arc magnets on the translators are expected to be more expensive. It is obvious that this configuration allows a better interaction between the magnets on the translators and the rotor. This mean, we can remove the I-cores to increase characteristics as mentioned it replaces two gaps with one.

In terms of transmission, either the translator or the rotor can be used as the driving part. In other words, this mechanism can be use in both motoring and generating applications. As the driving rotor, for example, we can use a motor to couple to the rotor's shaft to generate linear movement of the translator. Otherwise, if the translator is used as a driving port, e.g., in case of connecting with an oscillating system, then the translator reciprocates and causes the rotor to rotate which can in turn drive a rotary generator for example.

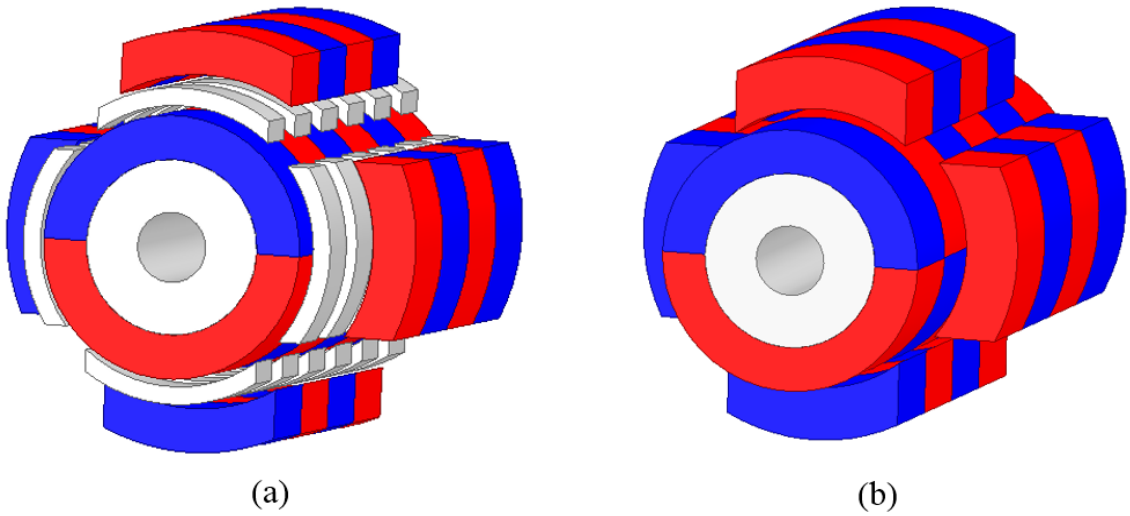

Figure 3. 5. The cylindrical topology: a) with I-cores b) without I-cores

In an actual design, either the rotor or the translator needs to be longer than the other one so that the magnets of the rotor and translator keep engaging as they move. Length of the shorter part is referred to as the active length, while the longer part is seen as the stroke length. The design aspect of the stroke length will be considered in the next chapter.

It is interesting to consider a basic unrolled system that consists of two simple rows of magnets on the rotor in Figure 3.6, without the I-cores and the core-backs. This reveals that the gear is equivalent to a discrete helical gear.

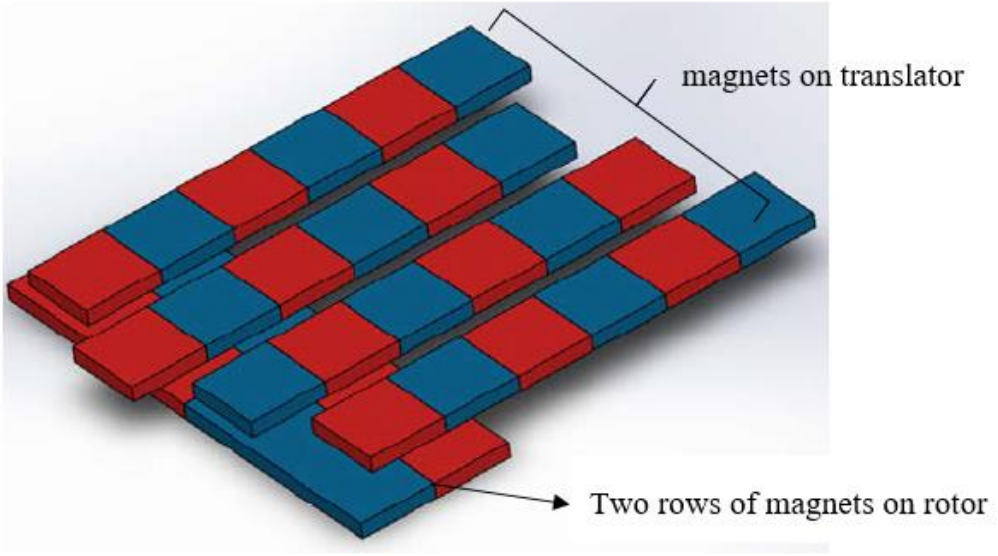

Figure 3. 6. Unrolled cylindrical magnetic gear without I-cores.

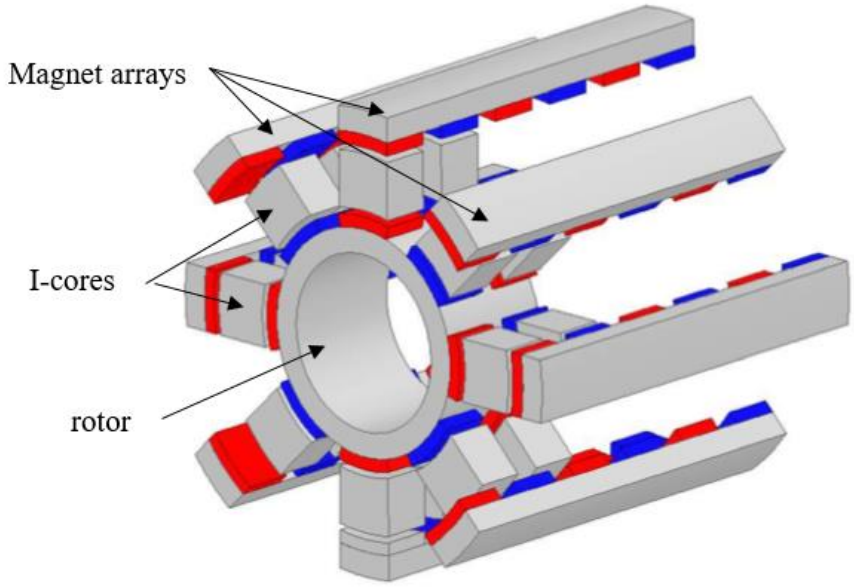

Figure 3. 7. A rotary-to-linear magnetic gear with 8 peripheral rotor poles.

Furthermore, we can also envisage having a rotor with multi-peripheral poles. In this case, the translator magnet arrays will form a polygon whose number of sides equals to the number of peripheral rotor poles as shown in Figure 3.7. The greater the number of peripheral poles, the closer the approximation to a helical disposition of the I-cores and magnets which,

based on the results reported in [55], will increase pull-out torque and improves the linearity of the relationship between torque and force, i.e., reduces the dependence of the gear ratio on the load.

3.1.2 Gear ratio

The speed of rotor is associated with the number of poles on the rotor in radial direction. If the number of poles on the rotor is decreased, speed of the rotor will increase. In other words, the number of poles on the rotor should be decreased to the smallest option, i.e., two poles in reality to get the highest rotor speed. In this configuration, two poles of the magnetic gear are designed, and its basic parameters are shows in Figure 3.8.

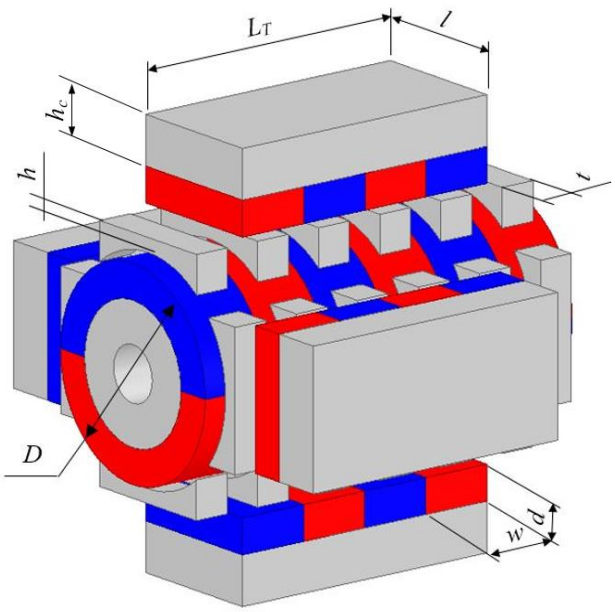

Figure 3. 8. A two-phase magnetic gear

Description	**Symbol** *(mm)*
Magnet width	*w*
Pole pitch	*λ (=w)*
Magnet thickness	*d*
I-core height	*h*
I-core width	*t*
Core-back width	*l*
Core-backs thickness	h_c
Air gap length	*g*
Active length	L_T
Rotor diameter	*D*

Table 2: Parameters description

Intuitively, when the translator moves one pole pitch, the rotor also rotates one pole pitch. This mean that the translator moves two pole pitches as the result of the rotor rotating a full turn. Consequently, having narrower pole pitch will result in higher angular velocity of the

rotor. If speed of the translator moves V meters per second. The rotor speed in term of revolution per second would be

$$n = \frac{V}{P\lambda} \tag{3.1}$$

where *P* are the number of poles on the rotor. The magnet width, *w*, is assumed to be at full pole pitch, λ (λ = *w*). The gear ratio is defined as the ratio of the rotor angular speed, (rad/s), to the translator linear speed, V (m/s), which is not a dimensionless quantity and is obtained by

$$G = \frac{\omega}{V} = \frac{2\pi}{P\lambda} \tag{3.2}$$

It is acceptable from Eq. (3.2) that two factors affect the gear ratio, namely the number of poles on the rotor and the translator's pole pitch. Obviously, the lower the number of poles and the narrower the magnets, a higher gear ratio can be obtained. It is observed that the magnet on the translator form a discretised helix. Furthermore, the derived Eq. (3.2) is similar to that described by Pakdelian [54] and [55]. It means that its performance is likely to be similar to the operation principles of a helical structure.

If we ignore power loss, the relationship in terms of movement powers of the rotor and translator can be expressed as

$$P_t = P_r \Longrightarrow F_t V = T_r \omega \Longrightarrow \frac{F_t}{T_r} = \frac{\omega}{V} = \frac{2\pi}{P\lambda} = G \tag{3.3}$$

where P_t and P_r are the power of the translator and the rotor, respectively. The relationship between the power of the machine will be considered in detail and also compared with the three-dimensional finite element analysis in the next section.

3.1.3 Force and torque characteristics

To investigate the performance of the magnetic gear, magneto-static modelling is carried out through three-dimensional finite element analysis. Figure 3.9 shows the structure of two

models, in which rectangular and arc magnet models are considered. They consist of three main parts: translators, rotor and I-cores (ferromagnetic pole pieces).

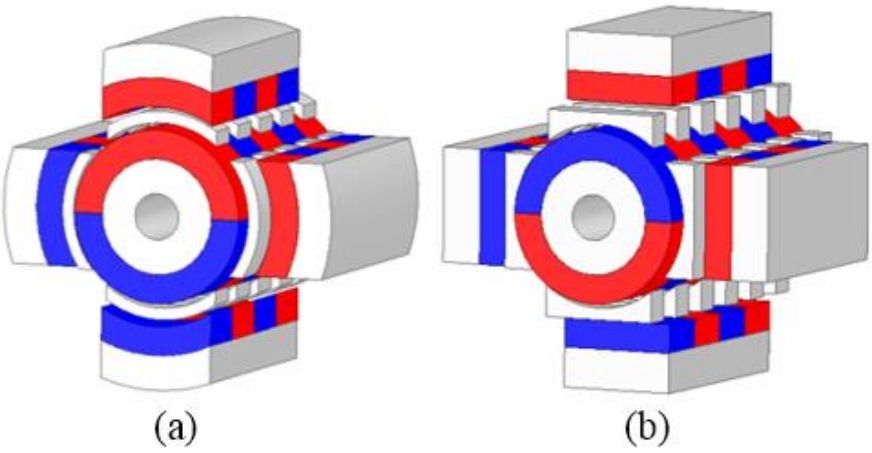

Figure 3. 9 Magnetic gear configurations: (a) arc segment magnets; (b) rectangular magnets.

The translators made up of rows of the rectangular magnets accompanied with the core-backs. There are four poles pitch on the translator that serves as an active length. The rotor consists of 180degree arc segment magnets embedded on a rounded core-back. A high-density force of NdFeB35 magnets are used. To enable high-speed operation, the I-cores need to be laminated and separated by a non-conducting material, but in the FEA model they were made of mild steel 1008. The rotor and translator's core-back were also made of steel 1008. Airgap length of the I-cores and others between phases must be large enough to reduce the leakage flux that occurs. This problem will be considered in the forthcoming optimising design chapter. ANSYS Electronic desktop software is used for the analysis. B-H curve characteristics of the steel and magnet materials are shown in Figure 3.10 and Figure 3.11, respectively.

To obtain static torque and force curve values, the translator and I-cores are held stationary, the rotor is rotated on its radial axis by 360 electrical degrees (which corresponds to 360 mechanical degrees rotation). Position of phase one is aligned with the magnets on the rotor and obviously unaligned for phase two. This is also the starting angle position (zero degree) of the rotor. The dimensional parameters are given in Table 3.

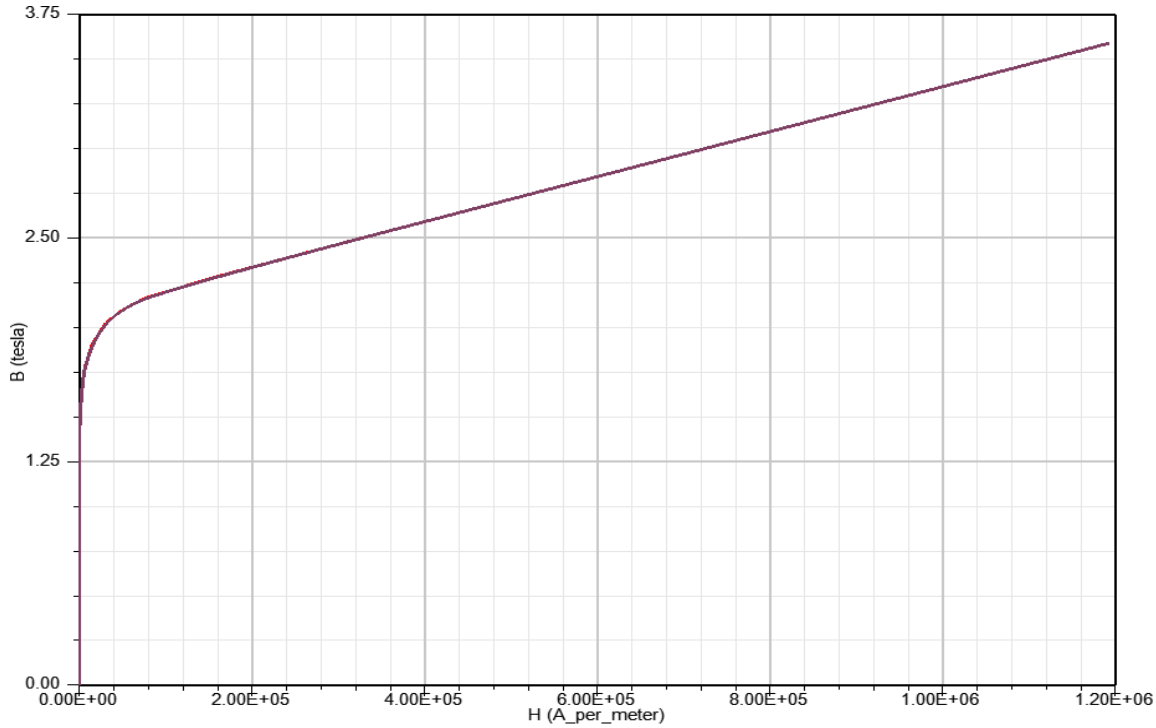

Figure 3. 10**.** B-H curve of the steel_1008 material

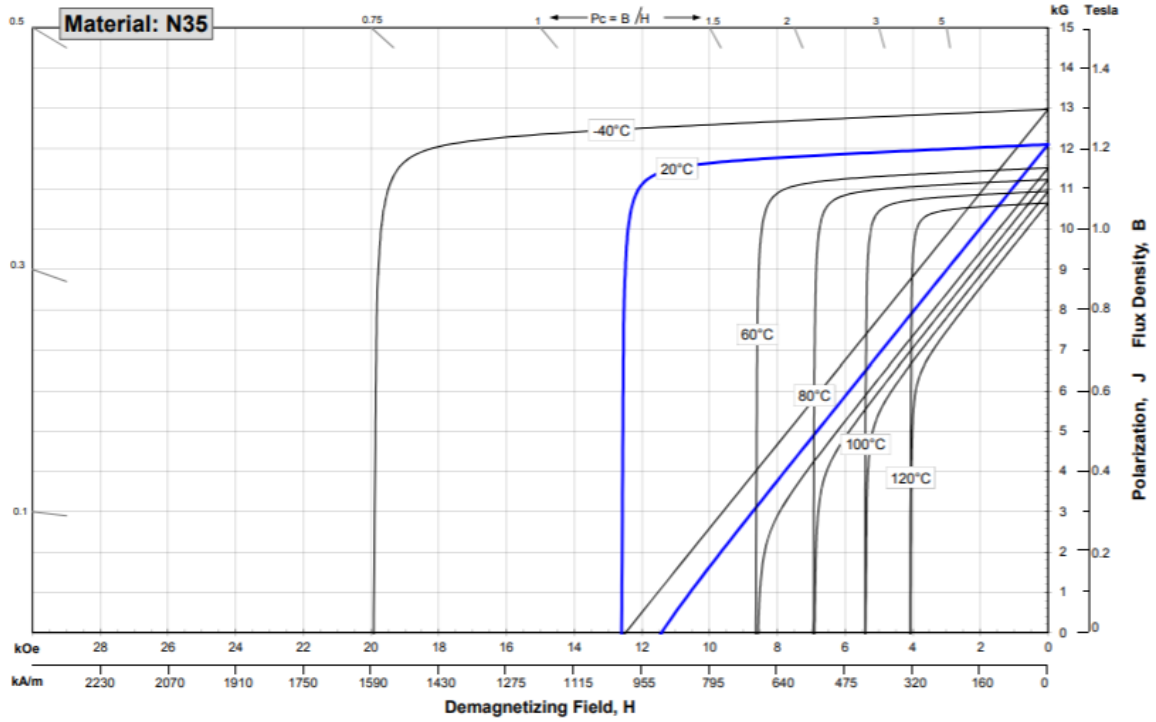

Figure 3. 11. B-H curve of NdFe35 permanent magnet material [75]

Table 3: Simulated design parameters

Parameters	**Symbol**	**Value (mm)**
Pole pitch	λ	10
Magnet thickness	d	5
I-core height	h	2
I-core length	l	20
I-core thickness	t	6
Inner and outer core-backs thickness	h_c	8
Air gap length	g	1
Translator length	L_T	40
Rotor length	L_R	80
Rotor diameter	D	30
Magnet coercivity (kA/m)	H_c	890
Magnet remanent flux density (T)	B_r	1.23
Steel 1008 resistivity (μOhm-cm)		14.2

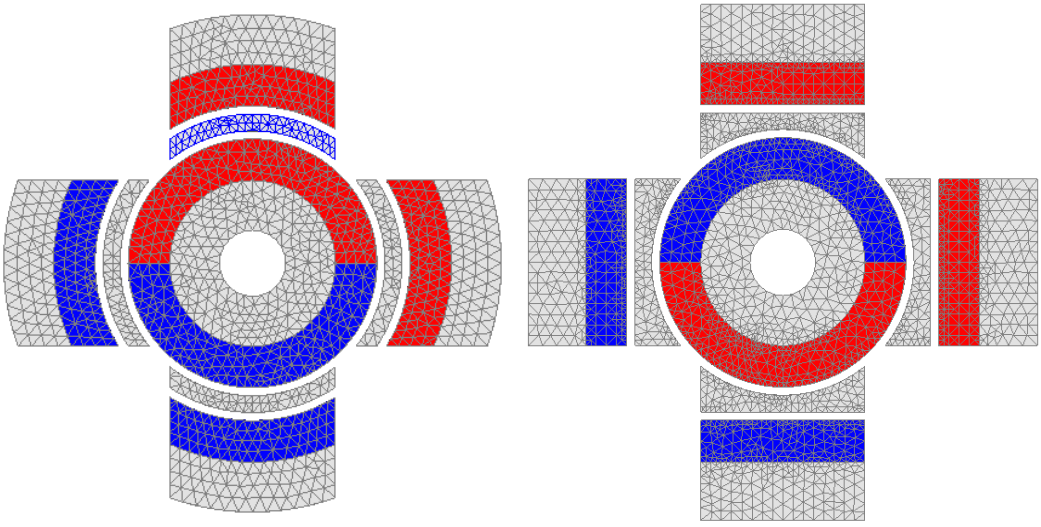

Figure 3. 12. Meshing models in ANSYS Electronics desktop

Figure 3.13 and Figure 3.14 show the flux distribution in vector and spectrum of two different planes at zero degree and 90 degrees, respectively. When the rotor is at 0 degree, either phase one or phase two is aligned with the rotor magnets, they generate a zero torque and force, or in other words, the rotor is at the rest state. It also can be seen that the flux distribution in the I-cores in the axial direction is uniform.

Nonetheless, when the rotor is rotated by 90 degrees in the clockwise, maximum torque and force values are achieved. The peak values of the torque and force profiles can then be analogously called pull-out torque and pull-out force. It is obserbed in Figure 3.14 that saturation occurred in the I-cores.

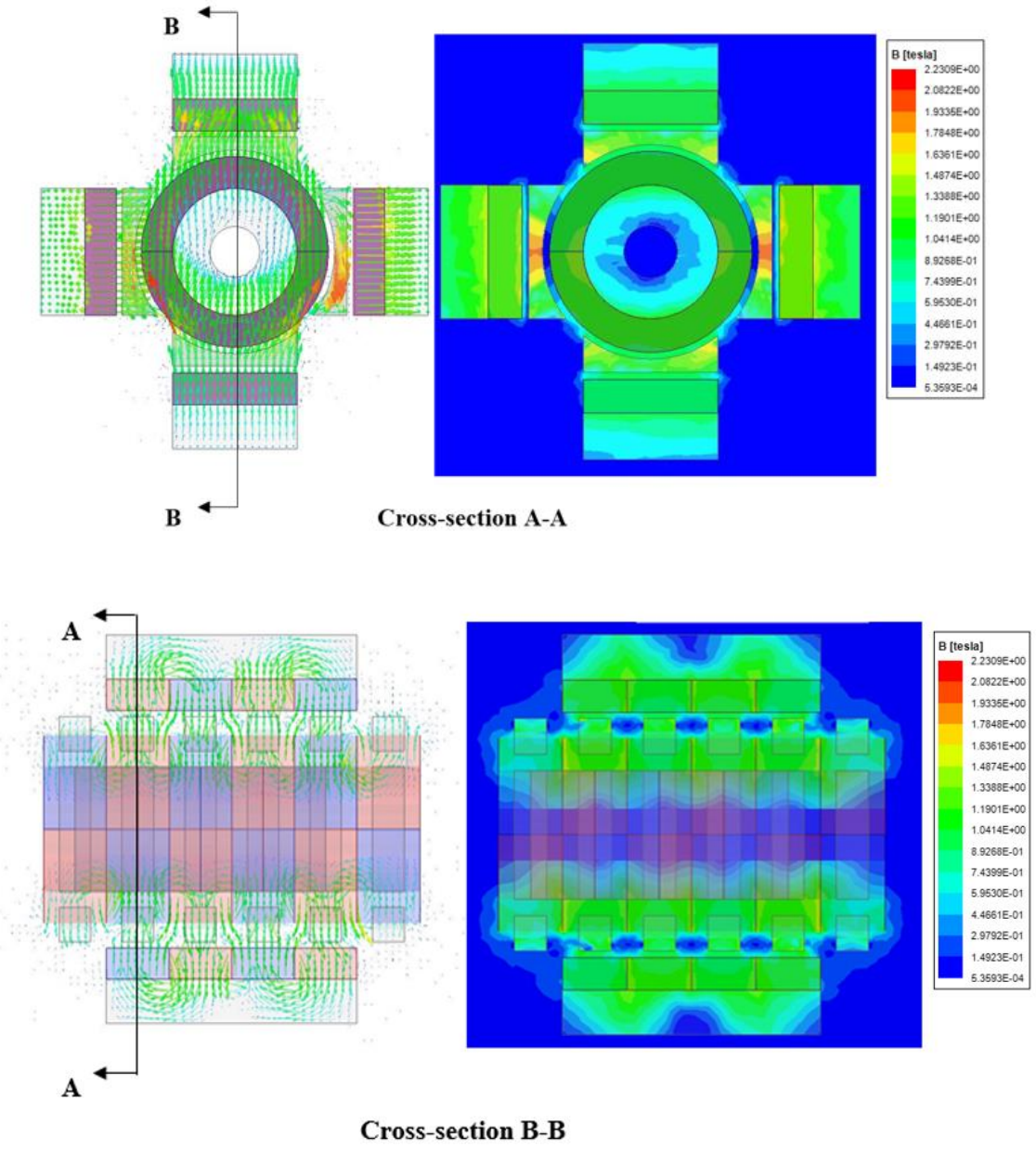

Figure 3. 13. Flux distribution in vector and spectrum at 0 degree of the rotor position

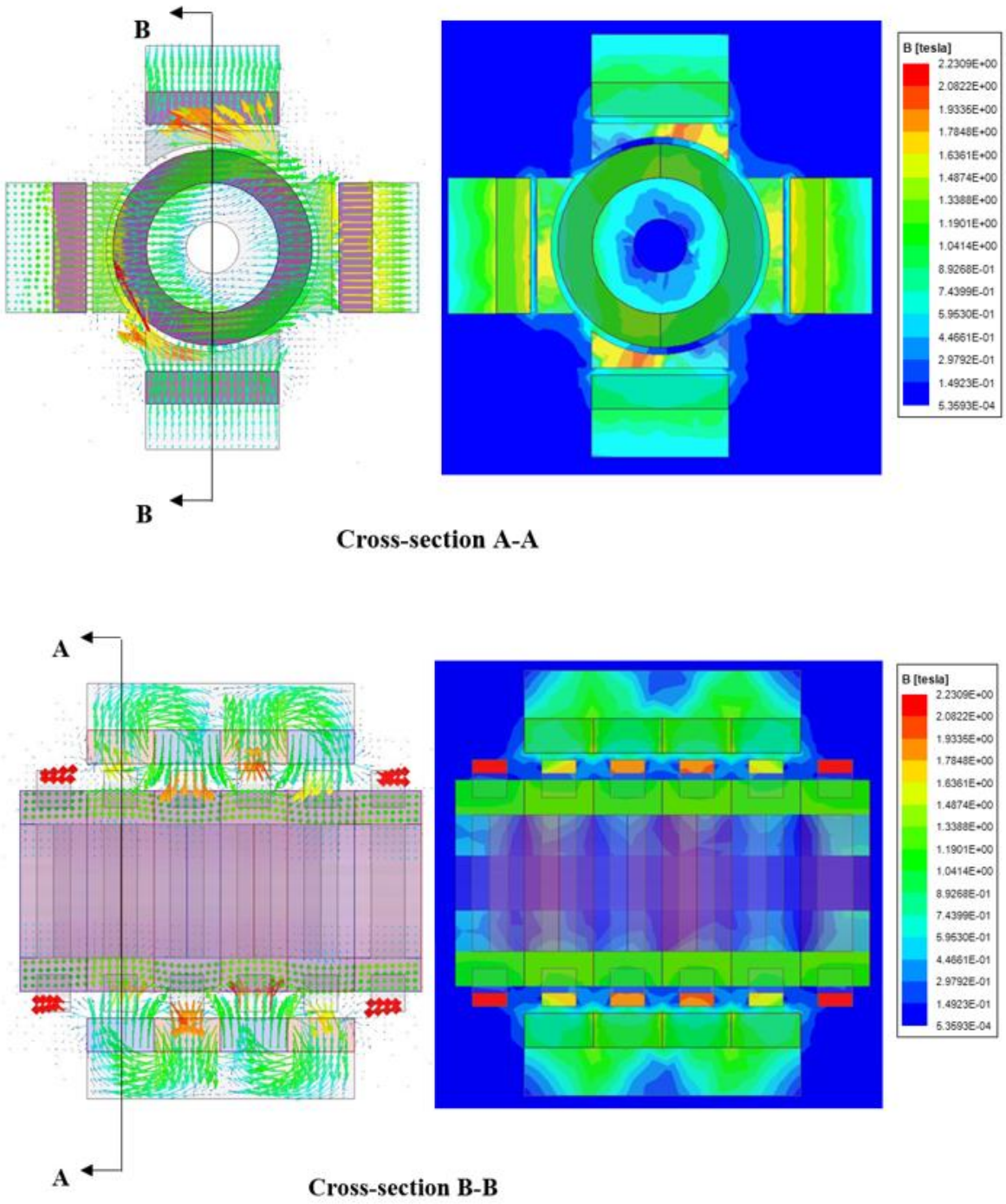

Figure 3. 14. Flux distribution in vector and spectrum at 90 degrees of the rotor position

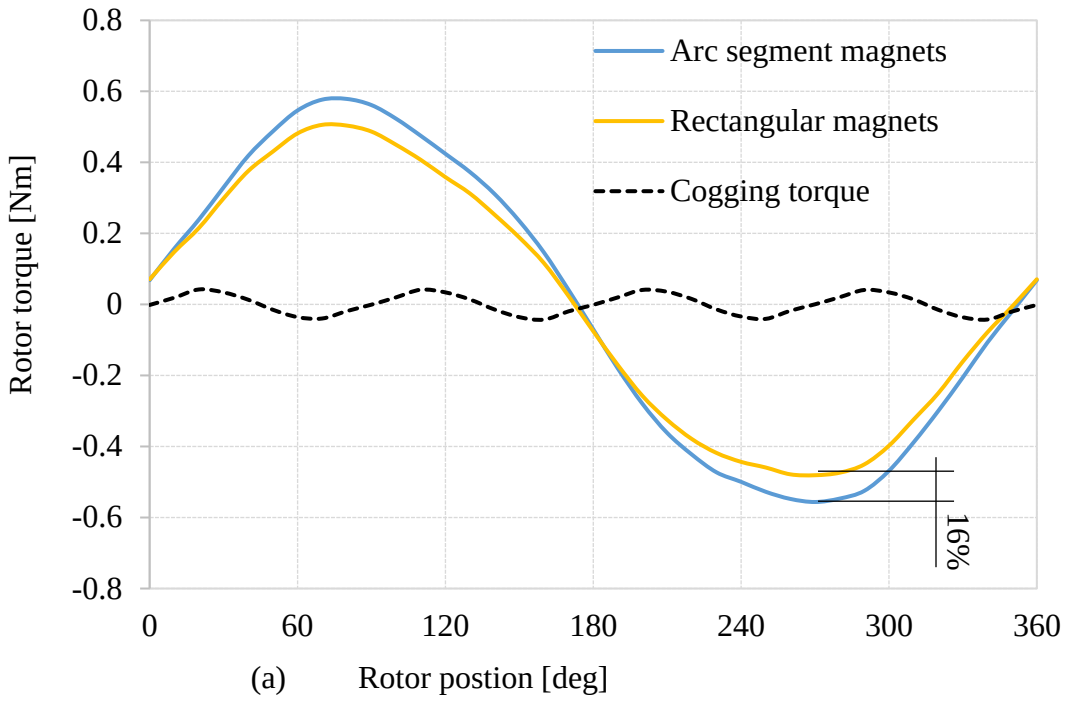

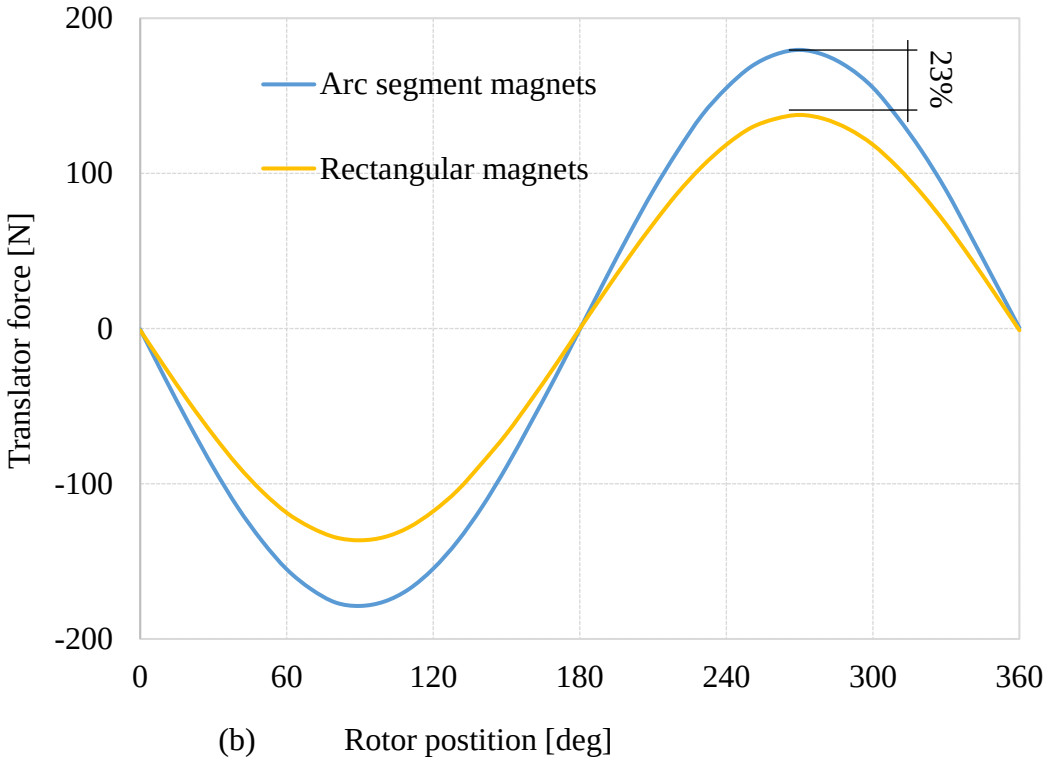

Figure 3. 15. Characteristics of the magnetic gears: (a) rotor torque; and (b) translator force.

The static characteristic results are given in Figure 3.15 from which several conclusions can be drawn, as follow:

- The torque peaks at 70 degrees not at 90 degrees, as expected, which is due to a combination of saturation of the I-cores and cogging torque. The force peaks at nearly 90 degrees.
- The model with arc magnet has higher torque than the rectangular one, i.e., 0.58 Nm and 0.52 Nm respectively.
- Cogging torque can be obtained by removing the translator. The I-cores are kept stationary, then the rotor rotates around its axial axis. The cogging torque is 8% of the rated torque.

Table 4: Gear ratio comparison between FEA and analytical caculations

Pole pitch λ (mm)	Rotor torque - FEA (Nm)	Translator force - FEA (kN)	Gear ratio	
			FEA $\left(\frac{F_t}{T_r}\right)$	Eq. (3.3) $\left(\frac{2\pi}{P\lambda}\right)$
10	3.9	0.963	289	314
12	4.3	1.1	247	262
15	6.64	1.34	198	209
20	10.14	1.5	148	157
30	15.1	1.45	96	105
40	17.38	1.23	70	79
60	20.25	0.898	44	52

To compare gear ratios between FEA and analytical calculations, a 3D-FEA model is simulated with a constant active length, then the pole pitch is changed to obtain torque and force characteristics. In order to modify the pole pitch, the active length is given at 120mm, and the rotor's radius is at 50mm. It is assumed that there is no saturation in the core-back. From FEA results, gear ratio can be obtained with different pole pitches and gear ratio is also calculated from Eq. (3.3), as given in Table 4. It is observed that the gear ratios obtained from

Eq. (3.3) give a higher value at the same pole pitch. This may be explained by the power losses that are calculated in the FEA simulations while the analytical calculations ignored this factor.

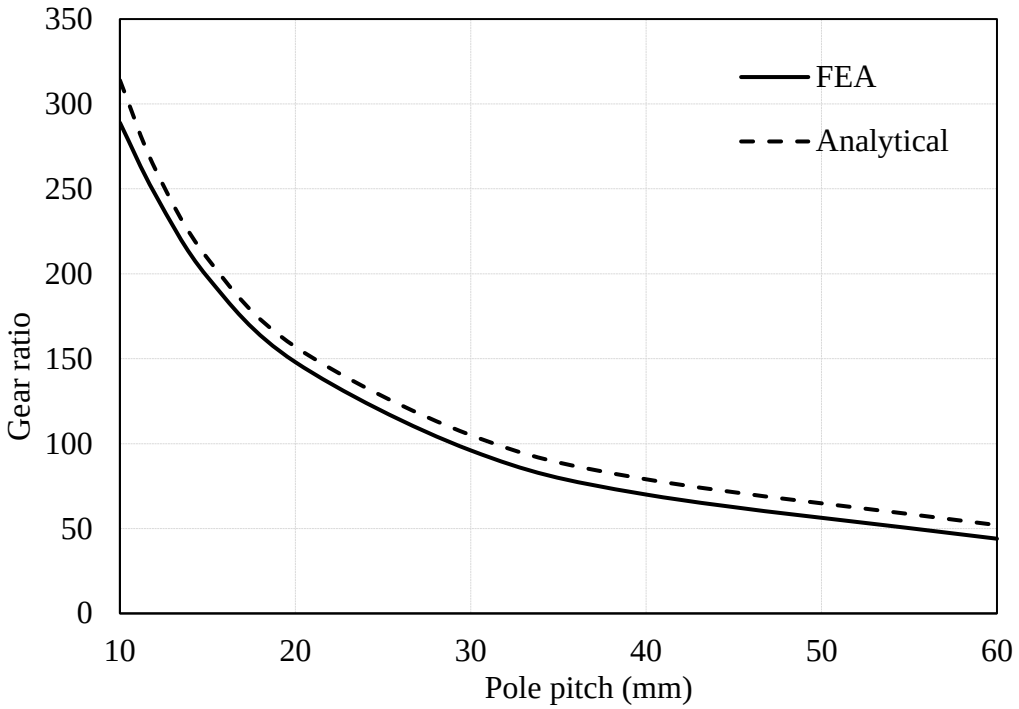

Figure 3. 16. Gear ratio vs pole pitch for FEA and analytical methods

3.2 Topology modification

In this section, few modified versions of the outer core-backs and I-cores (ferromagnetic pole-pieces) are considered. In previous analyses, the outer core-backs were separated in each magnet rows on the translator. This structure requires a simple process of fabrication and assembly. Similarly, I-cores are placed as a single piece and arranged into four rows with their positions corresponding to the magnet poles on the rotor. The purpose of these arrangements is to reduce flux leakage of a phase to another one on the translator.

3.3.1. Core-back combination

It is assumed that the core-backs are made sufficiently thick so as to avoid saturation. However, effect of outer core-back on flux leakage problem influences the characteristics.

Figure 3.16 shows two options for the outer core-backs and their isometric views: a version with outer core-backs combination and a separated one. In this analysis, a magnet arc segment is utilised on the translator, as a result, the geometry of the ferromagnetic pole-pieces is formed as arc segments. The aim of this comparison is to obtain an appropriate possible topology rather than implementing an optimal design.

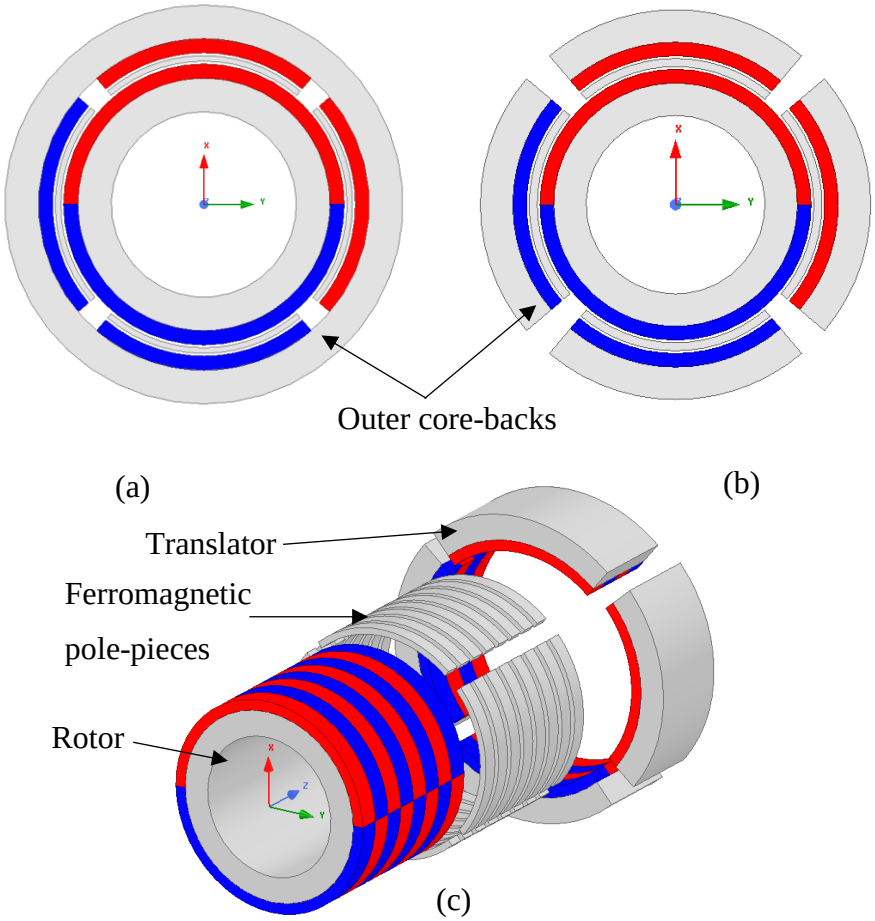

Figure 3. 17**.** A magnetic gear: (a) single core-back, (b) separated core-back, and (c) isometric break out view.

Three-dimensional analyses in Ansys are carried out to compare their torque and force characteristics. Figure 3.17 shows torque and force characteristics when using parameters in Table 3.2. It is observed that there are small errors in the amount of values of force and torque in two versions. Thus, both combined and separated core-backs give reliable results.

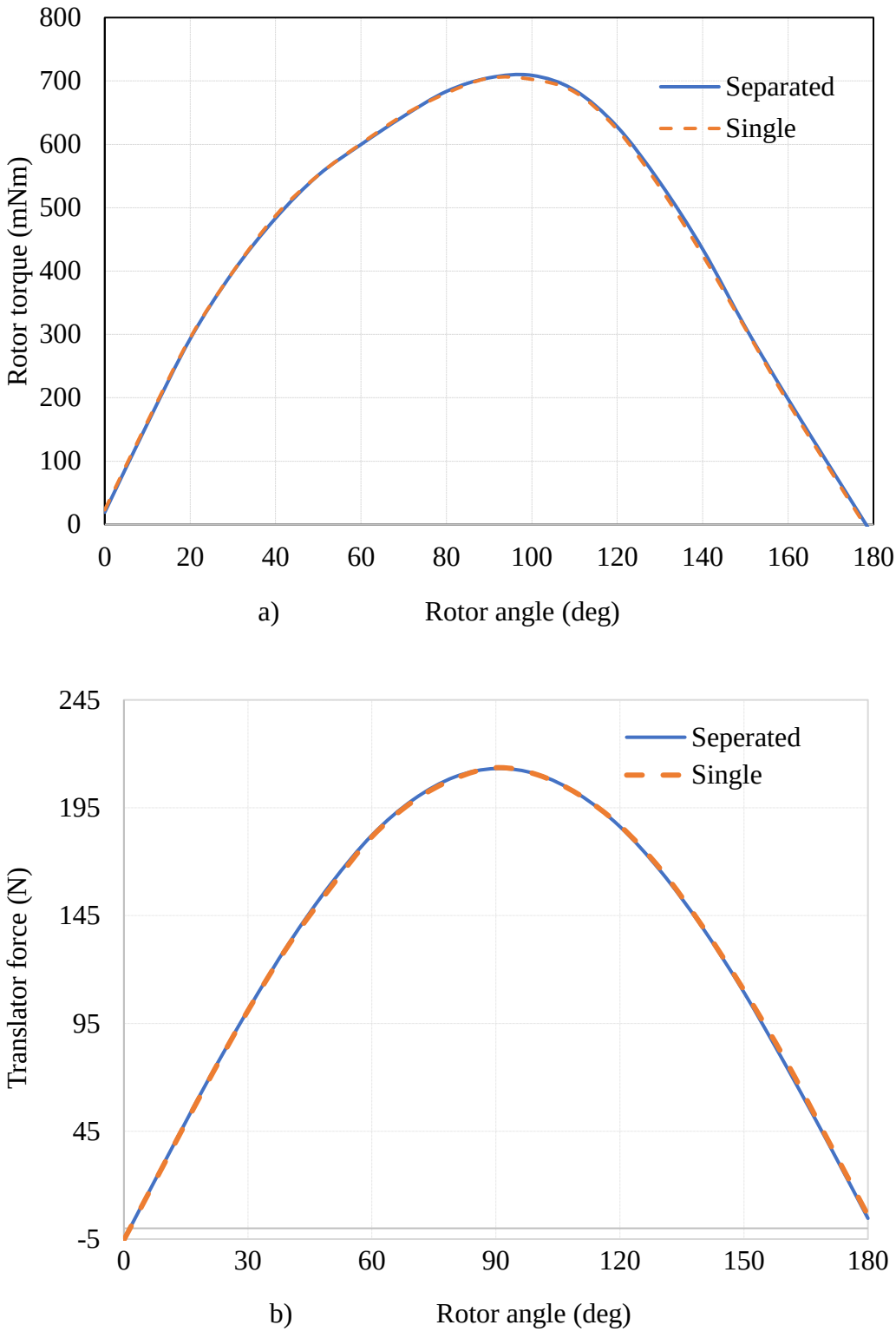

Figure 3. 18**.** Torque and force characteristics of the separated and single outer core-back: a) rotor torque; b) translator force.

3.3.2. United ferromagnetic pole-pieces

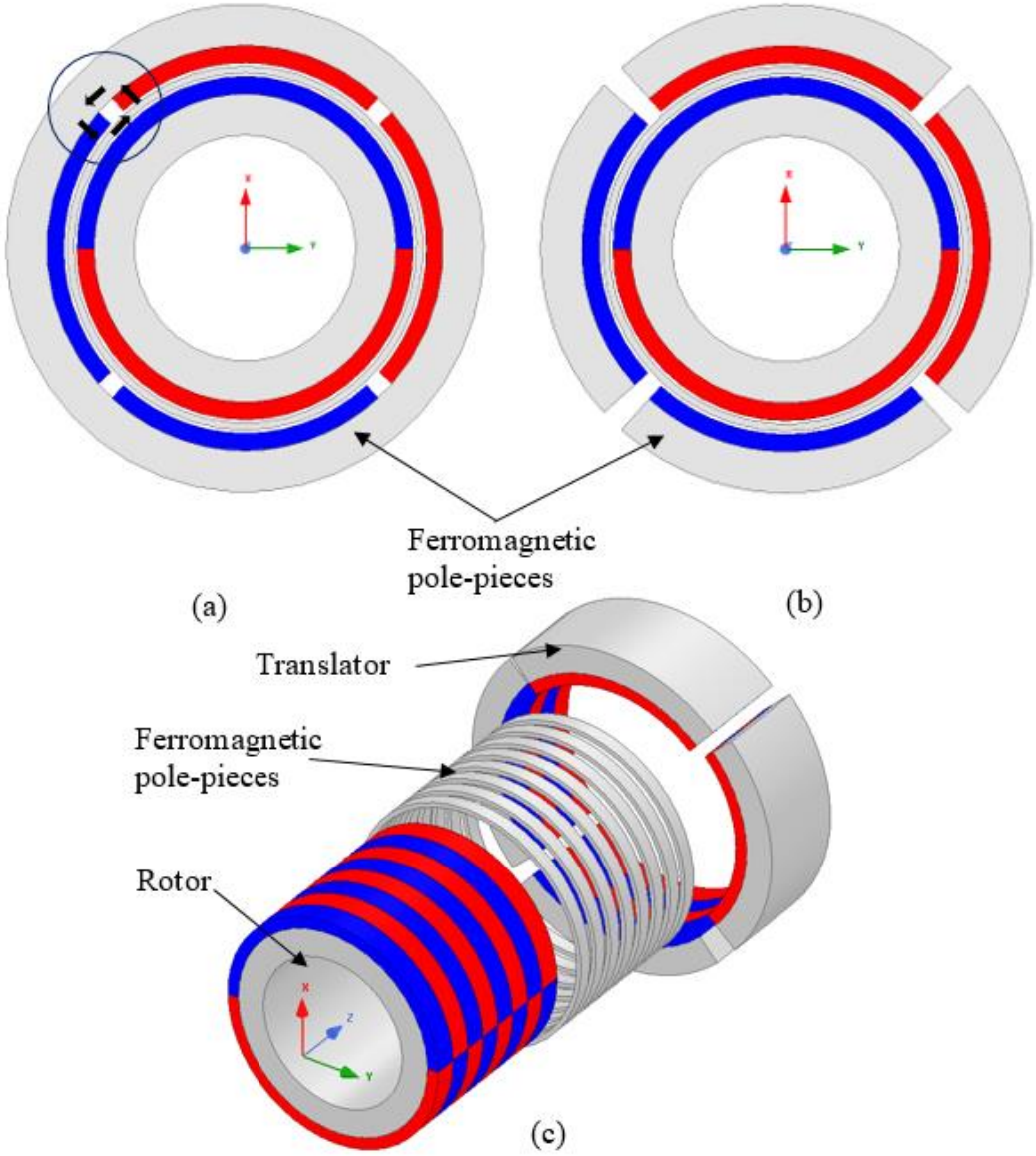

Figure 3. 19. Magnetic gears with single ferromagnetic pole-pieces: (a) single core-back and, (b) separated core-back, and (c) isometric break out view of (b).

Another option for a topology is the ferromagnetic pole-piece being continuous as a single circular part around the rotor. Figure 3.19 (a) combines both single core-back and ferromagnetic pole-pieces while Figure 3.19 (b) shows the separate core-back one. In Figure 3.19 (a), flux leakage may occur between two adjacent magnet rows of the translator because the flux path (black as rows) from a magnet rows flowing through the ferromagnetic pole-

pieces and then passing to the adjacent one rather than going through the rotor. In Figure 3.19 (b), flux leakage may occur through the ferromagnetic pole-pieces but, due to the separated core-back, they go through the adjacent pole rather than going back to the original magnet rows.

Figure 3.20 presents the rotor torque curves for three cases: (1) separated core-back and ferromagnetic pole-pieces; (2) separated core-back and single ferromagnetic pole-pieces; and (3) single core-back and ferromagnetic pole-pieces. The results show that torques obtained from the latter two cases drop approximately by 8% in comparison with the first case. Particularly, at the starting rotation angle, it can be seen that the starting torque of the first case is positive while the latter two cases give a negative value. This may be caused by flux leakage.

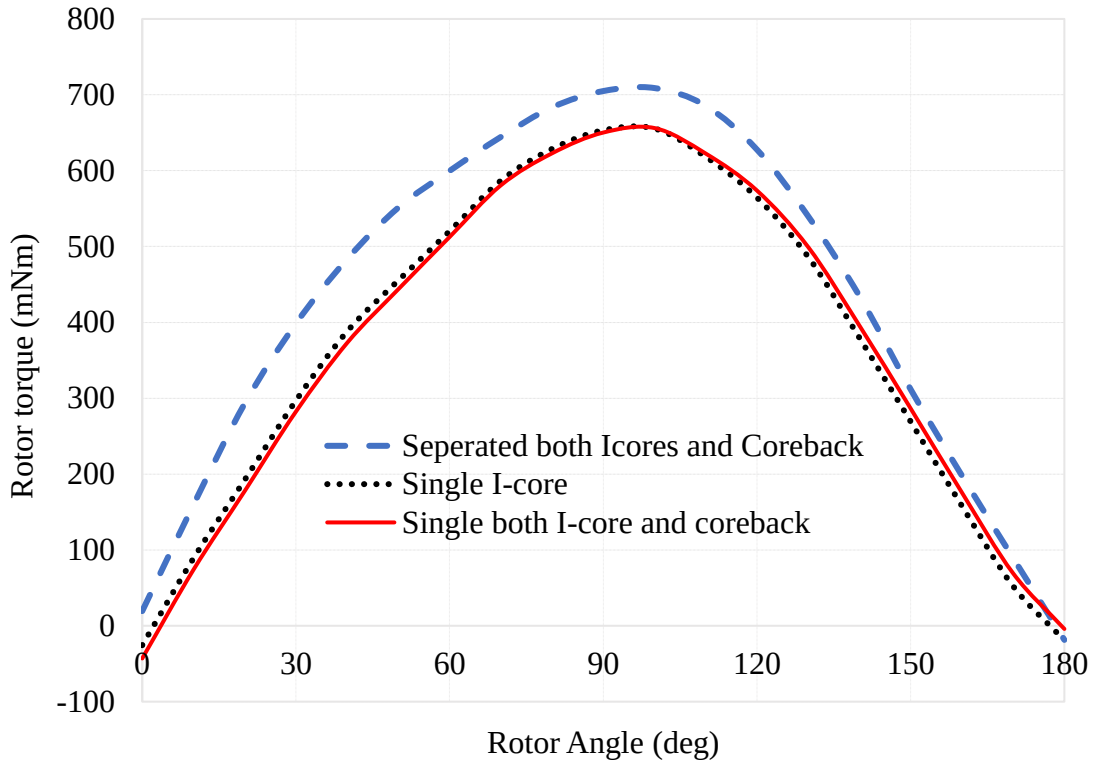

Figure 3. 20**.** Rotor torque for three cases: (1) separated both core-back and ferromagnetic pole-pieces; (2) separated core-back and single ferromagnetic pole-pieces; and (3) single both core-back and ferromagnetic pole-pieces.

3.3 Comparative design

As mentioned in the topology development section, in case of using rows of arc segment magnets on the translator, and the number of pole pitch on the translator and the rotor being equal, it becomes evident that the I-cores are not actually essential to the operation of this configuration. They can be advantageously removed to eliminate the associated core losses and replace the two gaps with one which consequently increases flux, force and torque.

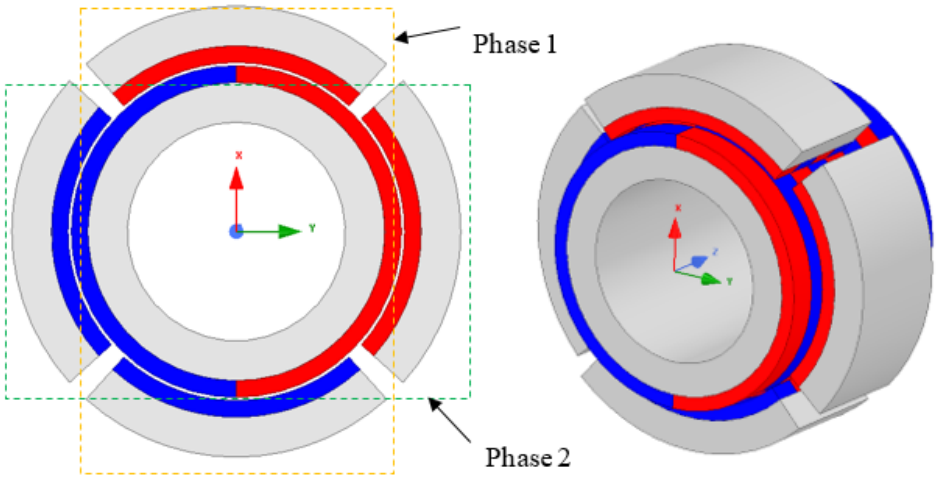

Figure 3. 21. A magnetic gear topology without I-cores: a) front view and b) isometric view

In order to compare the performance of the proposed magnetic gear to a helical magnetic gear structure, a three-dimensional finite element analysis is conducted with all parameters similar to that given in [55]. Figure 3.21 shows a magnetic gear without I-cores and presents its isometric view, in which the outer radius of the rotor is 50 mm, translator's active length is 40 mm and the magnet thickness on both rotor and translator is 5mm. As per discussions in the topology development section, the magnets on the translator are arranged in the form of a discretised helix and each segment angle is equivalent to 90 degrees. In this arrangement, the magnets on the translator of phase 1 are aligned with the magnets on the rotor, and as a consequence, the magnets on the translator of phase 2 are shifted by 90 electrical degrees (in other words, they move by a half pole pitch in the axial direction). If the inner rotor rotates about 360 degrees while the translator is kept stationary, a magneto-static axial force along

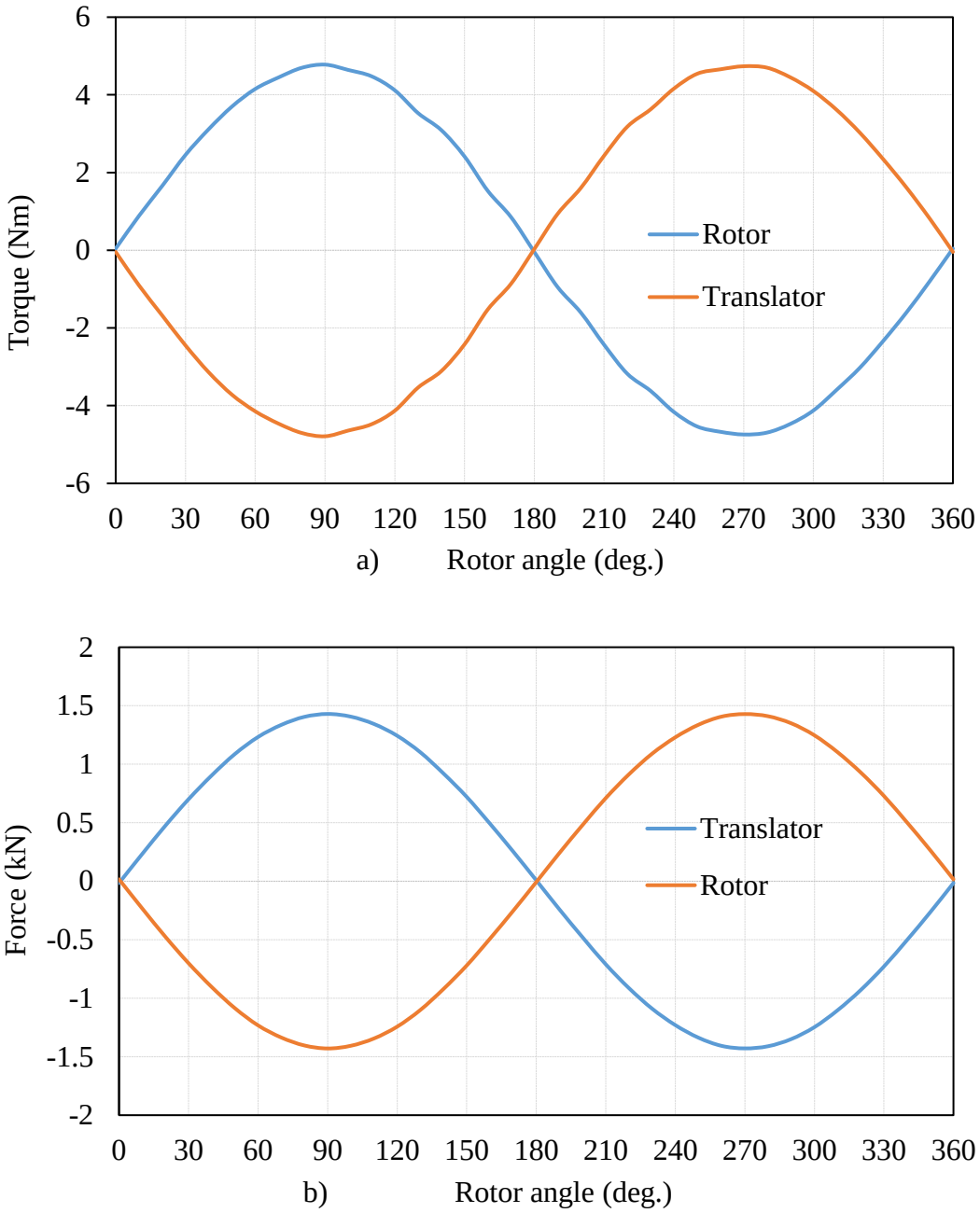

Figure 3. 22. a) Torque and b) Force of the magnetic gear due to rotation of the inner rotor.

the z-axis and torque are obtained. Theoretically, the amount of force and torque values on translator and rotor components are equal, but with inverse directions. Through three-dimensional finite element analysis, the obtainable force and torque profiles are proved to be in agreement with assumptions, as shown in Figure 3.22. It is observed on the graph that a maximum torque from the non I-cores proposed topology is approximately 4.78 Nm while

maximum torque of the helical topology [55] reaches 8.95 Nm. Similarly, maximum force achieved from two topologies was about 1.43 kN and 2.89 kN, respectively.

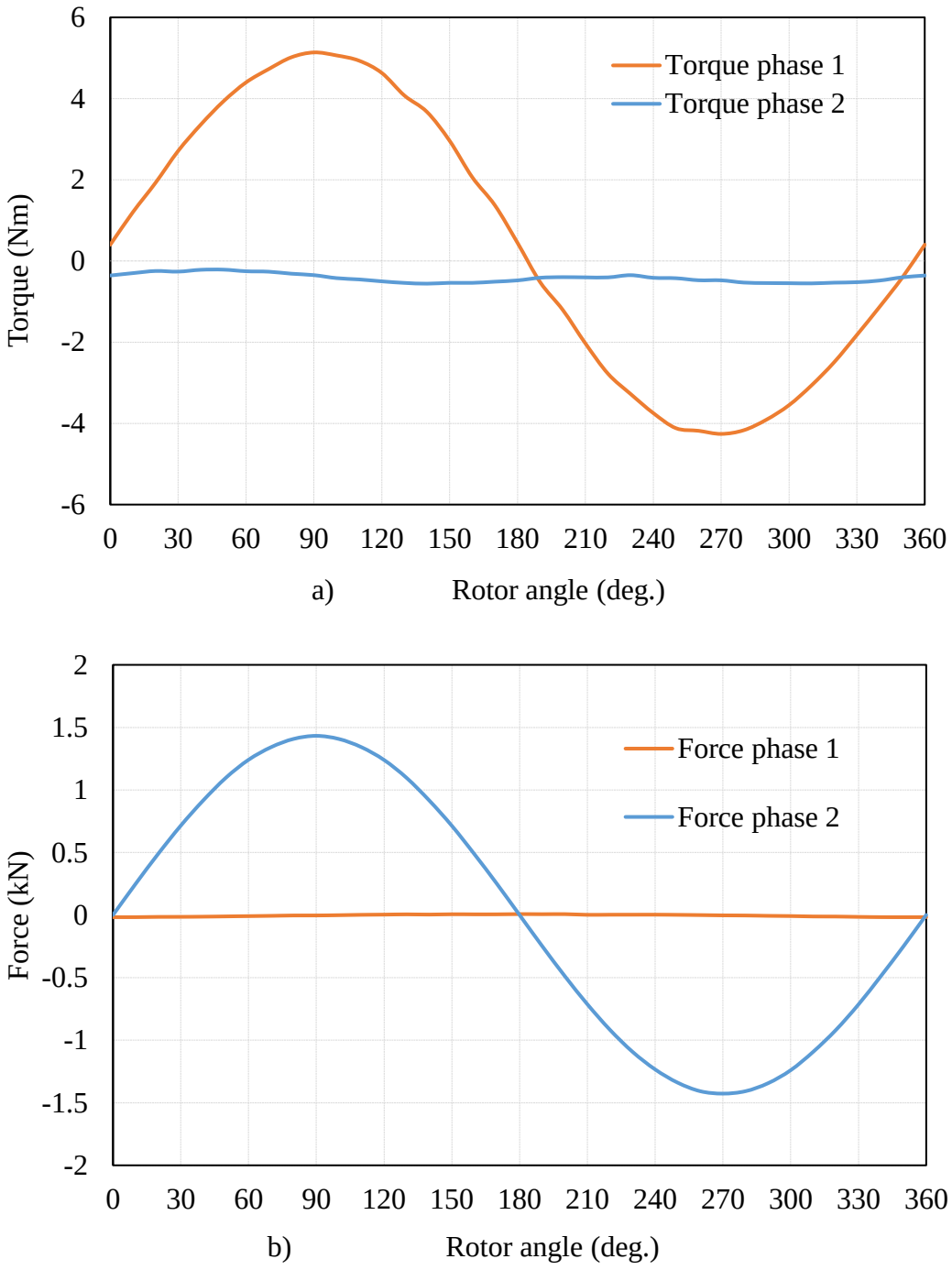

Figure 3. 23. a) Torque and b) Force of each individual phase of the magnetic gear due to rotation of the inner rotor

Intuitively, torque and force obtained from the helical structure have greater values of nearly two times those of the proposed magnetic gear. These may explain the results shown in Figure 3.23 when torque and force curves are presented in each individual phase. It is clear from the graph that most of the rated torque is contributed by phase 1 while phase 2 is kept constant at a small value. On the other hand, the force profile is initially generated by phase 2. It can be concluded that all active magnets in the helical topology contribute to force and torque characteristics while the proposed magnetic gear has only half of the active magnets contributing.

3.4 Varying pole pitch topology

A different pole pitch between the inner and outer rotating members of a rotary to rotary topology was deveoloped by Attalah and Howe [40] in 2001. In these, the number of poles on the ferromagnetic pieces equals the total number of poles on the inner and outer rotors. These authors, in 2005 [50], used a similar principle and the number of poles to develop a linear to linear topology. Wang et al. [48], in the same research group, have deveopled a magnetic screw gear that is based on the concept of a magnetic screw-nut, in which helical magnets are used on both the screw and the nut.

In 2016, Kouhshahi et al. [58-59] developed a rotary to linear magnetic gear topology that is based on the different number of poles principle and a helical structure. The inner rotor magnets and ferromagnetic pieces are skewed as a helix while the outer rotor magnets arranged in cylincrical form and kept stationary. The ferromagnetic pieces are used as a translator so that unusable magnet material (non active magnet material) can be removed.

In this section, a different number of poles magnetic gear is introduced and presented. This topology maintains a similar structure to the proposed magnetic gear, but with different pole pitch lengths on the rotor, translator and the I-cores. Figure 3.24 shows the structure of a varying number of poles magnetic gear topology, which consists of three components: an outer translater with p_t pole pairs; an inner rotor with p_i pole pairs; and a ferromagnetic piece that containts n_s pole-pieces. The number of pole pairs arrangement on the axial direction of

each component was selected to fit within the axial length *L*, and to satisfy requirements in [58]

$$n_s = p_i + p_t \tag{3.4}$$

Figure 3.25 depicts the cross-section in the axial direction and principal parameters. Thus, the length of pole pairs can be calculated by

$$\lambda_i = L/p_i \tag{3.5}$$

$$\lambda_t = L/p_t \tag{3.6}$$

$$\lambda_s = L/n_s \tag{3.7}$$

where $\lambda_i, \lambda_t, \lambda_s$ are the lengths of the pole pairs of the rotor, translator and ferromagnetic pole pieces respectively, therefore,

$$\lambda_s n_s = \lambda_i p_i = \lambda_t n_t \tag{3.8}$$

Magnets on the rotor and translator can be seen as a descrete helical structure that includes two 180 degree arc magnet segments. Eq. (3.4) may be presented in the form of wavenumbers, i.e.,

$$k_s = k_i + k_t \tag{3.9}$$

where

$$k_i = 2\pi/\lambda_i \tag{3.10}$$

$$k_t = 2\pi/\lambda_t \tag{3.11}$$

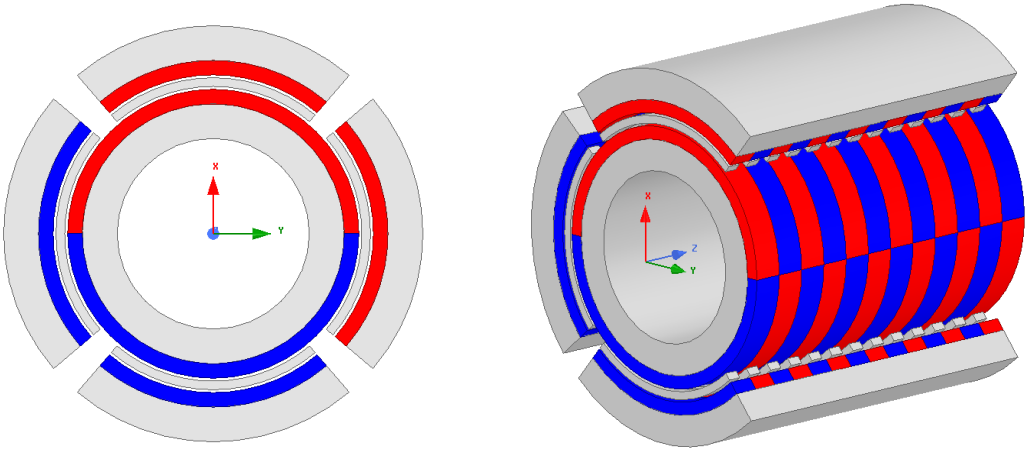

Figure 3. 24. A different poles magnetic gear with p_i = 6 pole pairs, $_{pt}$ = 7 pole pairs, and n_s = 13 pole pairs.

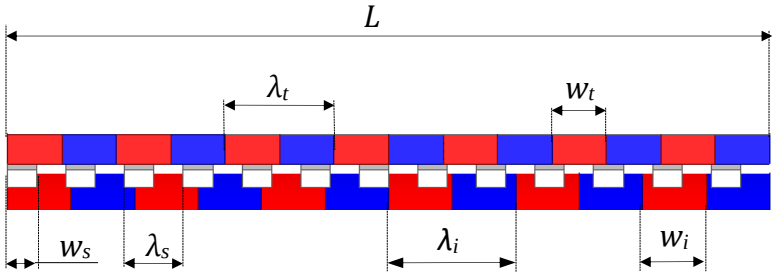

Figure 3. 25. Cross-section view of the magnetic gear showing pole pitch for rotor, translator and I-cores.

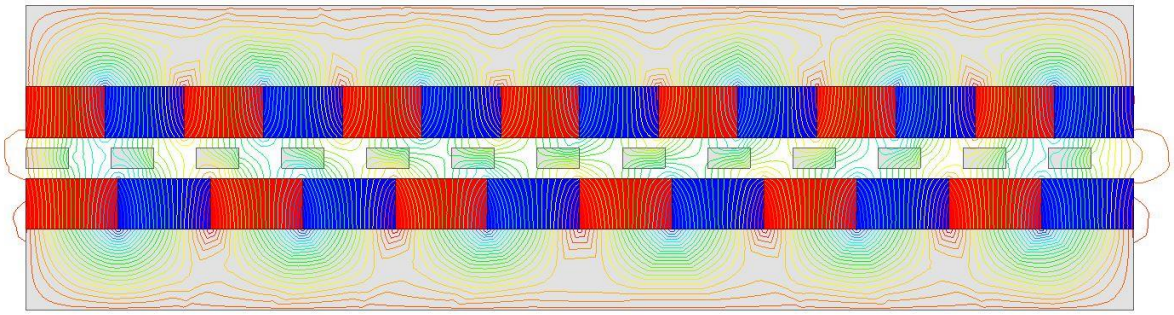

Figure 3. 26. Flux density lines of a 2D model of the different pole magnetic gear shown in the axial direction

Table 5: Geometric dimensions and material values

Parameters		**symbol**	**value**	**Unit**
Rotor	Pole pairs,	P_i	6	mm
	Pole pitch	w_i	35	mm
	Outer radius	R_i	53	mm
	Air gap length	g	0.5	mm
	Magnet thickness	d	7.5	mm
	Axial length	L	420	mm
Translator	Pole pairs	P_t	15	mm
	Pole pitch	w_t	14	mm
	Outer magnet radius	R_o	71	mm
	Magnet thickness	m	11	mm
Ferromagnetic pole-pieces	Pole pairs	n_s	21	mm
	Pole pitch	w_s	10	mm
	thickness	h	6	mm
Materials	Magnet coercivity	H_c	890	kA/m
	Magnet remanent flux density	B_r	1.23	T
	steel 1008 resistivity		14.2	μΩ-cm

As per geometric dimensions and material values given in Table 5, a 2D FEA model is established to show modulating effect of the ferromagnetic pieces in Figure 3.26. When the inner rotor is rotated by 360° while the translator and I-cores are kept stationary, an axial force along the *z*-axis is created as well as a torque, as shown in Figure 3.27.

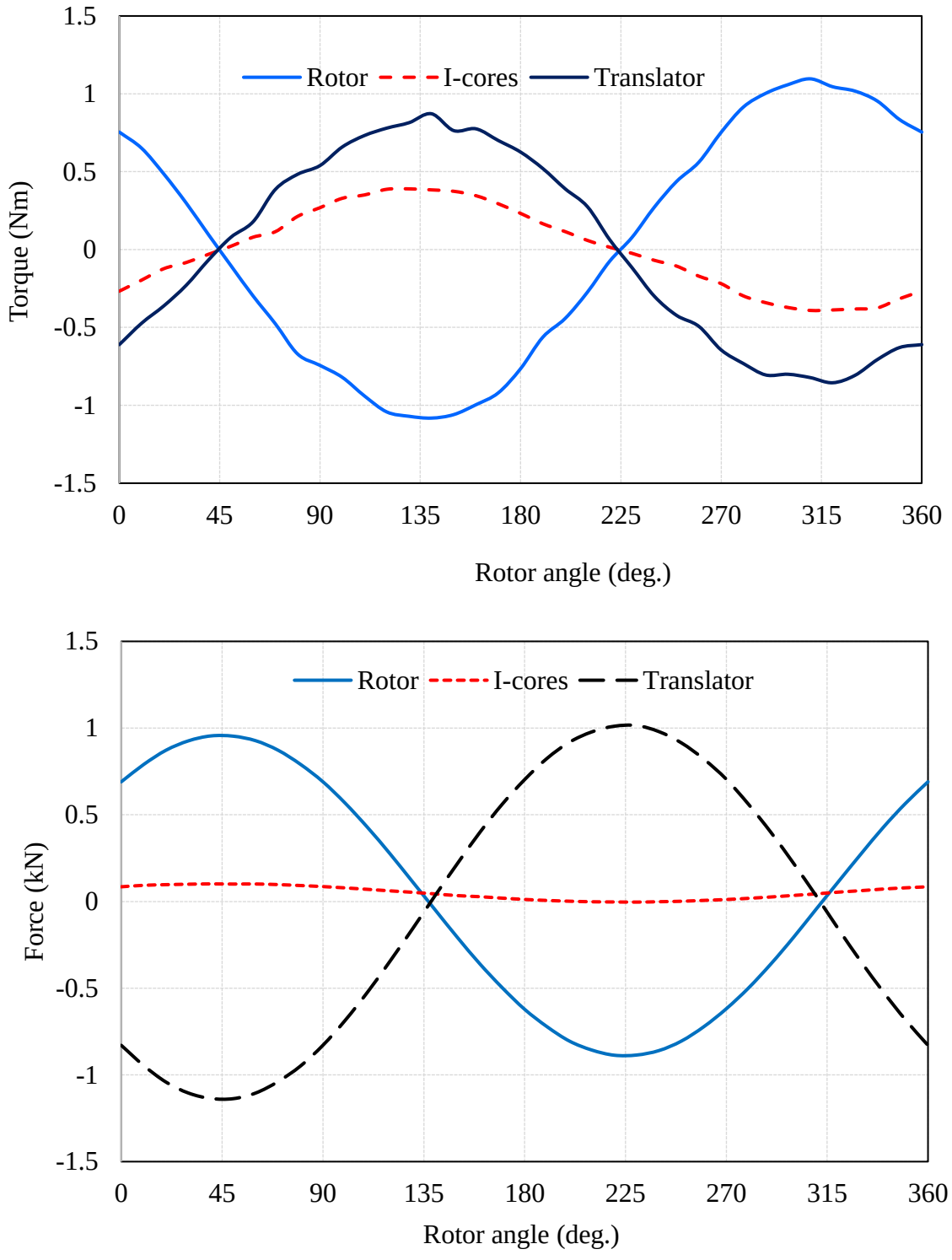

Figure 3. 27. Torque and force on different parts of the varying pole magnetic gear

3.5 Summary

Based on the concept of the transverse-flux machine, a magnetic gear was developed and presented. In terms of transmission from linear to rotary and vice versa, and the gear ratio was determined. In addition, by using three-dimensional FEA models the magneto-static torque and force were estimated. It was shown that torque and force were nonlinearly related. Moreover, the cogging torque was low in comparison with the rated torque.

At the beginning of this chapter, it was described how a novel magnetic gear has been developed, starting from the transverse flux machine's structure. According to the configuration of the transverse flux machine, however, C-cores modulating flux field were cut to become I-cores. In addition, the winding was replaced by four rows of hetero-polar magnets to produce flux ripples in the airgaps for generating the rotor torque. The number of poles on the rotor affected the gear ratio and the rotor torque, in that the higher number of rotor poles meant a lower gear ratio.

Furthermore, we can envisage having a rotor with multi-peripheral poles. In this case, the translator magnet arrays will form a polygon whose number of sides will be equal to the number of peripheral rotor poles. The greater the number of peripheral poles, the closer the approximation will be to a helical disposition of the I-cores and magnets. Based on the results reported in [31], this will increase the pull-out torque and improve the linearity of the relationship between torque and force, i.e., reducing the load dependency of the gear ratio.

A comparative design of the proposed magnetic gear was implemented by using the arc segment magnets on the translator and removing the I-cores to eliminate the associated core losses. Also, replacing the two gaps with one resulted in an increase in the flux, force and torque. The geometric dimensions were kept similar to the helical gear topology. Through 3D FEA, the torque and force of each individual phase were examined. It was shown that only half the active magnets on the translator contributed to torque and force characteristics. Consequently, the maximum values of the torque and force of the proposed magnetic gear were nearly half the value of the screw magnetic gear topology.

Chapter 4 Design optimisation of the magnetic gear

4.1 Introduction

In this chapter, design optimisation is implemented in order to investigate the influence of principal geometric dimensions on the magnetic gear performance. A two-dimensional finite element analysis (2D FEA) is implemented here because it is faster whilst can produce accurate computations in predicting the behaviour and characteristics of a design. A 2D model is generated that represents the pattern of a pole pitch so that the field distribution repeats in the next periodic pole pitch in the axial direction. The flux density is calculated in the air gap and the effects of key parameters on performance are determined. However, 2D FEA is not able to calculate radial direction of the magnet, therefore, the results do not represent the full characteristics of the device. Thus, 3D FEA is also utilised in the optimisation process.

As mentioned in chapter 3, if the magnets on the translator are the arc segment, the I-core can be removed to eliminate the associate core loss and to decrease the gap between rotor and translator magnets, which increases the flux, force and torque. However, the optimasation process in this study will be carried out by using the configuration with the I-cores. The reason for choosing this can be explained as: 1) the bar magnets are practical to make a demonstrator because they are available in commercial market; 2) gear ratio can be variable by varying the number of poles on the rotor, translator and I-cores. This is an advantageous option for development a magnetic gear to a certain inquired that it can combine an optimal objective between gear ratio and the performance.

In the first analysis, a single design parameter is optimised while others are kept constant. Then a parametric sweep analysis is implemented to maximise performance characteristics. The results are provided and discussed with the optimal parameters. The trade–off between maximising force density and force-per-kg magnet is presented.

4.2 Two-dimensional finite element analysis (2D-FEA)

This section is concerned with predicting the influence of the design parameters of a magnetic gear by using two-dimensional finite element methods.

4.2.1. 2D FEA model

Performance of the magnetic gear is a function of the magnets' dimensions, material and sizes of the ferromagnetic pole-pieces (I-cores), and the air gap length. In this section, the relationship between these parameters is considered and discussed. Two-dimensional finite element analysis (2D-FEA) is used to investigate the effects of the above mentioned on the performance of the magnetic gear. In this analysis, the magnet width w is assumed to be at full pole pitch λ (*i.e.*, $w = \lambda$).

Figure 4.1 shows the 2D-FEA model in the axial direction of the magnetic gear. At both aligned and nonaligned positions, the force and torque are zero, while at the half-way position, the magnetic gear operates at its pull-out values of force and torque. Therefore, from here onwards, halfway position is used for simulation in all models.

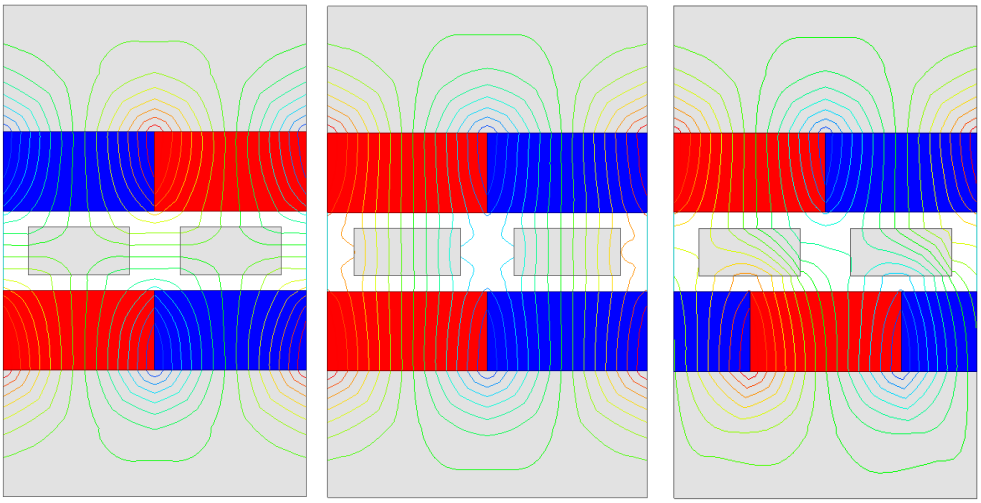

(a) (b) (c)

Figure 4. 1. Flux line in the magnetic gear with equal magnet thicknesses on rotor and translator: (a) aligned (b) non-aligned (c) half-way

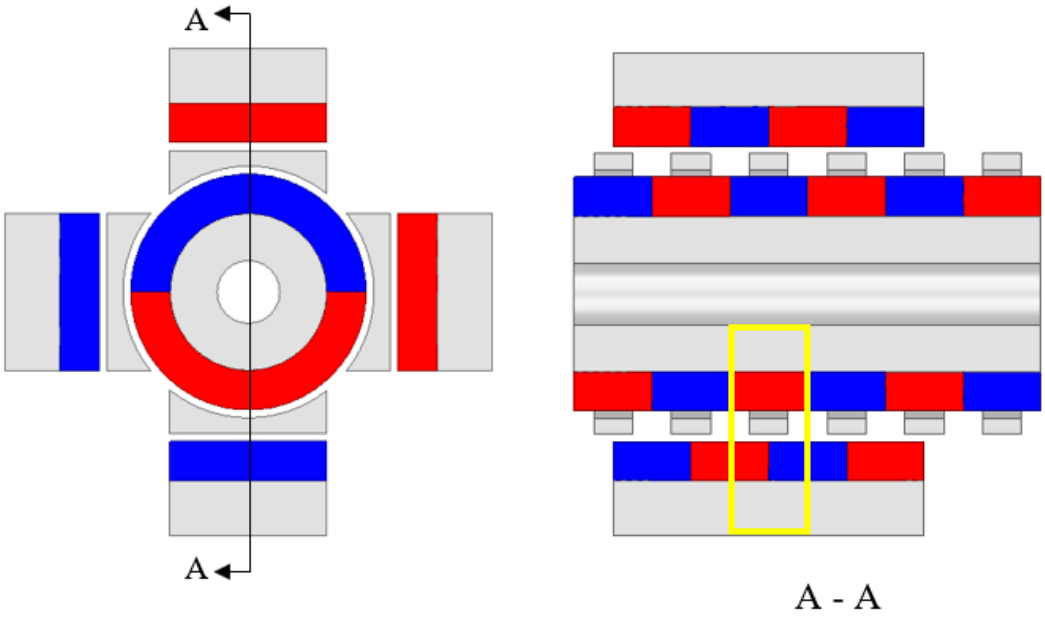

Figure 4. 2. Front and cross-section views of the magnetic gear

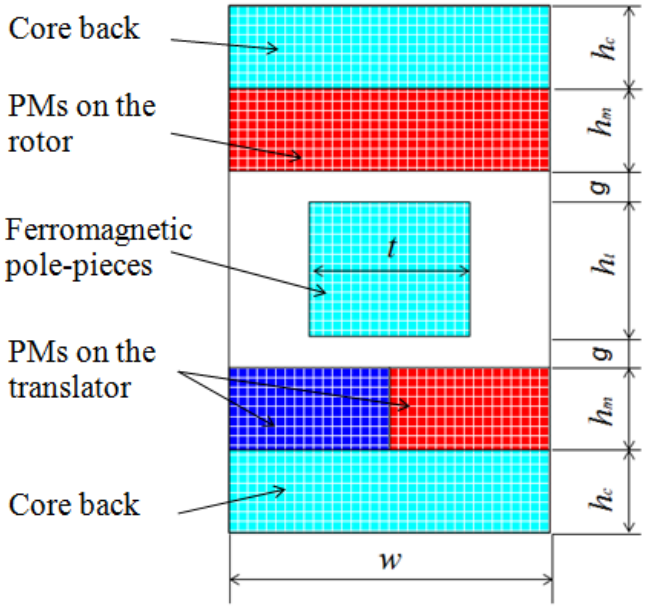

Figure 4. 3. 2D-FEA model of the magnetic gear

4.2.2. Results

In order to determine optimal parameters, the magnetic flux density in the air gaps is calculated by using a 2D-FEA model in ANSYS Maxwell. A high force density permanent magnet material NdFe35 and steel_1020 (Ansys library) are used for the PMs, I-cores and core backs, respectively. Figure 4.2 shows a cross-section of the magnetic gear and Figure 4.3 depicts a 2D-FEA model with labelled components. Periodic boundary conditions are imposed to exclude the end effects originating from the open-ended structure of the device. As a result, the field distribution repeats in the next periodic pole pitch in the axial direction. The magnetic flux distribution in the examined model can be seen in Figure 4.4. It is shown that the magnetic flux distribution is not uniform. It is also observed that the I-cores' magnetic field is saturated at the bottom right corner. This effect can increase the pull-out force rapidly at half pitch position of the translator. Also, the thickness of the core-back should be taken into account to eliminate the high magnetic flux density distribution.

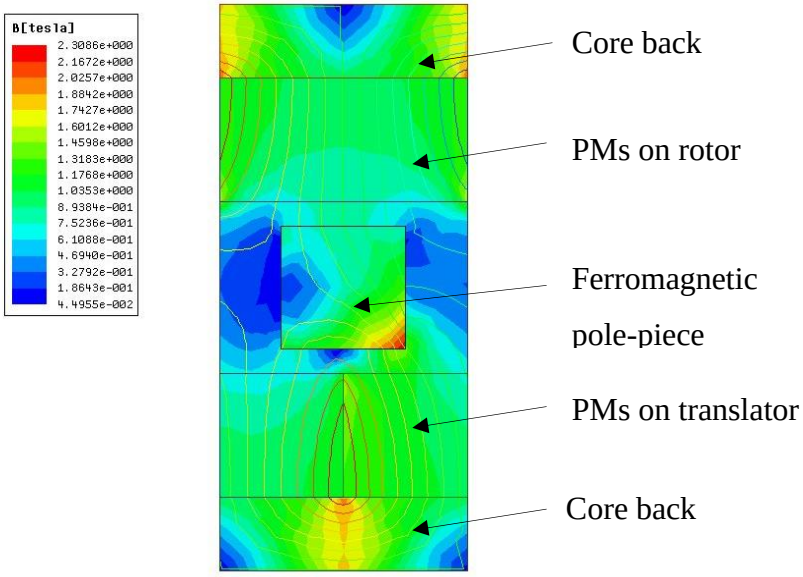

Figure 4. 4. Magnetic flux distributions in 2D-FEA model

4.2.3. Effects of the I-cores' dimensions

Generally, in the design and operation of the gears, the rotor length will be made as long as the stroke of the translator. However, it should be noted that the I-cores are arranged along the rotor, thus, this will increase the number of I-cores and results in increasing the cogging

torque. Therefore, the magnetic gear should be carefully designed in order to avoid this problem.

In this section, the thickness of the I-cores is considered based on the 2D-model. Figure 4.5 shows the variations of the pull-out force versus I-cores' width for several values of magnet thickness. To obtain this result, the width of the I-cores is increased from 1 to 10 mm, and the pull-out force is calculated for values of the magnet thickness in the range of 2 to 8 mm, and the air gap is fixed at 1 mm.

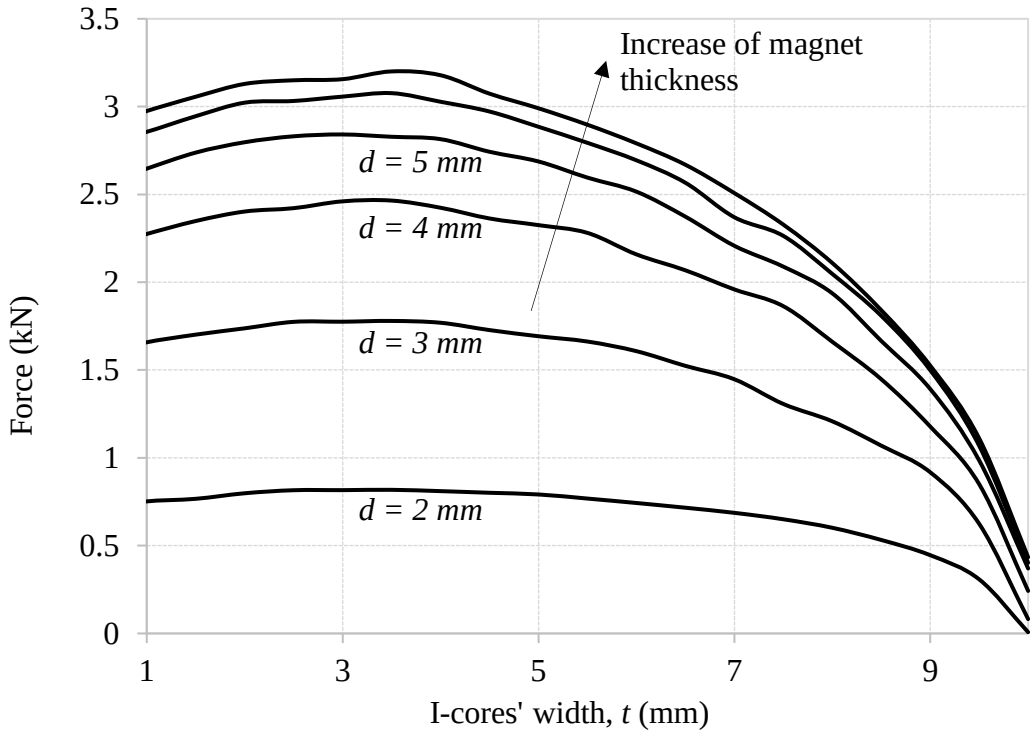

Figure 4. 5. Variations of the pull-out force versus I-cores' thickness, *t*, for several values of magnet thickness.

The pole-pitch is kept at a constant value of 10 mm. It is observed that the maximum pull-out force is achieved in each magnet thickness at a certain I-cores' width. For example, for the case of 5 mm magnet thickness, the resultant pull-out force is maximized at 6 mm width of the I-cores. Another conclusion that can be drawn from the results is that, for a given

air gap length, increasing the magnet thickness will increase the pull-out force, which becomes saturated when the magnet thickness increases to a certain value.

Another result of the pull-out force is calculated by considering the effect of I-cores' thickness, as shown in Figure 4.6. From the plot, it is concluded that for any given magnet thickness, the pull-out force is maximized at a certain value of the I-cores' width. The curves presented in Figure 4.6 can also be looked upon as another form of demonstrating the conclusion made in Figure 4.5, i.e., for a given air gap length, increasing the magnet thickness increases the pull-out force. However, increasing the thickness eventually will result in the saturation of the pull-out force.

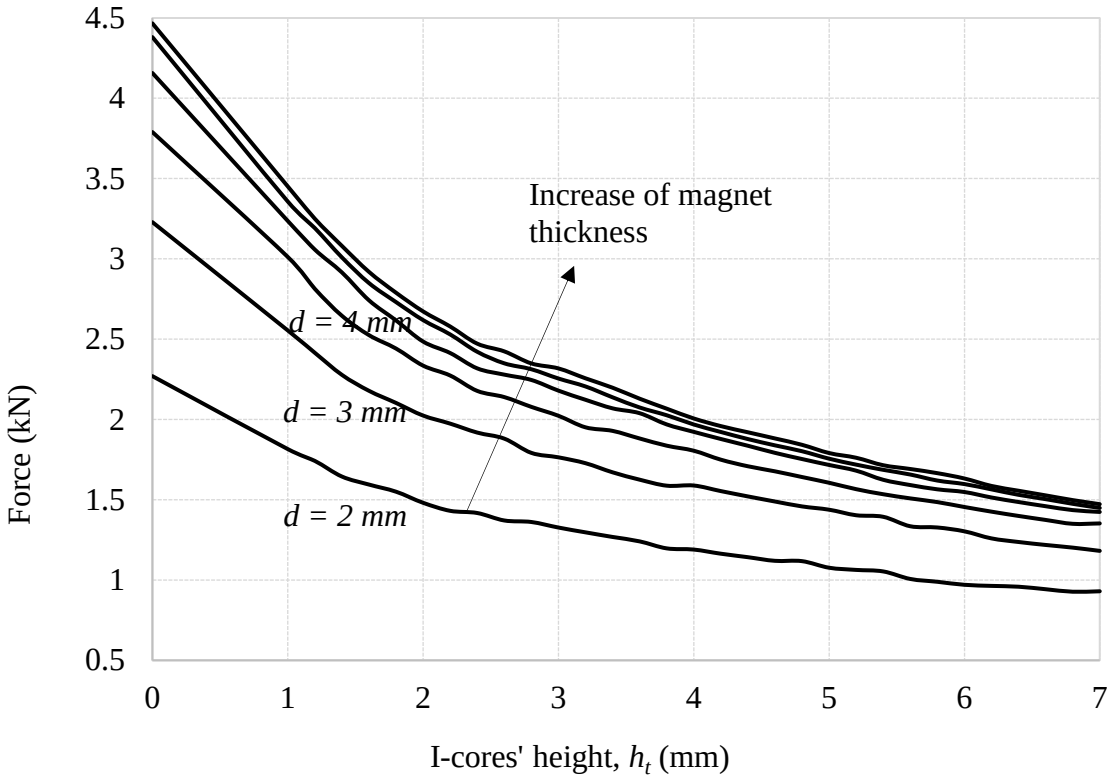

Figure 4. 6. Variations of the pull-out force versus I-cores' thickness for several values of magnet thickness

4.2.4. Pull-out force versus permanent magnets' dimensions

To increase the torque, in a magnetic gear we can increase either radius of the rotor or its length or both. For example, if a topology is chosen with a small radius and long length

then a more compact design will be obtained. Therefore, some associated factors need to be considered, such as cost, weight and maximum torque transmission that are very important in making a decision. In addition, the stroke of the translator should be considered.

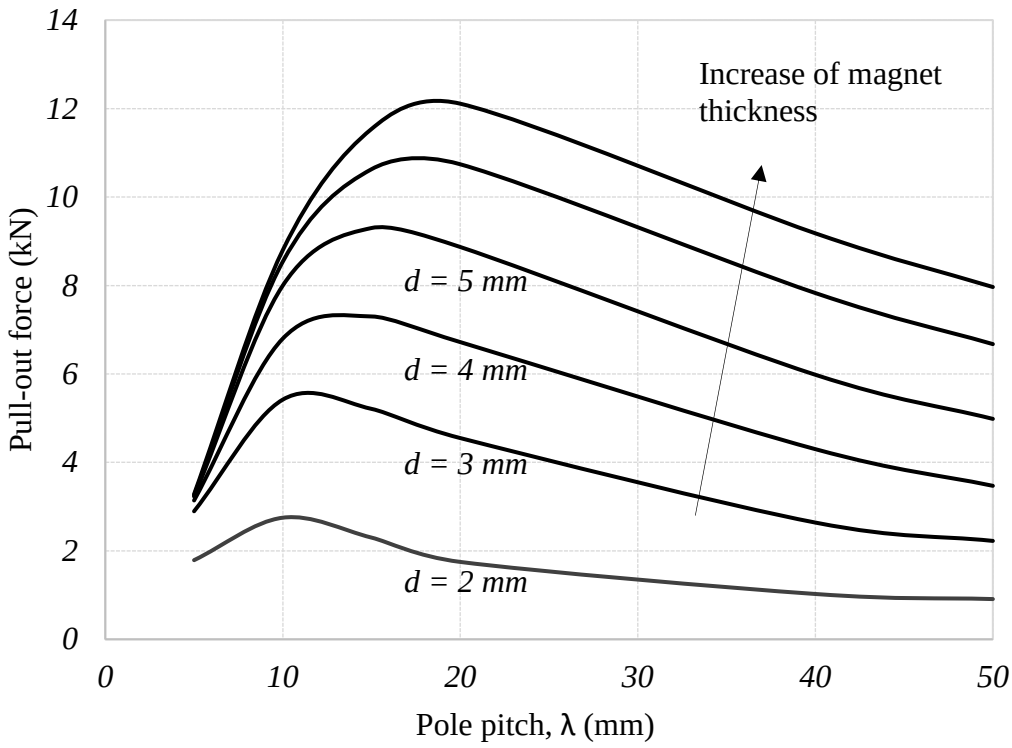

Figure 4. 7. Variation of the pull-out force versus magnet width for several values of magnet thickness

Analytical models are also used to investigate the influence of magnet thickness, width, and pole pitch. Figure 4.7 shows variations in the pull-out force versus magnet width for several values of magnet thickness. In this section, magnet width is assumed to be at the full pole pitch. The air gap length is fixed at 1 mm while the magnet thickness is increased from 2 to 8 mm in steps of 1 mm. As seen in the result, a conclusion can be drawn that for any given magnet thickness, there would be an optimum pole pitch for which the pull-out force is maximised. For example, for the case of 5 mm magnet thickness the optimum pitch is 30 mm and the resultant pull-out force is about 8.9 kN.

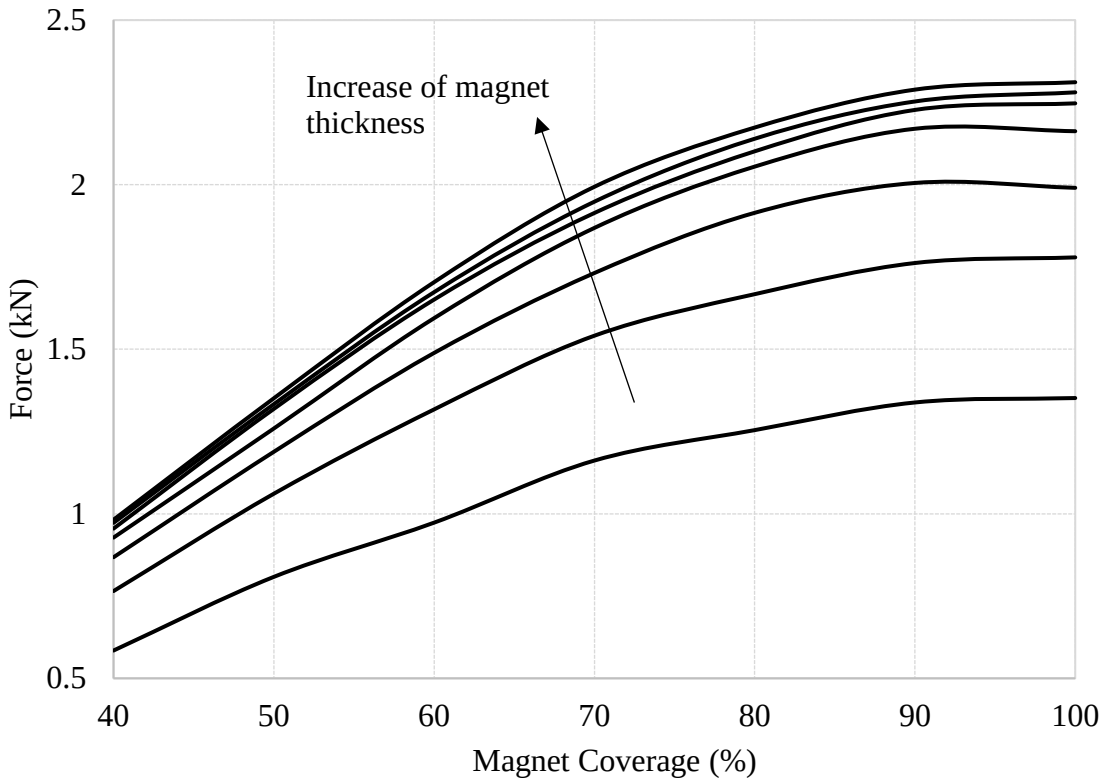

Figure 4. 8. Pull-out force versus magnet coverage for several values of magnet thickness

The effect of the magnet width to pole pitch ratio w/λ, the so-called *magnet coverage*, on the pull-out force is also examined by using the FEA model, as seen in Figure 4.8. The air gap length is fixed at 1 mm, and the magnet coverage has increased from 40% to 100% of the pole pitch, set at 10 mm, for several values of the magnet thickness from 2mm to 8 mm. It is observed that for each magnet thickness there is a range of magnet coverage over which the pull-out force increases almost in a linear fashion.

4.2.5. Effects of air gap length

The effect of increasing the air gap length on the pull-out force is shown in Figure 4.9. In this case, the pole pitch is set at a constant value of 10 mm, the air gap length increases from 1 to 5 mm, and the pull-out force is calculated for several values of the magnet thickness in the range of 1 mm to 8 mm. It is seen that increasing the air gap length at a certain magnet thickness reduces the pull-out force.

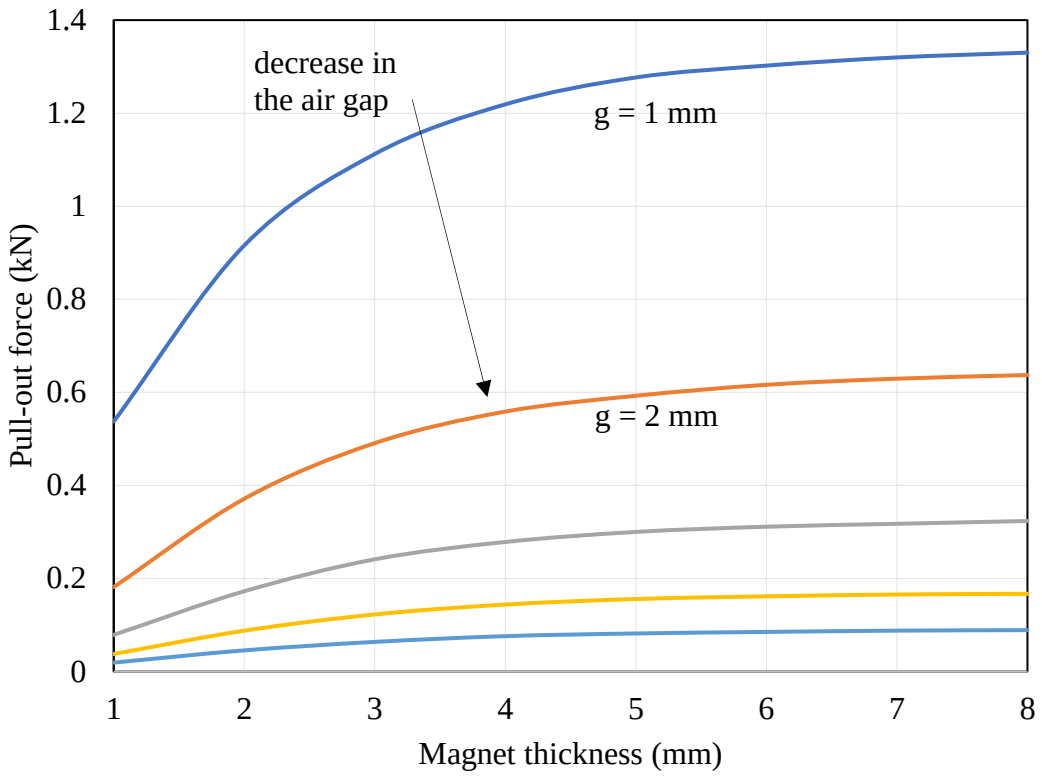

Figure 4. 9. Variations of the pull-out force versus air gap lengths for several magnet thickness

To maintain the constant pull-out force, as the air gap length increases, both magnet thickness and pole pitch (the magnet width in this case) must increase proportionally. However, increasing the pole pitch is the result of reducing the gear ratio, according to Equation (1). Moreover, an increased magnet width requires a thicker core-back to carry the resultant magnetic flux.

4.3 Three-dimensional finite element analysis (3D-FEA)

4.2.1. The Model

In the previous section, two-dimensional computation was unable to account for the flux in the radial direction, this obviously causes less accuracy in the predictions of torque and flux. In chapter 3, a magnetic gear was proposed and developed. Here in this section,

aspect design studies are carried out by utilising three-dimensional computations and several principal parameters are optimised and presented.

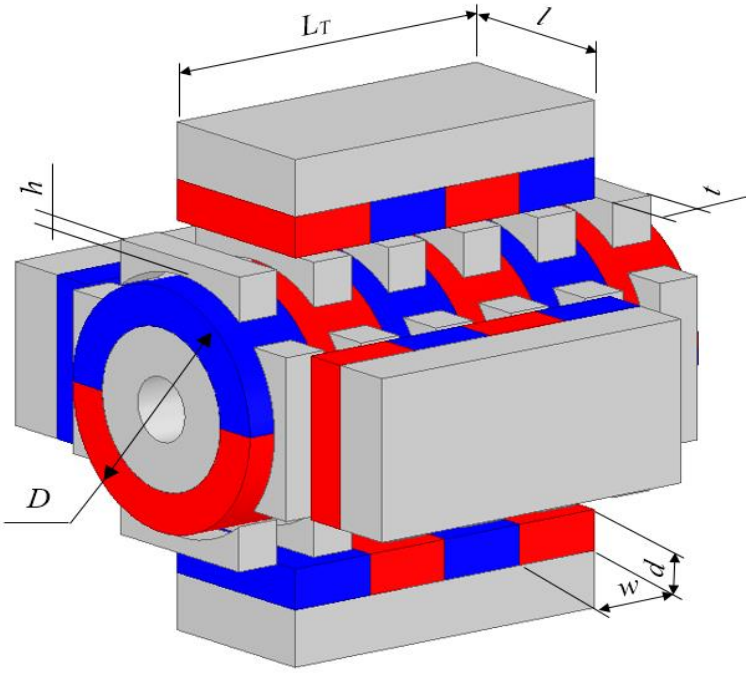

Figure 4. 10. Parameters scheme of the proposed magnetic gear

Figure 4.10 presents the proposed magnetic gear configuration in order to investigate the effects of key parameters. The configuration includes a rotor, a translator and I-cores, all isolated by air gaps in between. The translator consists of four magnet stacks which are divided into two phases. Magnets on phase 1 are aligned with magnets on the rotor, and magnets on phase 2 are shifted by half of the pole pitch, which is also referred to as the nonaligned position. While the translator moves back and forth along the axial axis, the rotor also rotates about the same axis. In this picture, the rotor rotates 90 degrees in the clockwise direction. General geometric parameters for all simulated models are given in Table 6.

4.2.2. Aspect design of the principal parameters

In this section, design studies are carried out to examine the effects of principal parameters on the performance of the proposed magnetic gear. In turn, magnet thickness, air gap length, and I-core dimensions are examined by fixing the other parameters listed in Table 1. For high

accuracy, the design process is implemented through a 3D-FEA model, as shown in Figure 3.10.

Table 6: Geometric design parameters of the proposed magnetic gear

Parameters	**Symbol**	**Value**	**Units**
Magnet width	*w*	10	*mm*
Magnet thickness	*d*	5	*mm*
I-core height	*h*	2	*mm*
I-core length	*l*	20	*mm*
I-core thickness	*t*	6	*mm*
core-backs thickness	h_c	8	*mm*
Air gap length	*g*	1	*mm*
Translator active length	L_T	40	*mm*
Rotor diameter	*D*	30	*mm*
Pole pitch	λ	10	*mm*
Magnet coercity		838	kA/m
Magnet remanent flux density		1.23	T
Steel 1008 resistivity		14.2	μΩ-cm

Due to lack of radial flux calculations in a 2D-FEA model, the effects of pole pitch length are reconsidered in 3D-FEA models with a variety of magnet thicknesses. In order to modify the pole pitch, the translator active length is made longer and is set at 120 mm. Meanwhile, the rotor diameter is kept constant at 50 mm. The pole pitch is modified from 10 mm to 60 mm in step of 5mm, and the magnet thickness is various from 2 mm to 20 mm. Figure 4.11 shows the variation of force versus the pole pitch for several values of magnet thickness. It is shown on the graph that force increases significantly between 2mm to 10mm and then the value rises slightly between 10mm to 20mm. Obviously, the trend is in agreement with the 2D-FEA calculations.

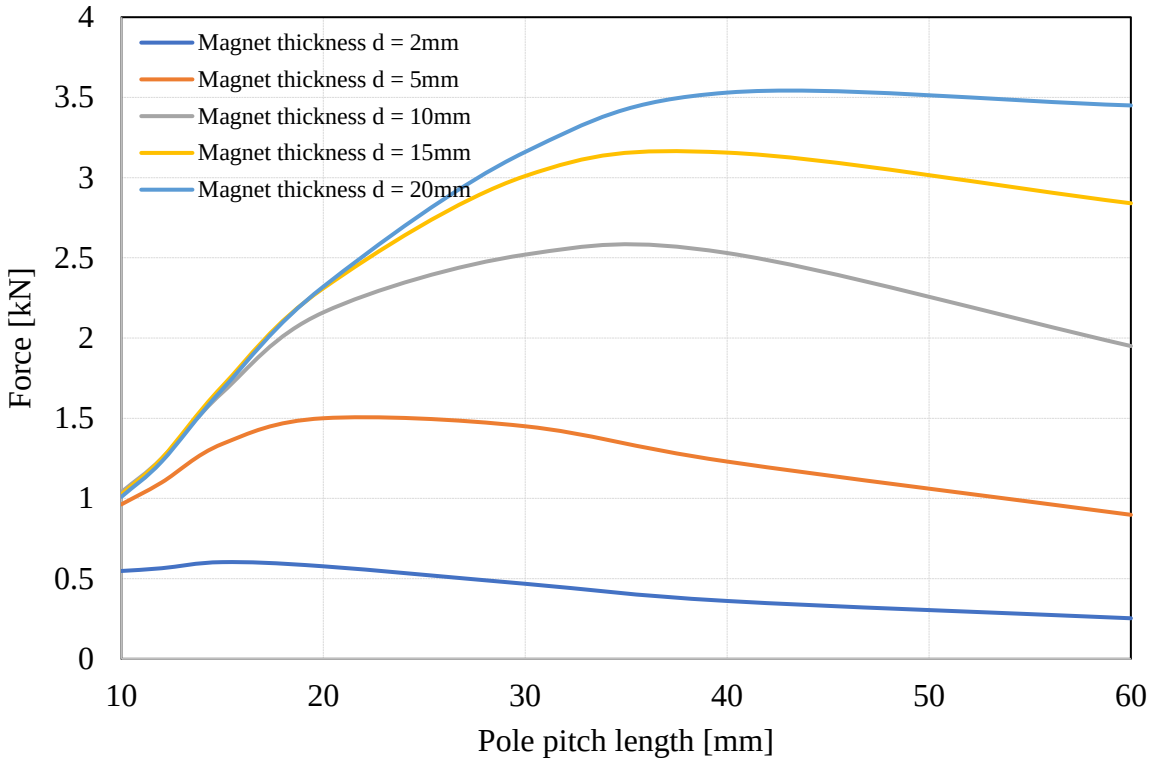

Figure 4. 11. Variation of force versus pole pitch length with several values of magnet thickness

Figure 4.12 shows variation of maximum torque for several values of magnet thickness that is increased from 2 to 10 mm in steps of 1 mm. A conclusion can be drawn that increasing the magnet thickness will increase the torque; however, the effect will saturate beyond a certain point. More specifically, the torque increases very gradually after the magnet thickness value of 6 mm. This may happen due to an increase in the reluctance of the flux path when magnet thickness is increased beyond this threshold value. Moreover, if the core-back is kept constant while the magnet thickness increases, as a result, the saturation inside the I-cores may occur at a higher magnet thickness.

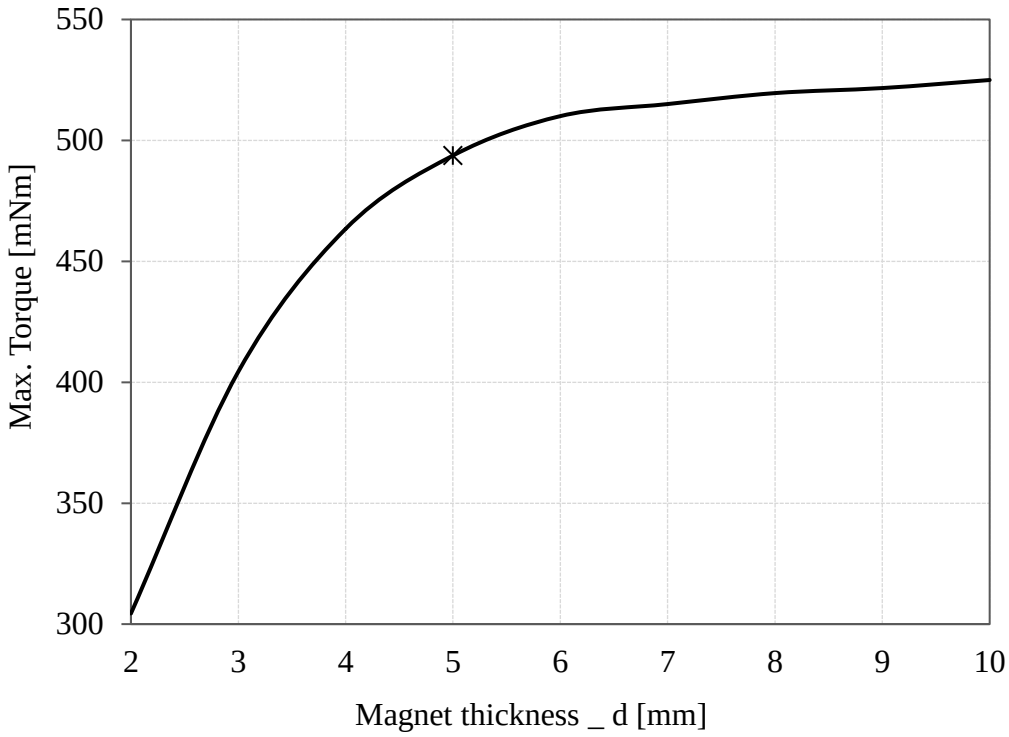

Figure 4. 12. Variation of the maximum torque with different magnet thicknesses: D = 30, *L_T = 40, λ = 10, t = 6, l = 20, h = 2 and g = 1 constant* (all units in *mm*)

In [31], it is suggested that magnet material not only has an effect on the performance, but also contributes to the cost. The effect of the magnet material can be examined by considering the effect of the magnet width to pole pitch ratio, *w/λ*, on the transmitted torque. This is done by using 3D-FEA, as presented in Figure 4.13. The air gap length and magnet thickness are fixed at 1 mm and 5 mm, respectively. For the simulation, this ratio, the so-called magnet coverage, has increased from 60% to 100% of the pole pitch, at 10 mm. It is observed that the maximum torque increases rapidly as magnet coverage goes from 60% to 90%, and then it has a small increase. As far as the rate of maximum torque rise due to the increased magnet coverage is concerned, it can be shown that the torque tends to saturate as the coverage approaches the full pole pitch, which it dues to the increase in leakage flux between adjacent magnets.

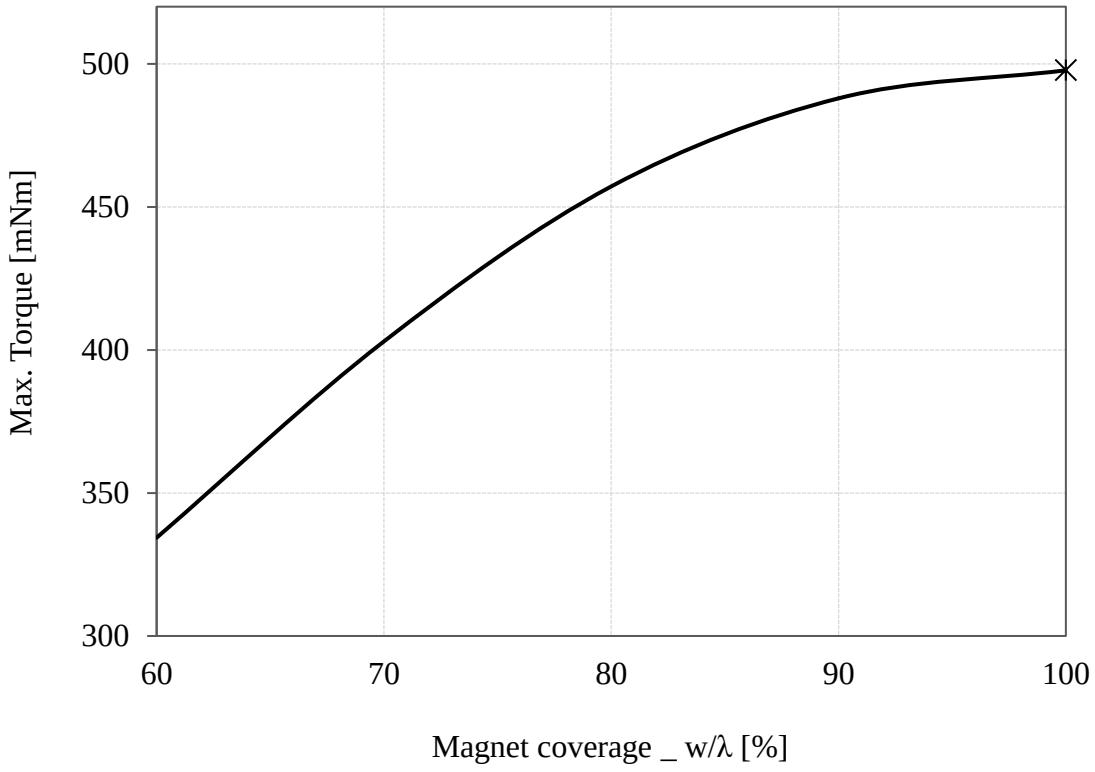

Figure 4. 13. Variation of maximum torque with different magnet coverages: L_T = *40, λ = 10, t = 6, l = 20, h = 2, d = 5 and g = 1 constant*

Also, the effect of the air gap length on maximum torque is illustrated in Figure 4.14 by using a 3D-FEA model. The magnet thickness is kept at 5 mm while the air gap length increases from 0.5 to 3.0 mm in steps of 0.5 mm. As can be seen, increasing the air gap length at a constant magnet thickness reduces the torque. In reality, the air gap length needs to be increased for larger designs. Thus, proper selection of the air gap length and magnet thickness proportion, as shown in Figure 4.15, contributes to obtaining the desired maximum torque characteristics. However, a small air gap length combined with small radius and long length of the translator may lead to a more compact design.

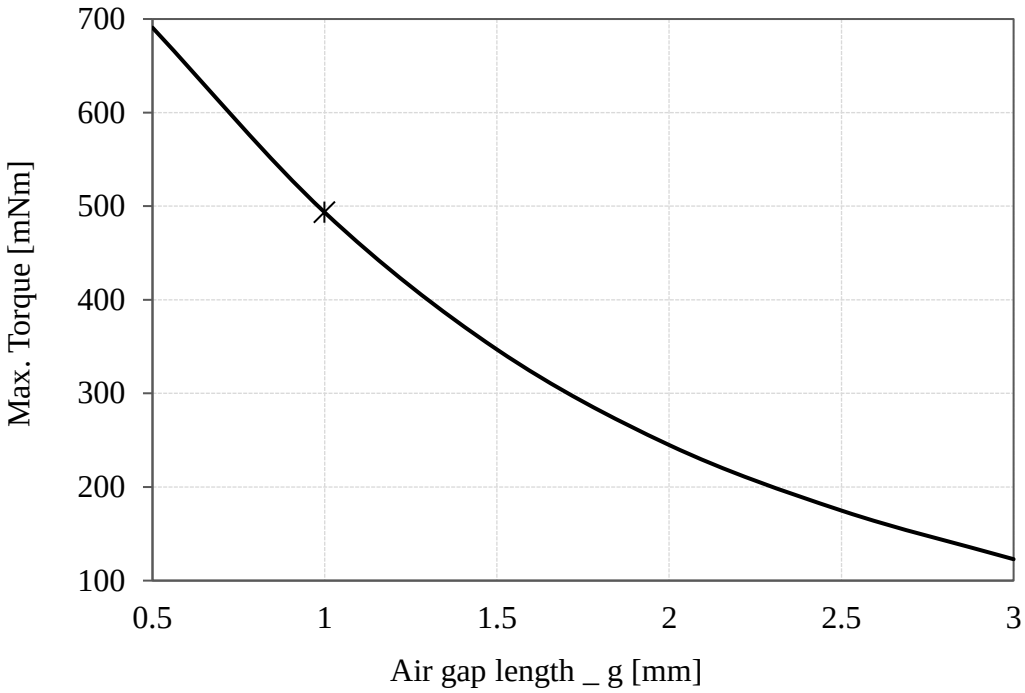

Figure 4. 14. Variation of the maximum torque with different air gap length: L_T = *40,* λ *= 10, t = 6, l = 20, h = 2, and d = 5 (unit: mm) constant*

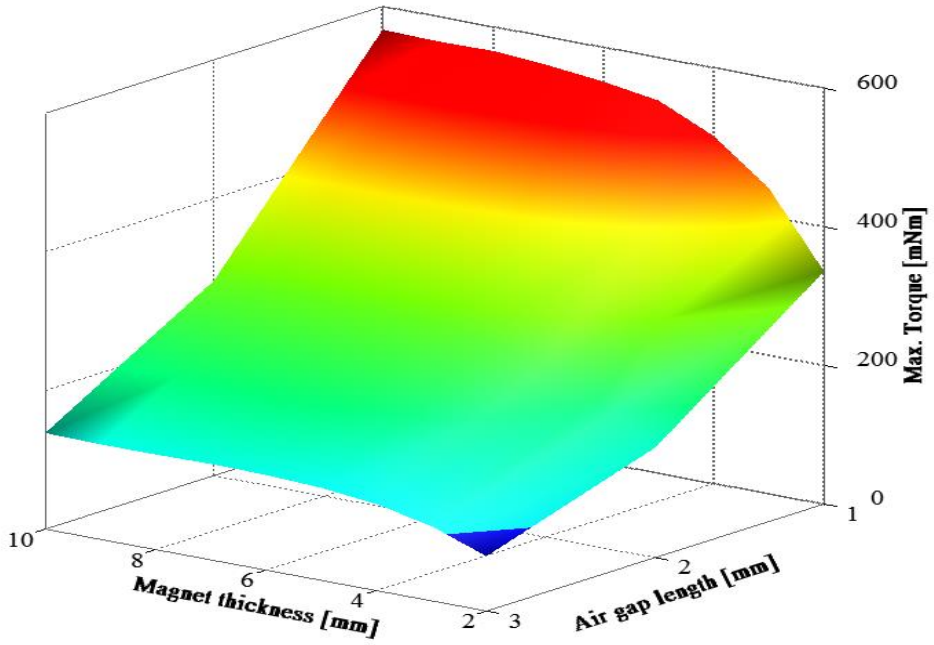

Figure 4. 15. Variation of the maximum torque versus magnet thickness and air gap length: L_T = *40,* λ *= 10, t = 6, l =20, and h = 2 constant (*unit: *mm)*

The function of the I-cores is to modulate the magnetic field towards the magnets and then to the core-backs. Thus, I-cores' dimensions are essential factors that contribute to the performance of the magnetic gear. I-core head presents two dimensions in which I-core thickness, *t*, is in the axial direction and I-core length, *l*, is in radial cross section. If I-core thickness is axially shorter than the magnet (pole pitch), then the fringing flux in the axial direction will be actually producing torque (or force). In the case when the I-core thickness is equal to the pole pitch, the leakage flux between two adjacent magnets will deteriorate the performance. The effect of the I-core thickness and I core length on maximum torque are examined by using a 3D-FEA model, as seen in Figure 4.16 and Figure 4.17. Meanwhile, the effect of the I-core height, *h*, on the maximum torque is examined, as seen in Figure 4.18. It is observed that increasing the I-core height reduces the torque.

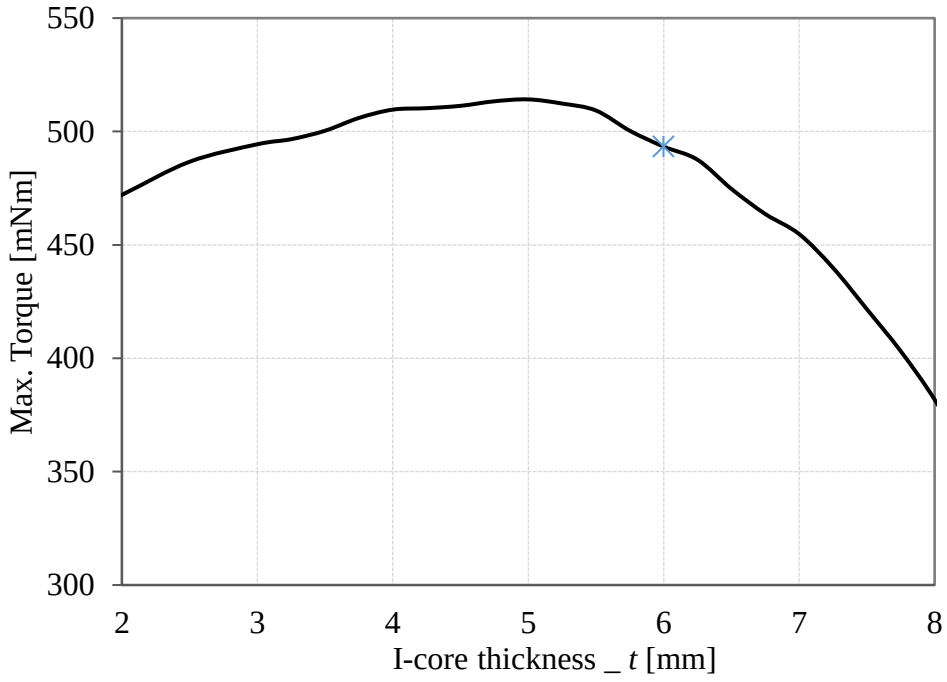

Figure 4. 16. Variation of the maximum torque with different steel thicknesses: L_T = *40,* λ = *10, l = 20, h = 2, d = 5, and g = 1 constant (*unit: *mm)*

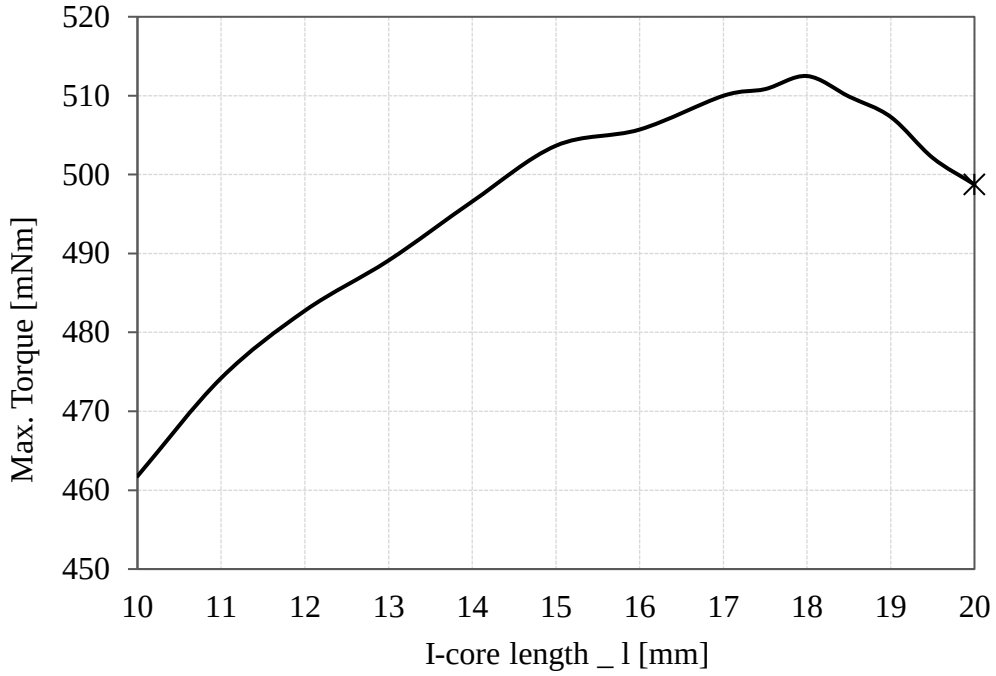

Figure 4. 17. Variation of the maximum torque with different I-core length: $L_T = 40$, $\lambda = 10$, $t = 6$, $h = 2$, $d = 5$, *and* $g = 1$ *constant (*unit: *mm)*

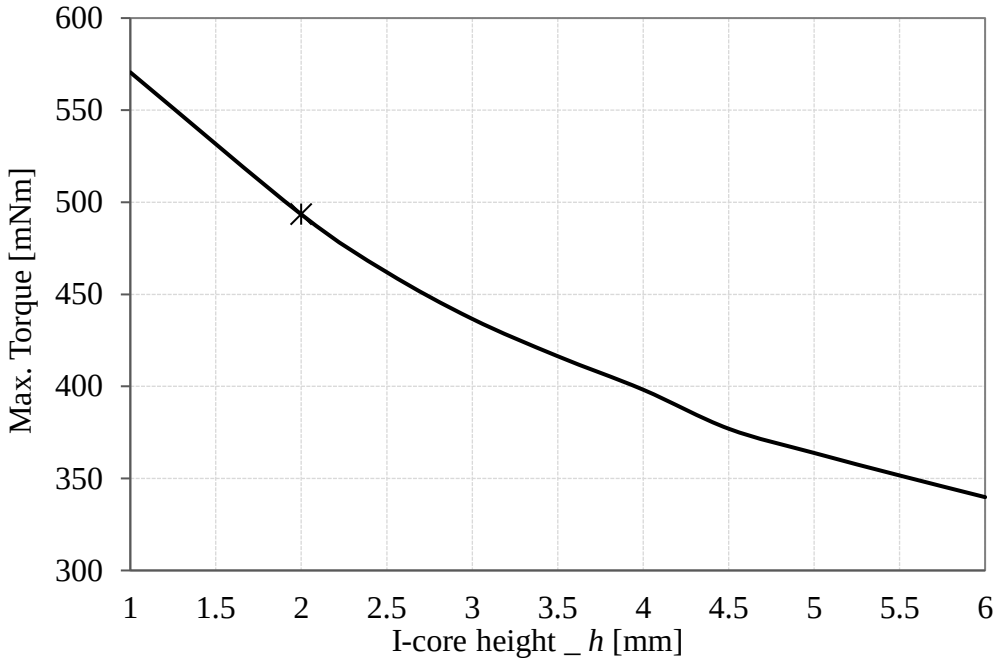

Figure 4. 18. Variation of maximum torque with different I-core heights: $L_T = 40$, $\lambda = 10$, $t = 6$, $d = 5$, *and* $g = 1$ *constant (*unit: *mm)*

4.4 Scaling

Theoretically, the torque and force of the magnetic gear are linearly proportional to the air gap area and active length. The air gap area depends on the air gap length and the rotor radius. If the air gap length is kept at a certain constant value, then the air gap area will depend on the rotor radius. A 3D-FEA that uses rectangular magnets on the translator is employed to verify linear proportionality of the characteristics. The rotor radius, *R*, is increased from 15 mm to 40 mm while the active length is fixed at 40 mm and the magnet thickness is kept constant at 5mm, as shown in Figure 4.19. Similarly, another simulation is carried out with a constant radius of 15mm and the active length, L_{ac}, is changed from 40mm to 100mm. The results present a linear trend for both simulations, as seen in Figure 4.20.

It is assumed that the core-back thickness is sufficient to avoid magnetic saturation and the volume of the active magnets is calculated for comparing torque densities in order to identify which methods lead to a better design. Meanwhile, the core-back space of one phase to another is kept at a certain distance (5 mm in this study) to minimise flux linkage. Obviously, increasing the rotor radius results in an increase in the magnet width on the translator. Thus, the total active volume contributions to torque change can be given by

$$V_{ac} \cong \pi R^2 L_T + 4 \times (h + d + c) l L_T \tag{4.1}$$

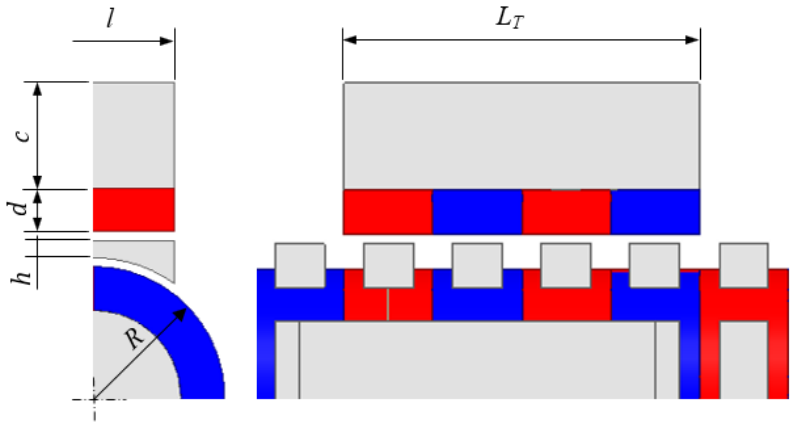

Figure 4. 19. Geometric Parameters of the magnetic gear.

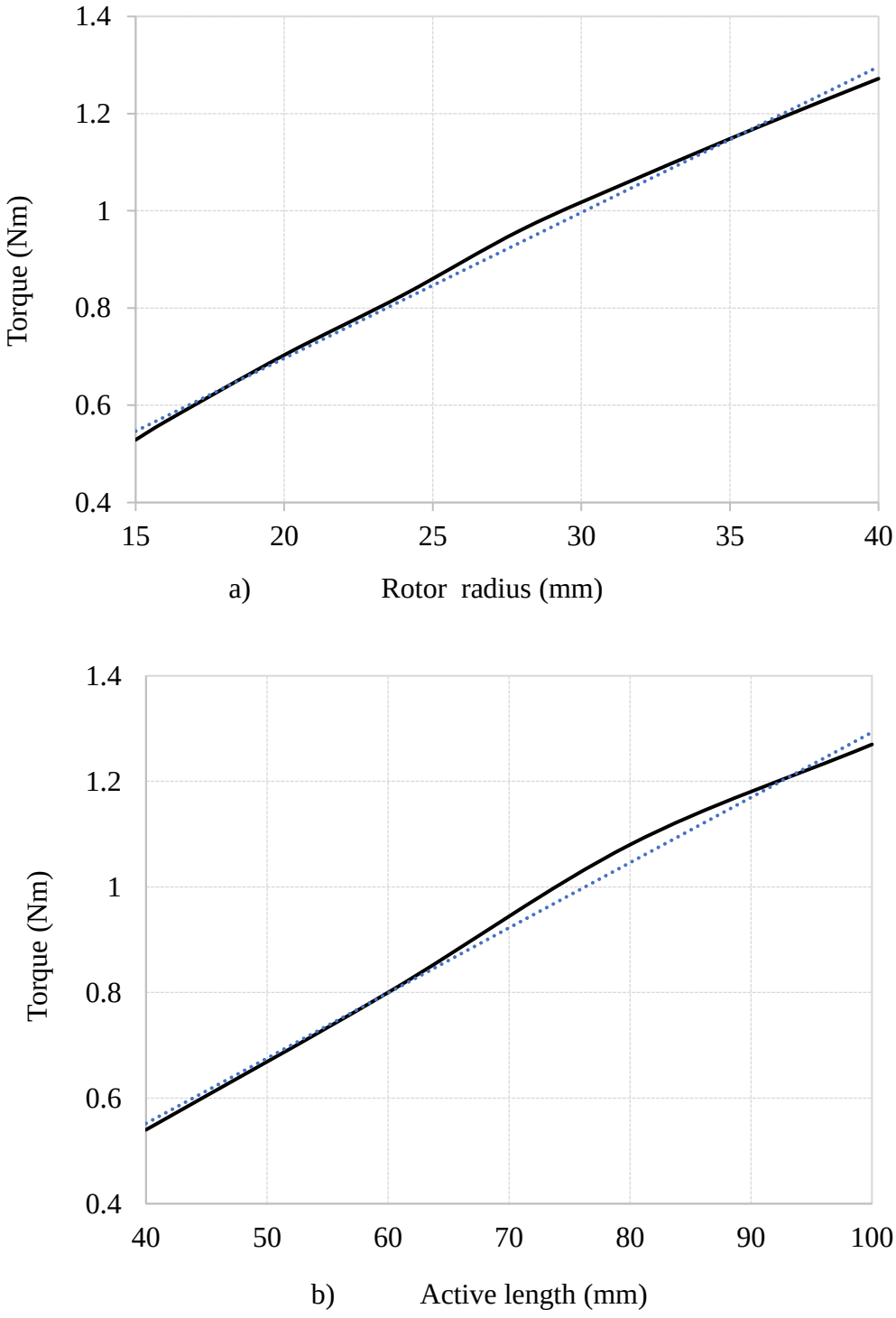

Figure 4. 20. Variation of torque with varying a) rotor radius and b) active length.

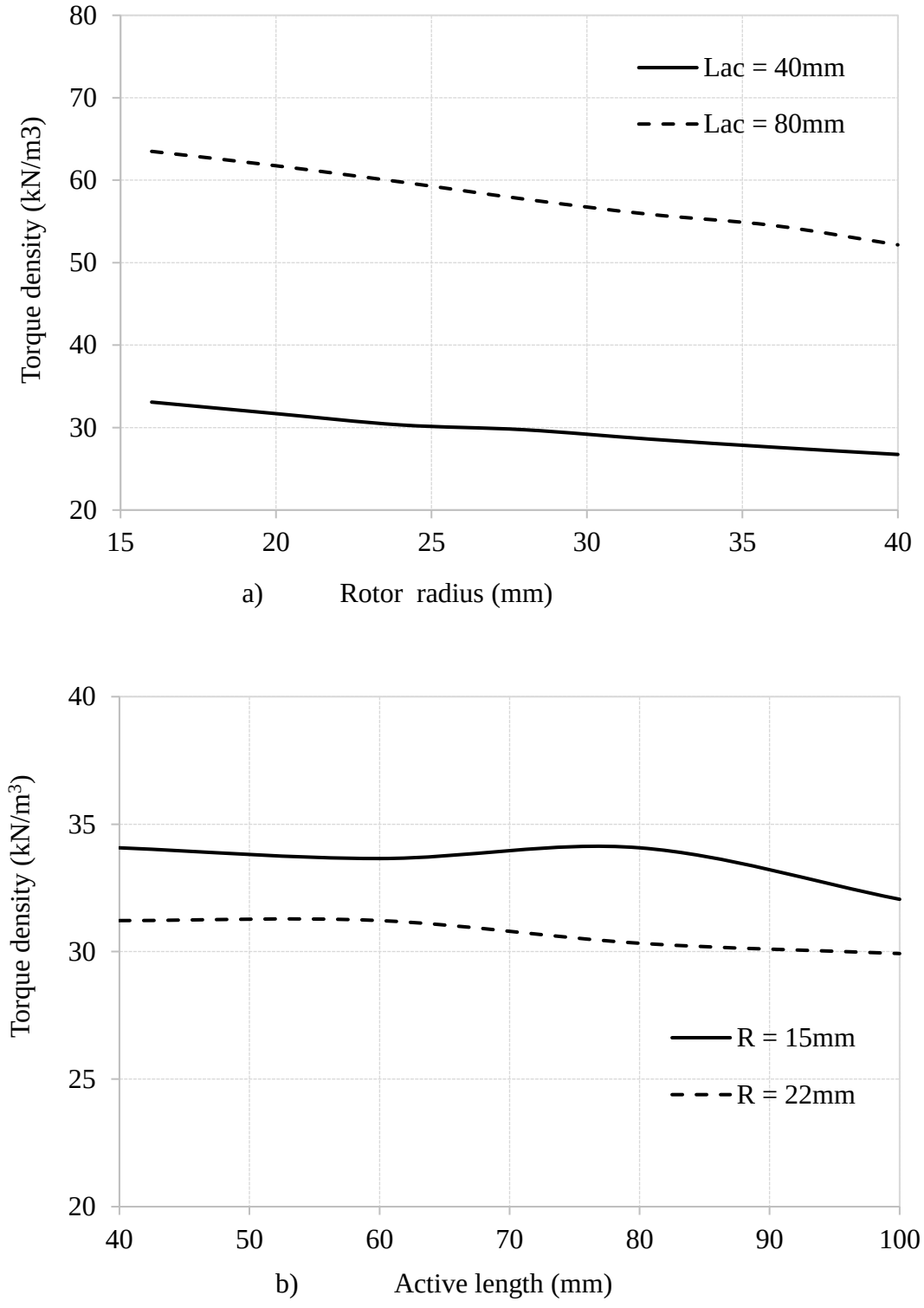

Figure 4. 21. Variation of torque density with varying: a) rotor radius; and b) active length

Based on Eq. (4.1), torque density is calculated by combining with the 3D-FEA results, as seen in Figure 4.21. It is observed that increasing the rotor radius imposes a higher rate of magnet material consumption than in the case of increasing the active length. Thus, increasing the rotor radius results in a slight decrease in torque density while torque density is almost constant with increasing the active length. However, when increasing the active length, the amount of magnet material consumption of the whole device will be related to the stroke when robustness will also be a matter of concern in the design.

4.5 Design analysis

In previous sections, individual parameters were analysed while other parameters were kept fixed in order to find out local optimal values. In this section, a 3D-FEA iterative parameter sweep analysis is implemented to design a globally optimised magnetic gear. As all the parameters in the radial direction are interrelated, only three parameters are analysed to describe the process.

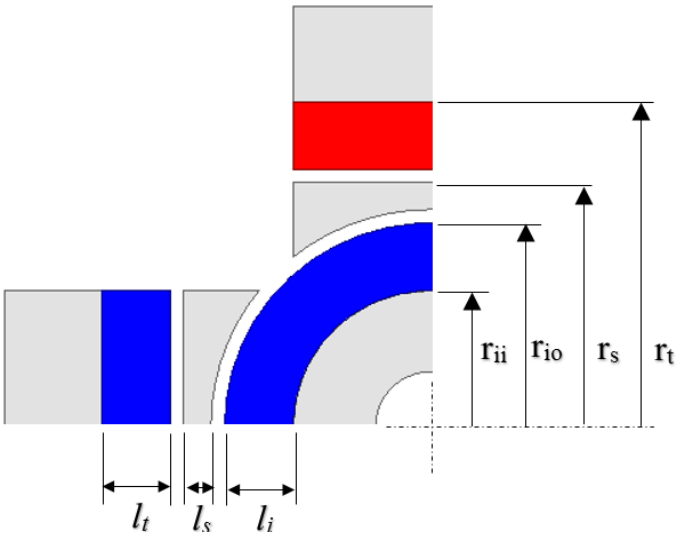

Figure 4. 22. Cross – section dimensional parameters

They are the inner rotor radius, r_{ii}, the outer rotor radius, r_{io}, and the outer dimension of I-cores, r_s, as shown in Figure 4.22. The other geometric parameters, given in Table 2, were kept fixed. The outer dimension of the magnet, r_t, in radial direction is set to 24 mm and the

axial active length of the translator is fixed at L_T = 40 mm. It is assumed that the inner and outer back cores are made sufficiently thick to avoid saturation.

The objective is to maximise the active region volumetric force density, defined as:

$$V = F_t/[\pi r_{io}^2 L_T + 4(r_t - r_{io})L_T l] \quad (4.2)$$

Table 7: Geometric and material parameters

Parameters	Symbol	Value *(mm)*
Magnet width	w	10
Outer dimension of translator magnet	r_t	24
I-core thickness	t	6
Air gap length	g	1
Translator length	L_T	40
Magnet coercity (kA/m)		838
Magnet remanent flux density (T)		1.23
Steel 1008 resistivity (μΩ-cm)		14.2

There are three iterations in the parametric sweep analysis. In iteration I, the inner radius of rotor, r_{ii}, is fixed at 8 mm, and the parametric sweep is carried out for varying outer rotor magnets radius, r_{io} and I-cores outer dimension, r_{to}. The results for a fixed I-core thickness value of 2 mm, that will produce a robust mechanism, are given in Table 7. It is observed that a peak force density is obtained at 2.79 kN/L, and a peak force-per-kilogram magnets is reached at 0.58 kN/kg with (r_{ii}, r_{io}, r_{to}) = (8, 16, 19) mm. Similar analysis for the iteration II is carried out but the inner radius of rotor, r_{ii}, is fixed at 10 mm. The results in Table 8 show that a peak force density is obtained at 2.75 kN/L, and a peak force-per-kilogram magnets is reached at 0.64 kN/kg with (r_{ii}, r_{io}, r_{to}) = (10, 16, 19) mm. A pattern analysis in iteration III is carried out for the inner radius of rotor, r_{ii}, fixed at 12 mm. The peak force density is reduced slightly at 2.63 kN/L, but the peak force-per-kilogram magnets is increased in comparison with the previous iterations to 0.75 kN/kg with (r_{ii}, r_{io}, r_{to}) = (12, 16, 19) mm.

Table 8: Iterations of radial dimensions in the design optimisation process

Iteration number		I				II				III			
Outer dimension, r_t		24				24				24			
Rotor	Outer radius, r_{io}	15	15.5	16	17	15	15.5	16	17	15	15.5	16	17
	Inner radius, r_{ii}	8	8	8	8	10	10	10	10	12	12	12	12
I-core outer dimension, r_s		18	18.5	19	20	18	18.5	19	20	18	18.5	19	20
I-core thickness, l_s		2	2	2	2	2	2	2	2	2	2	2	2
Rotor magnet thickness, l_i		7	7.5	8	9	5	5.5	6	7	3	3.5	4	5
Trans magnet thickness, l_t		5	4.5	4	3	5	4.5	4	3	5	4.5	4	3
Trans force, F_t , N		156	159	161	160	125	156	159	159	137	146	152	155
Rotor torque, T_r , mNm		578	587	602	664	553	577	591	596	501	536	563	579
Volumetric force density, kN/L		2.73	2.78	2.79	2.7	2.2	2.7	2.75	2.7	2.4	2.54	2.63	2.6
Force per–kg magnet, kN/kg		0.57	0.53	0.58	0.5	0.53	0.6	0.64	0.64	0.68	0.73	0.75	0.62
Volumetric torque density, kNm/m^3		10.1	10.3	10.4	11.3	9.7	10.1	10.2	10.1	8.8	9.3	9.7	9.8
Torque per – kg magnet, Nm/kg		2.1	1.97	2.2	2	2.3	2.2	2.3	2.4	2.55	2.7	2.79	2.3

Figure 4.23 shows the variations of the translator force versus the outer rotor magnets radius, r_{io}, for iteration I, when the inner rotor magnet radius, r_{ii} = 8 mm, and for different outer I-core dimensions, r_s. It is shown that increasing the outer rotor magnet radius increases the translator force. The same pattern is observed in the case of reducing the outer I-cores dimension. In other words, decreasing the outer I-cores dimension increases the translator's magnet thickness, l_t, and also reduces I-cores thickness, l_s. It was proved in the previous section that the I-cores can be removed in order to reduce the two air gap lengths to one, which subsequently increases flux, torque and force values. However, the I-cores are needed

when bar magnets are used on the translator in order to interface the rectangular geometry of the translator magnets with the cylindrical rotor. Thus, I-cores thickness should be considered as a trade-off between the maximum force and torque and the stiffness of the mechanism.

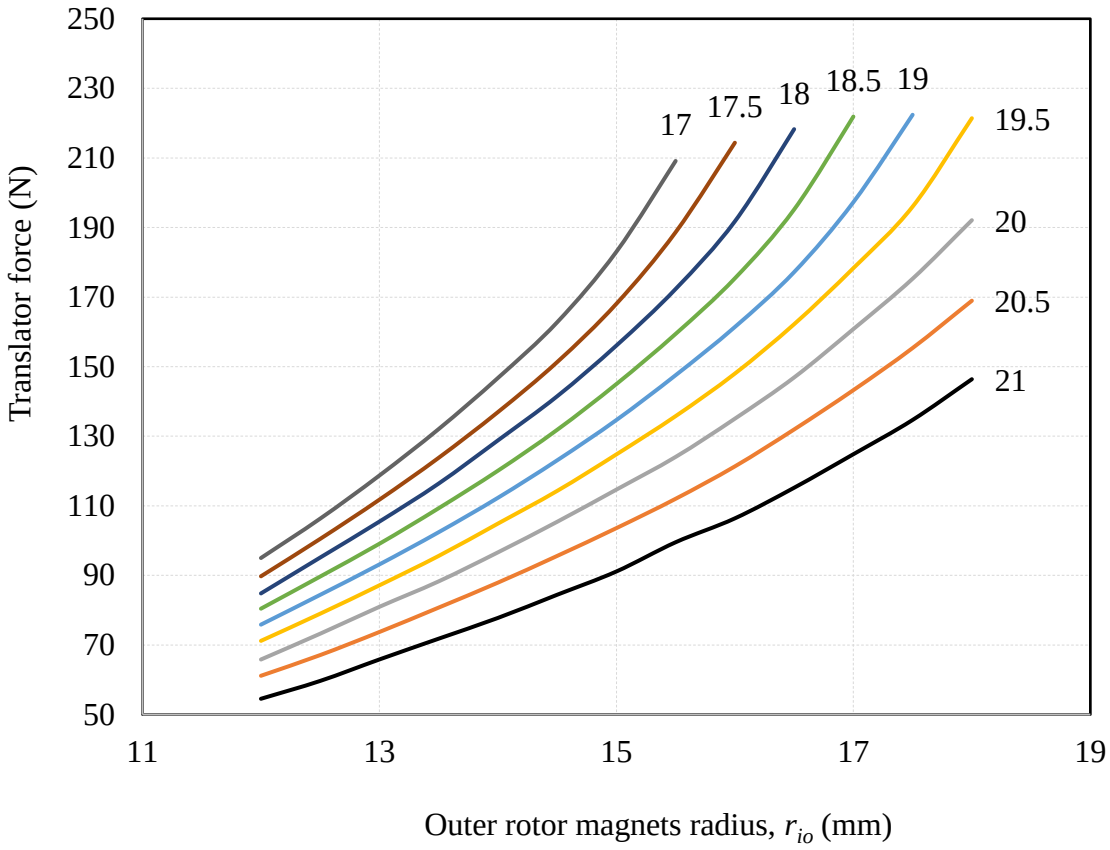

Figure 4. 23. Variations of translator force versus the outer rotor magnets radius, r_{io}, for iteration I, inner rotor magnet radius, r_{ii} = 8 mm, and varying outer I-core dimensions, r_s.

In Figure 4. 24, the trade-off between volumetric force density and force-per-kg of the magnet material is presented as a function of the inner rotor magnet radius while the outer rotor magnet radius and I-cores' outer dimension are fixed. It is observed that increasing the inner rotor radius decreases the volumetric force density but by increasing the force per-kg magnets up to a certain value, it declines dramatically. Based on these results, a magnetic gear can be obtained depending on whether we choose to maximise the force density or the volumetric mass.

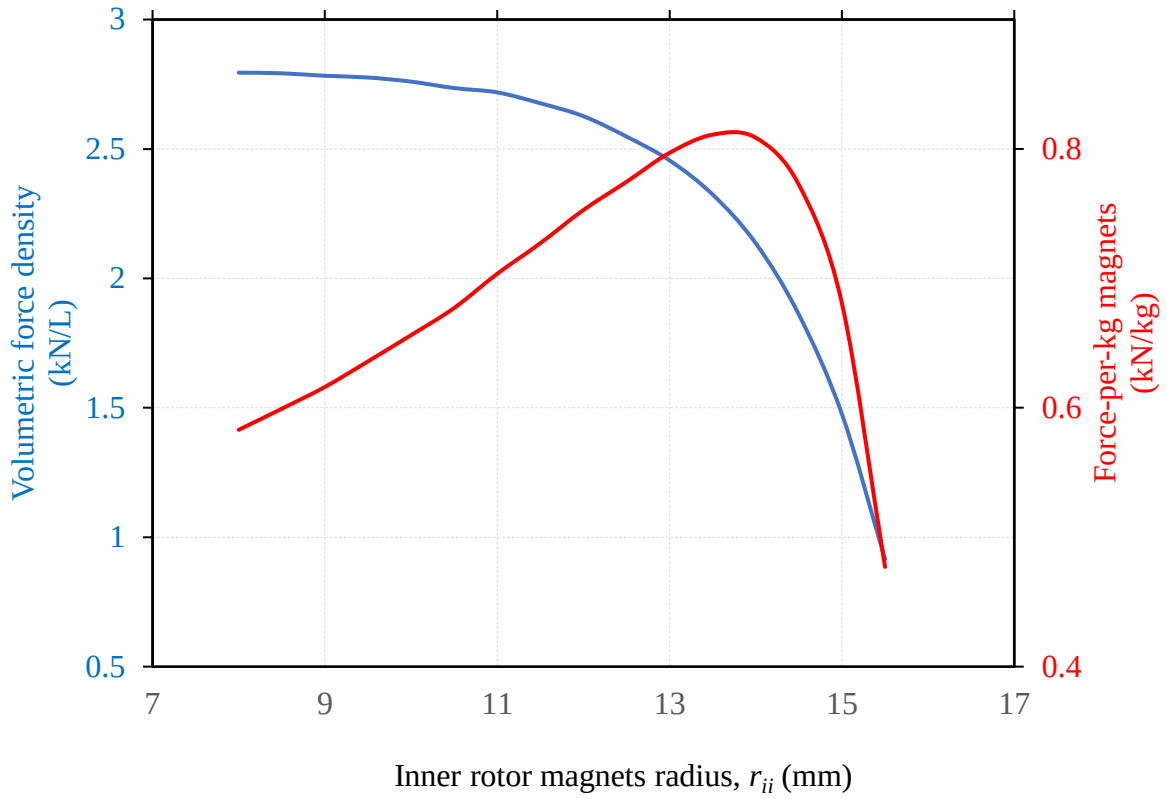

Figure 4. 24. The trade-off between volumetric force density and force-per-kg magnets as function of inner rotor magnets radius, r_{ii}, for (r_{io}, r_s) = (16, 19) mm.

4.6 Summary

In this chapter, design optimisation of the magnetic gear was studied numerically, and results were presented. Two and three dimensional FEA were also employed to investigate the effects of principal geometric parameters on performance. The 2D-FEA gave a general understanding of each component that effects the characteristics; however, it was not able to compute the radial components of flux. The 3D-FEA accounted for all components of flux in a reliable manner and accurate force and torque characteristics were also computed. In the design a rectangular magnet was used on the translator, I-cores were used as a function of an interfacing geometry of the translator magnets to the cylindrical rotor. Unless the translator magnets are used as arc segments, they could be removed to eliminate the reluctance and hence replace the two air gaps with one.

Through 2D and 3D FEA simulation results, it was observed that principal geometric parameters such as the air gap length, I-cores' dimensions, pole pitch, etc., had huge impacts on the performance of the magnetic gear, and thus, they need to be accounted for in a design optimisation process. The air gap length needs to be selected in a way that the right balance between maximising forces and the fabrication feasibility is hit. Furthermore, I-cores' dimension associated with flux linkage, leakage and core losses, contributes to a higher reluctance. The optimum values were found while rotor radius and pole pitch were fixed at 15 mm and 10 mm respectively. They were; magnet thickness, d = 6 mm; I-core length, t = 5 mm; and I-core width, l = 18 mm.

A global optimisation was implemented in the radial direction (cross section) with an iterative parameter sweep analysis. Because the parameters are interactive in the radial direction, only three radial parameters were used to constrain the analysis. The outer radial dimension of the translator was fixed at 24 mm. The parametric sweep analysis accounted for the rotor radius and outer radial dimension of the I-core while the inner dimension of the rotor magnet was set in turn to 8, 10 and 12 mm. the results in Table 8 showed that a peak force density is obtained at 2.79 kN/L with (r_{ii}, r_{io}, r_{to}) = (8, 16, 19) mm, and a peak force-per-kilogram magnets is reached at 0.75 kN/kg with (r_{ii}, r_{io}, r_{to}) = (12, 16, 19) mm. Also, there was a trade-off between maximising force density and minimising the volumetric mass by sweep is the inner rotor radius while other parameters was used in iteration I with (r_{io}, r_s) = (16, 19) mm. This is related to key parameters such as magnet thickness, active length, pole pitch and radius of the rotor. It was concluded that a small rotor radius may give a more compact structure but requires a higher axial length and a larger pole pitch with a higher force and torque results in a lower gear ratio.

When considering the torque and force at different positions of the translator, the value is not constant, and it is so-called the ripple torque and force. Figure 4.25 shows the ripple torque and force of the proposed magnetic gear as given the rotor radius is 50mm and the active length is 120mm. When the translator moves 20 mm, it is equivalent with a revolution of the rotor. It is observed from the graph that the variations of torque value is from 19.79 Nm to 20.87 Nm (around 6%), and the variations of force value is from 2.96 kN to 3.39 kN (around 13%).

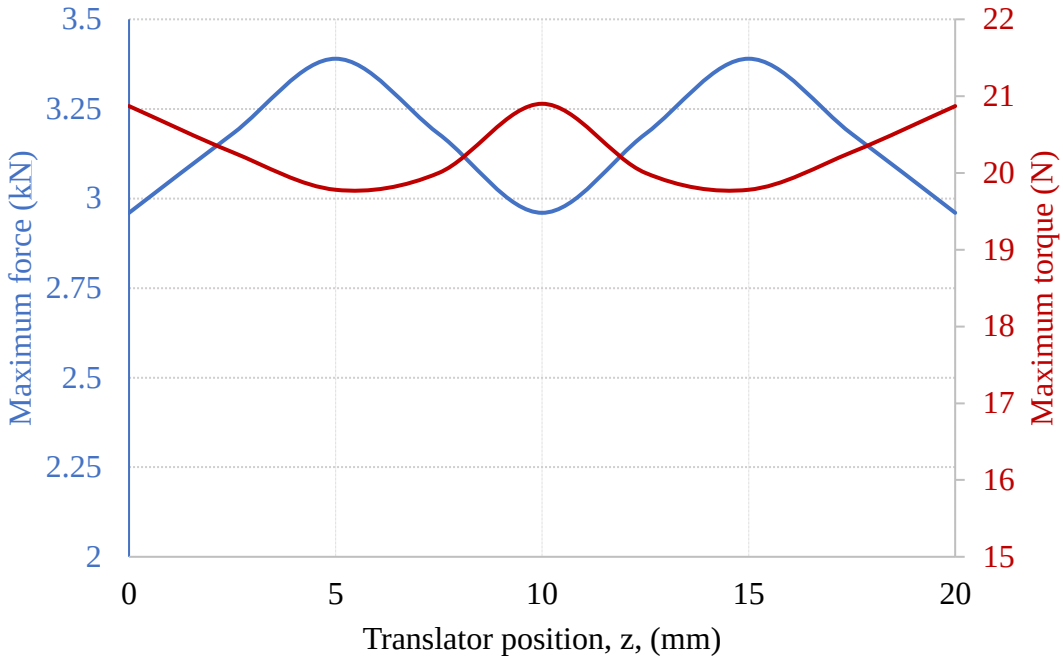

Figure 4. 25. Ripple torque and force of the magnetic gear: the rotor radius is 50 mm and the active length is 120 mm.

Chapter 5 Prototype of the linear to rotary magnetic gear

5.1 Introduction

The concept of linear to rotary magnetic gear based on transverse-flux machine was proposed. In previous chapters, numerical analysis was developed by using finite element analysis to investigate the performance of the proposed magnetic gear. Based on 2D and 3D FEA models, the effects of magnet thickness, ferromagnetic pole-pieces' dimensions and air gap length, were determined. To validate the ideas behind the concept, a demonstrator is designed, built and tested. Firstly, a prototype is designed based on the FEA simulations. The aim of testing is to prove working principles and measure the static state of the device. Therefore, a simple demonstrator is built with a long rotor and a translator that moves back and forth with a fixed stroke that is related to the rotor's length. In order to fabricate the prototype, the thickness of the rotor magnet is obtained from a commercial supplier. The parameters of the prototype are given in Table 9.

Figure 5.1 shows a 3D model of the prototype. In this model, ferromagnetic pole-pieces are arranged along the rotor and are held stationary. The magnets on the rotor do not skew and hence, the arrangement may increase the cogging torque of the rotor. In order to calculate the static torque of the rotor and the force of the translator, a magnetic software Ansys Maxwell is used. Steel_1008 and FeNd35 in Ansys material library are used as materials for ferromagnetic pole-pieces and permanent magnets, respectively. A mesh is applied with the inside length of 2mm. The model is placed into an air environment with the surrounding volume being threefold of the model. To obtain the response characteristics of the prototype, the translator is held stationary while the rotor is rotated 360 degrees around its radial axis.

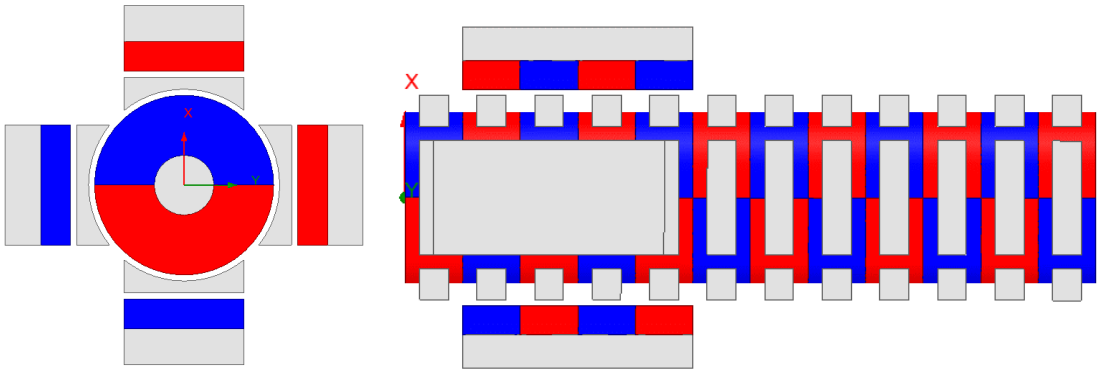

Figure 5. 1. A 3D-FEA model of the prototype

5.2 Prototype fabrication

Figure 5.2 shows detailed isometric view of the mechanical design of the prototype. The prototype includes rotor, translator, ferromagnetic pole-pieces and the supporting frame. The rotor is supported by two end plates with holding bearings to allow rotational motion. The translator moves along the rotor's length by using two sliders that maintain a fixed position between the rotor and translator. The ferromagnetic pole-pieces are held stationary by a frame that consists of aluminium plates and four shafts that keep the assembly together. This frame is fixed to the end plates, as can be seen in Figure 5.3. A bottom plate supports all the parts in order to enable measuring devices such as the load cells to be added. If the ferromagnetic pole-pieces are assembled in advance, then it will be difficult to install the rotor inside due to the attraction force between the permanent magnets on the rotor and the ferromagnetic pole-pieces. It was also noted that the permanent magnets on the rotor should be installed properly to ensure that the poles of the magnets align with each other.

In this prototype, N42 Neodymium ring magnets that were used for the rotor were purchased from a commercial supplier. The poles of the magnet are polarised and built in a solid part. The N42 Neodymium rectangle magnets on the translator, shown in Figure 5.4, were supplied by Expert Magnet Ltd.

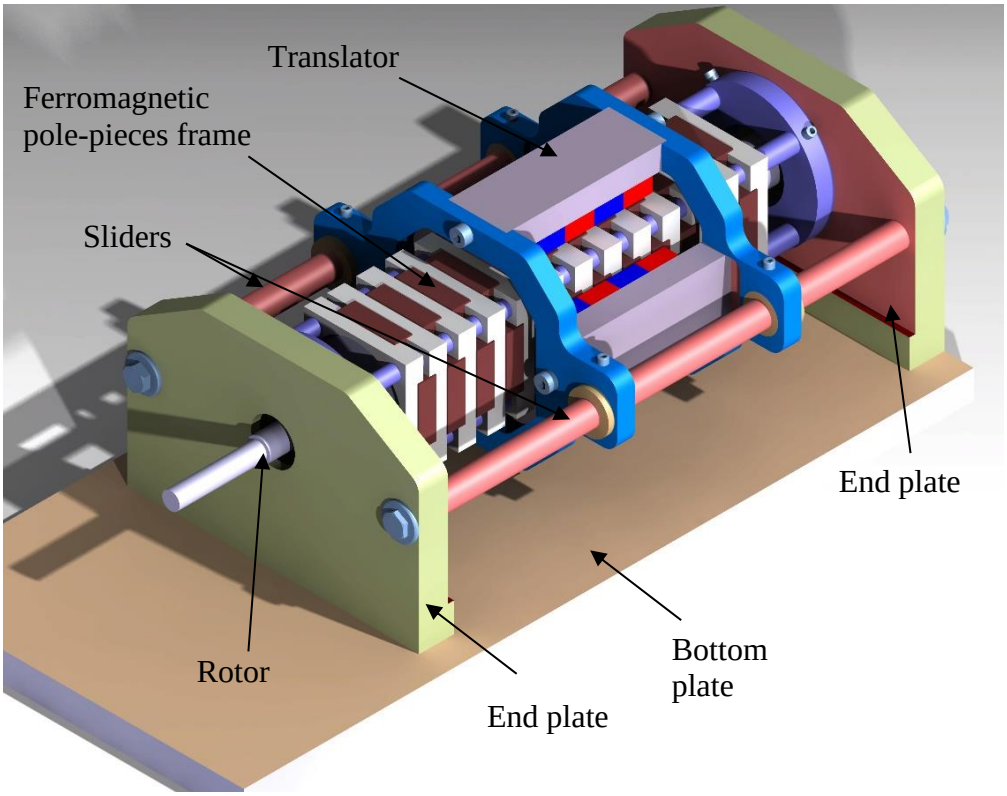

Figure 5. 2. 3D isometric view of the prototype

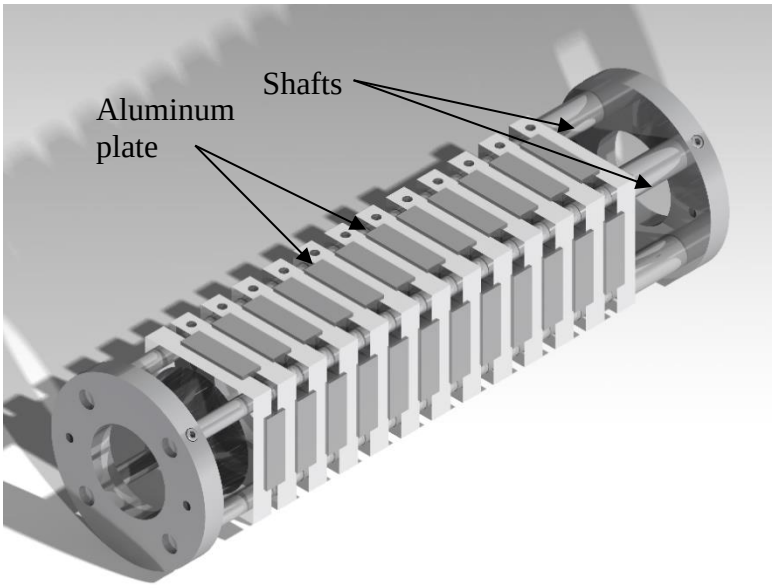

Figure 5. 3. A frame to hold the ferromagnetic pole-pieces

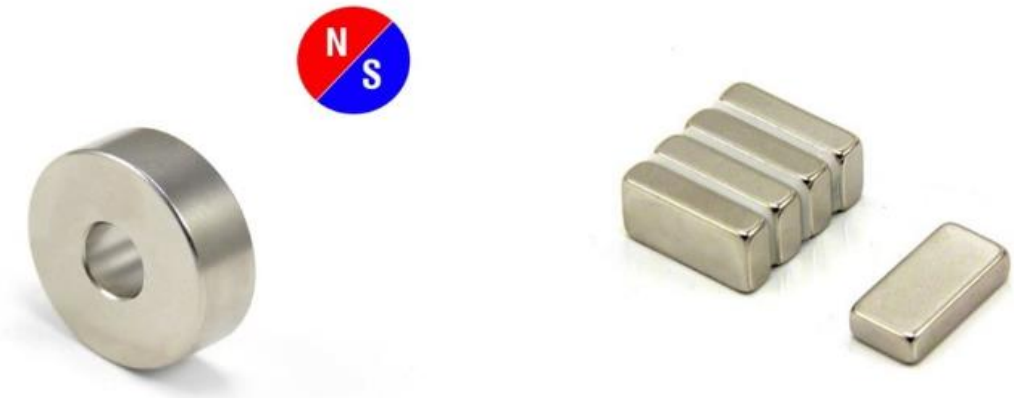

a) b)

Figure 5. 4. Magnets for the prototype: a) rotor magnets and b) translator magnets

Table 9 : Parameters of the prototype

Parameters	**Symbols**	**Value**
Number of pole pitch on rotor	N_r	12
Number of pole pitch on translator	N_t	4
Pole pitch	τ_P	10 *(mm)*
Magnet width on translator and rotor	w	10 *(mm)*
Magnet thickness on translator	h_m	5 *(mm)*
Magnet thickness on rotor	h_r	10 *(mm)*
Outer radius of magnet on rotor	R	15 *(mm)*
Thickness of ferromagnetic pole-pieces	h_t	2 *(mm)*
Width of ferromagnetic pole-pieces	t	6 *(mm)*
Thickness of core-back	h_c	6 *(mm)*
Air gap	g	1 *(mm)*

To avoid magnetic field interference that occurs between parts, all parts and fasteners are made of aluminium or stainless-steel, with the exception of the rotor's shaft, ferromagnetic pole-pieces and the core-backs that are made from mild steel (C45 steel). A demonstrator of the linear to rotary magnetic gear is fabricated, as shown in Figure 5.5.

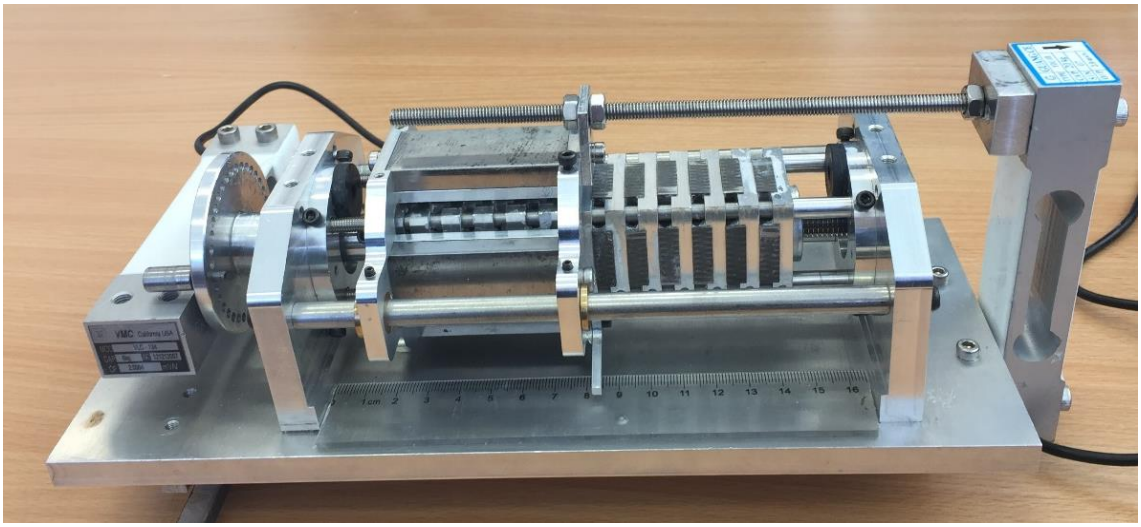

Figure 5. 5. The demonstrator of the linear to rotary magnetic gear

5.3 Experiment set up

The aim of this experiment is to prove the working principle of the prototype and measure the static torque on the rotor and the static force on the translator. In the prototype, a nut screw mechanism is used to move the translator back and forth and therefore the rotor rotates by the generated torque. Figure 5.6 shows the nut and screw installation. The translator can be pushed and pulled to move on the sliders along the length of the rotor (i.e., the stroke length), while the rotation of the rotor will be observed.

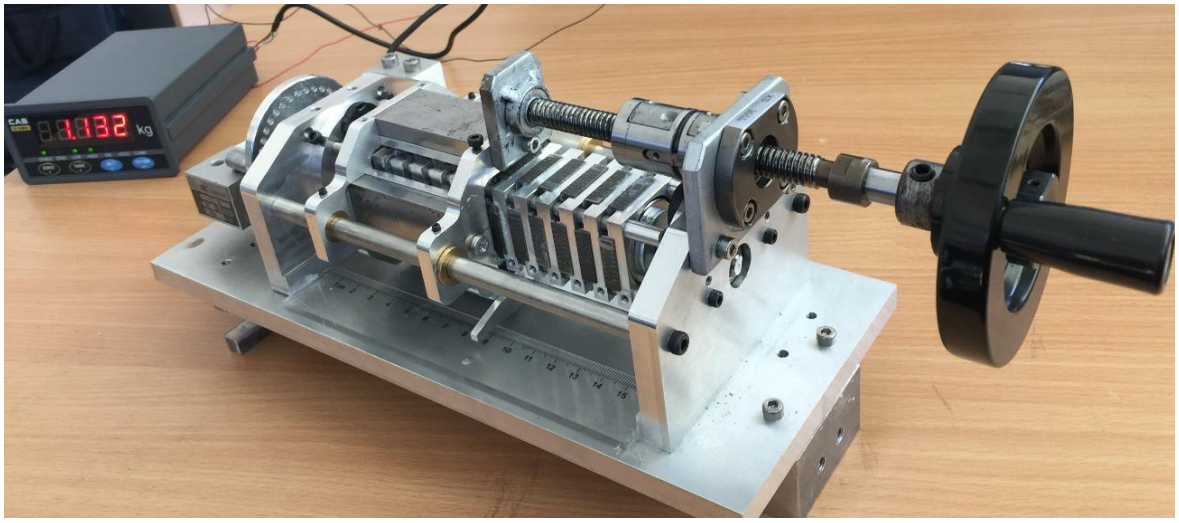

Figure 5. 6. Nut and screw mechanism to move the translator

To measure the static torque and force, two load cells from VMC California Ltd with the capacities of 6kg and 20kg, used for the rotor and the translator, respectively, were installed on the demonstrator, as can be seen in Figure 6.7. A load cell digital indicator by CAS, shown in Figure 6.8, is used to display the rotor torque and force of the translator along that rotor's axis. On the output shaft of the rotor, a disc is placed with circular holes drilled in step of 10 degree around it, that determine the resolution of each measuring step.

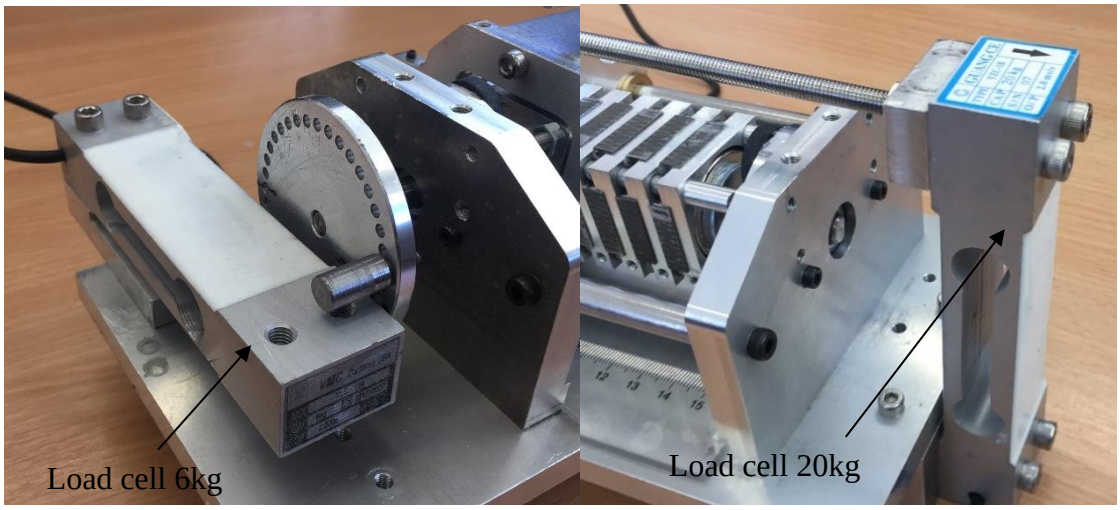

Figure 5. 7. Load cell installation for measuring a) torque and b) force along the rotor's axis

Figure 5. 8. Load cell digital indicator for displaying the measured torque and force values

5.4 Experimental results

Firstly, the working principle of the prototype was checked in order to confirm the concept of the linear to rotary magnetic gear, derived from the transverse-flux machine. Figure 5.9 shows the installation of the testing rig. It was observed that when the translator moves to the right, the rotor rotates clockwise and the reverse rotary motion happens when the translator

reverses direction. It was also observed that the rotor rotates a complete revolution when the translator moves a length of two pole pitches.

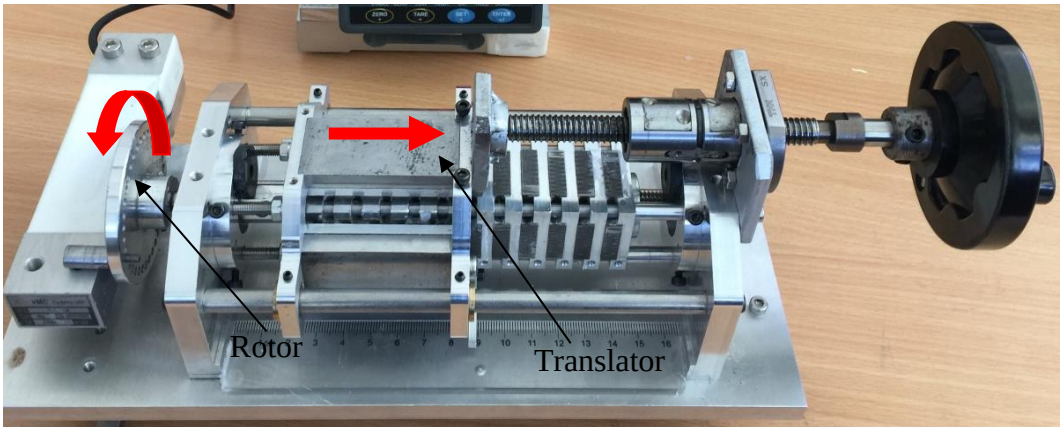

Figure 5. 9. Moving the translator to show working principle

Next, the static torque of the rotor was measured while the translator was kept fixed. In this test, phase 1 of the translator was aligned with the rotor, meaning that phase 2 was unaligned. The measured rotor torque results are shown in Figure 5.10. It was observed that a maximum torque of 0.47 Nm occurred at the position of the rotor corresponding to 70 degrees. Obviously, the static torque is smaller than the simulation results which is due to the difference in materials used for the magnets and the core-back in the prototype.

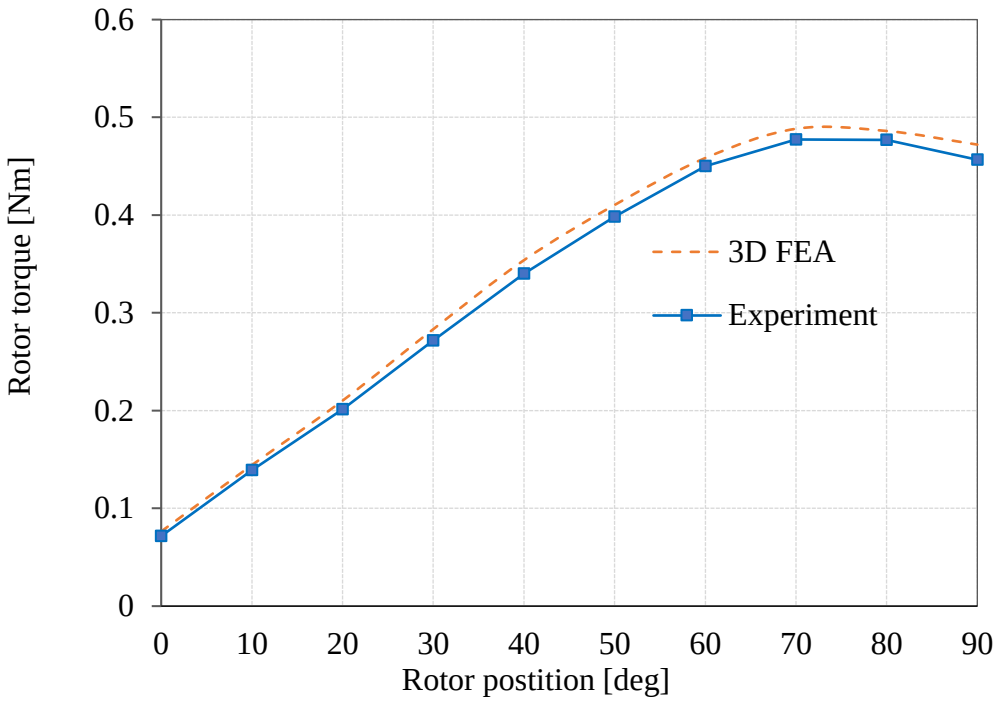

Figure 5. 10. Rotor torque in comparison between simulation and experiment

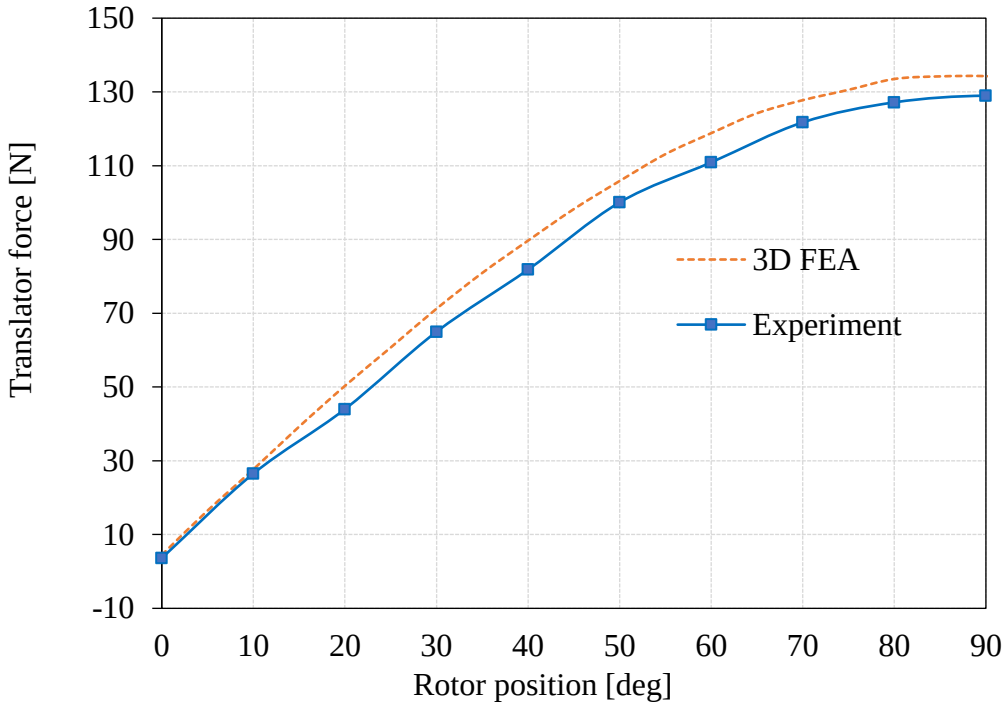

Figure 5. 11. Translator force in comparison between simulation and experiment

Other measurements were carried out by moving the translator while the rotor was kept fixed. For the initial position, magnets on the rotor and translator were aligned, and hence the rotor torque was zero. When the translator moves, the rotor torque is recorded and the maximum rotor torque was achieved in the middle of the pitch, as can be seen in Figure 5.11. The FEA values are slightly higher than the experimental values, which is probably due to the uncertainty of the magnet characteristics, and effect of mechanical tolerances when positioning the magnets and the I-cores – this matter will be investigated further.

The torque peaks at 70 degrees, not 90 degrees as expected, which is due to a combination of saturation of the I-cores and cogging torque. The force peaks at nearly 90 degrees. The characteristics in Figure 6.11 suggest that ratio of torque per force is largely independent of the load up to about 60 degrees. However, at higher angles, we observe significant load dependency. In practice, this will be acceptable as gears are not usually operated near to their pull-out loads.

5.5 Summary

The realisation of the idea of linear to rotary magnetic gear based on transverse-flux machine was presented in this chapter. A demonstrator was designed, built and tested. Intuitively, it operated as prediction in the theory. A prototype with the rotor diameter of 30 mm generated a maximum torque of 0.47 Nm. It was also shown that the rotor makes a complete revolution when the translator moves by two pole pitches. Also, observation of the torque curve indicates that the device works quite smoothly. However, the measured rotor torque is quite small in comparison with the simulation results. This may be due to different materials being used for the magnets and core-back in the prototype and simulations.

Chapter 6 Conclusion

In this thesis, the idea of a linear to rotary magnetic gear was presented. The working principle and the relevant theories were analysed and discussed. A demonstrator was designed and built for conducting experiments in order to confirm the validity of the concept. The following sections contain brief summaries of all the chapters in this thesis.

Chapter 2 Magnetic field theory

In this chapter, basic magnetic field theories were reviewed to show the most relevant methods for calculating the magnetic field in an airgap. Analytical analysis provides an exact solution and a good insight into the behavior of simple models while finite element analysis provides reliable results and allow the modelling of more complicated geometries, even though they are calculated by using approximate solutions. For those reason, FEA method is used intensively throughout this thesis to predict the performance characteristics.

Chapter 3 A linear to rotary magnetic gear

This chapter presented the concept of a rotary to linear magnetic gear, the configuration of which is based on the transverse flux machine topology. It was shown that the magnet arrangement on the translator forms a discretised helix. In other words, the proposed magnetic gear is similar to the helical magnetic gear in terms of working principle. However, I-cores are needed when bar magnets are used on the translator to interface with the rectangular geometry of the translator to the cylindrical rotor. Through a specific configuration, the gear ratio of the proposed magnetic gear was estimated and was shown that it depends on the pole pitch and the number of poles on the rotor. By using three-dimensional finite element analysis, the torque and force characteristics were obtained. The torque peaks at 70 degrees, not 90 degrees as expected, which is due to a combination of saturation of the I-cores and the cogging torque. The force peaks at nearly 90 degrees. It was observed that, in the case of using rectangular magnets on the translator, the maximum rotor

torque was 0.52 Nm while the translator force occurred at 142 N. Furthermore, the cogging torque was also estimated and was shown to be small in comparison with the rated torque, i.e., it was %8 of the rated torque. To develop a deeper understanding of the proposed configuration, different geometries of the parts such as the core-back and the I-cores were examined. They imposed a large effect on the characteristics when the arrangement is not proper such as the i-cores being in a single combination. Moreover, a comparative magnetic gear design was examined for comparison with its counterpart helical structure. By using the same geometrical dimensions, the proposed magnetic gear shows inferior characteristics than those shown by the helical structure. This may be due to the contribution of magnets that produce the torque. Thus, from the 3D FEA results, it is shown that in the helical magnetic gear, all the magnets on the translator contribute to producing torque while only half the magnets on the translator play the same rule in the proposed design. Based on the proposed magnetic gear's configuration, a different pole pitch topology is also introduced. From 3D FEA simulations, the characteristics of this configuration are obtained and shown to be far inferior in comparison with a helical structure in which the rotor's magnets and ferromagnetic pole-pieces are skewed.

Chapter 4 Design optimisation of a magnetic gear

This chapter assessed the performance improvement of the proposed magnetic gear though a design optimisation process. A local optimisation was carried out by using 2D and 3D FEA models to investigate the effect of the basic design variables such as thickness of the magnets, the dimensions of the ferromagnetic pole pieces and the air gap length. It was shown that increasing the magnet thickness resulted in increased interactive force, but it was saturated upon a certain point. In other words, the interactive force increases by a small amount until the magnet thickness increases up to a certain value. In addition, the thickness of the ferromagnetic pole pieces gave a maximum interactive force at a certain proportion with the specific pole pitch length. For example, if the pole pitch length is 10 mm, a maximum torque can be obtained at the ferromagnetic pole pieces' thickness is about 6 mm and the height is at 2 mm. It was also recognised that smaller values of the airgap length result in larger interactive forces. However, fabrication of a very small airgap length is a real challenge. The scaling of the proposed magnetic gear was also investigated to compare the torque densities

between the options of a longer stroke or a bigger radius prototype. An optimisation process was implemented in the radial direction (cross section) using an iterative parameter sweep analysis approach. The parametric sweep analysis accounted for the rotor radius and the outer radial dimension of the I-core. It was concluded that a small rotor radius may give a more compact structure but requires a higher axial length and a larger pole pitch with a higher force and torque results in a lower gear ratio.

Chapter 5 Prototype of linear to rotary magnetic gear

In this chapter, a demonstrator was designed, fabricated and tested of the proposed magnetic gear that relied on the FEA simulation results. It was shown that the prototype worked properly and its performance agreed with the theoretical predictions. The measured rotor torque was 0.47 Nm for a given 30 mm rotor's diameter. However, a ripple force occurred when the translator moved along the rotary's axis. In other words, the magnetic force of the translator was varied during its movement. This caused a descretised form of the magnets on the translator that created a rough movement of the translator.

Chapter 7 Future work

7.1 Overview

The studies presented in this thesis has revealed several potential aspects for further work and investigation which are discussed below:

The topology of the proposed magnetic gear was developed from a transverse-flux machine. However, when the final version of the magnetic gear was obtained in chapter 3, in which the rotor and translator was unrolled, and it looked like a helical magnetic gear, but in a discretised helix. Three-dimensional finite element analysis was used to calculate force and torque characteristics. The results shown that a ripple force occurred when moving the translator. Thus, the number of poles, *P*, in the radial direction should be considered to minimise the ripple force by the effect of the helical form of the translator on the characteristics.

A comprehensive finite element analysis was carried out of the two-dimensional and three-dimensional calculations in Chapter 4. The finite element analysis allowed machine designers to have very accurate solutions for the air-gap magnetic field even considering the non-linear behaviour of materials. Therefore, numerical methods are very useful tools for the validation and the refinement of the final design. Analytical method, however, gives a deep insight structure for an initial design and provide tools for subsequent parametric analysis. In the future work, an analytical calculation should be implemented to compare to 3D FEA. In addition, I-cores loss calculation is needed to get a better design. The I-cores losses are mainly due to eddy currents and leakage. Design optimisation implemented for I-cores' dimension in Chapter 4 that decreasing leakage occurred between adjacent parts. The remaining problem of eddy current loss can be solved through choosing the magnetic material property. The eddy current loss is caused when the lines of flux pass through the core, inducing electrical currents in it. These currents are called eddy currents and produce heat in the core. If the electrical resistance of the core is high, the current will be low; therefore, a

feature of low-loss material is high electrical resistance. However, a high electrical resistance restricts flux lines get through then less effectiveness of the excitations. The trade-off between effectiveness and eddy current loss becomes a problem in the I-cores loss calculation.

After all issues mentioned above have been solved, a design guideline process for the proposed magnetic gear should be generated in order bring the design into the real applications. The potential applications of the magnetic gear can be in harvesting systems, non-contacted place like medical devices.

7.2 Dynamic modelling of the magnetic gear

7.2.1 Analytical model

In this section, the magnetic gear dynamic behaviour is described through a nonlinear analytical model. Figure 7.1 illustrates the magnetic gear in which arc segment magnets on the translator are used. As mentioned in chapter 3, the I-cores can be removed to eliminate the associate core losses and replace the two gaps with one, which increases flux, force and torque. Figure 7.2 shows the force and torque characteristics of the magnetic gear while the parameters are given in Table 10. It is observed that there are two equilibrium points which refer to the curve profile when they cross the zero-horizontal line at two points ($\theta =$ 0 and 180 degrees).

The equilibrium point at zero degree of the rotor position corresponds to the relative position of the rotor and translator in which magnets of the same polarity are fully aligned, i.e., a stable equilibrium point. The equilibrium point at 180 degrees of the rotor position, however, is an unstable equilibrium point because the relative position of the rotor and translator in which magnets different polarity direction and are fully unaligned.

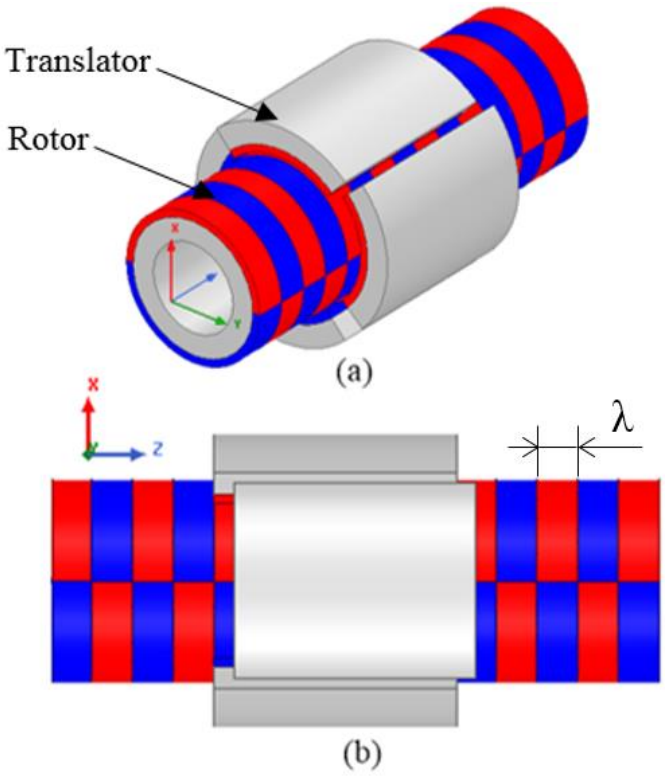

Figure 7. 1. View of a linear to rotary magnetic gear; (a) 3D view, and (b) side view

Table 10: Geometric and material parameters of magnetic gear

Parameters	Symbol	Value	Units
Magnet thickness	*d*	5	*mm*
Air gap length	*g*	1	*mm*
Translator length	L_T	60	*mm*
Rotor radius	*R*	50	*mm*
Pole pitch	λ	20	*mm*
Magnet coercity		838	kA/m
Magnet remanent flux density		1.23	T
Core-back material steel 1020			

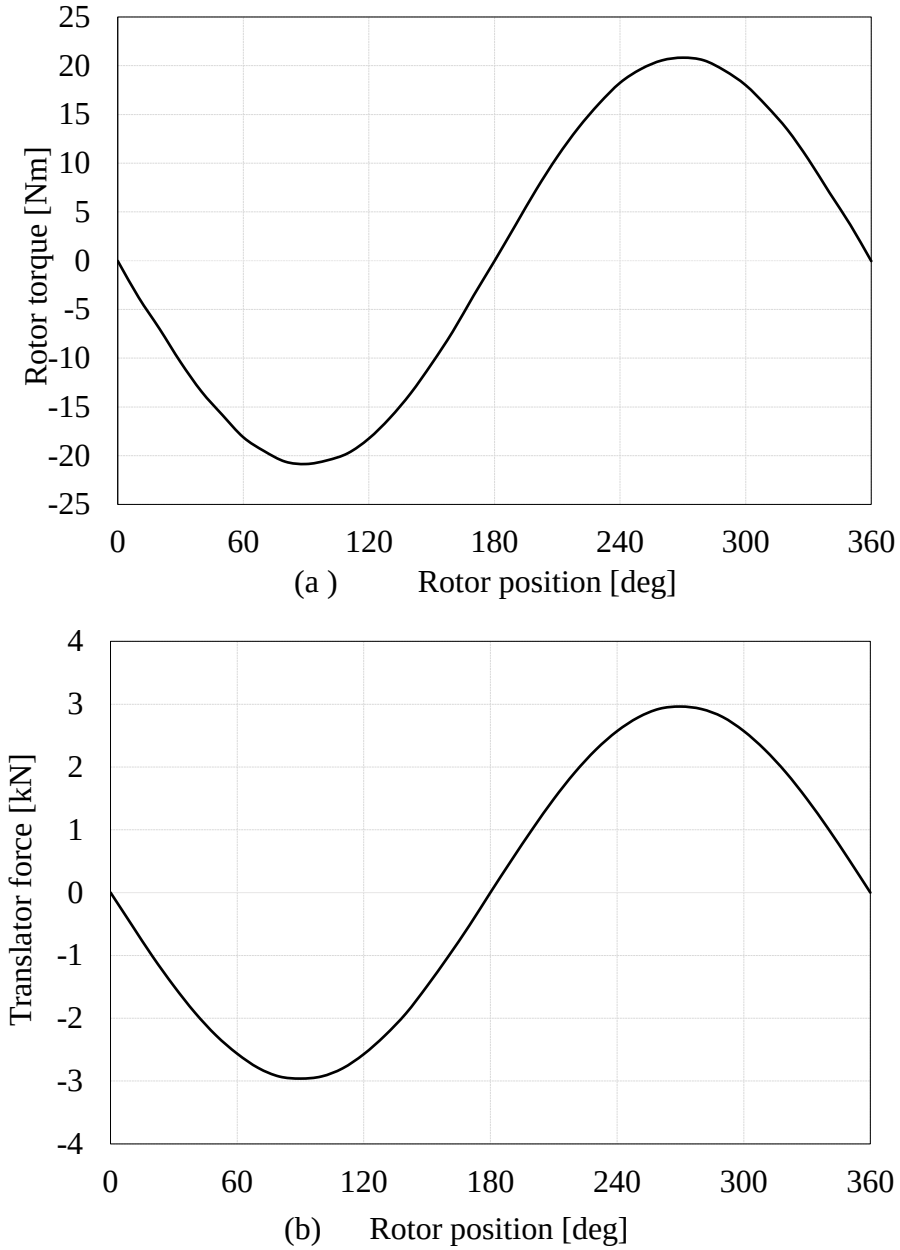

Figure 7. 2. Characteristics of the magnetic gears; (a) rotor torque, and (b) translator force.

From a dynamic viewpoint, the relationship between the rotor and translator of the magnetic gear may be described as a mass-spring system with non-linear stiffness that is similar to concentric magnetic gears described in [76], [79], [80] and [81]. Based on the description of a linear-rotary magnetic gear in [77] and [78], the following non-linear model can be described for the proposed magnetic gear.

$$T_r = -T_m sin\phi \tag{7.1-a}$$

$$F_t = -F_m sin\phi = GT_r = -GT_m sin\phi \quad (7.1\text{-b})$$

where T_r is rotor torque, F_t is translator force, $\phi = \theta + Gz$ describes the relative position of rotor and translator with respect to each other, θ and z denote the positions of the rotor and translator with respect to a stable equilibrium point respectively, and T_m presents the maximum torque that is obtained from a 3D-FEA, also called a pull-out torque.

The proposed non-linear model in Eq. (7.1) can be linearised about a stable equilibrium point in order to be able to present it in the Lablace domain, as given by

$$T_r \cong -T_m(\theta + Gz) \quad (7.2\text{-a})$$

$$F_t = GT_r \cong -GT_m(\theta + Gz) \quad (7.2\text{-b})$$

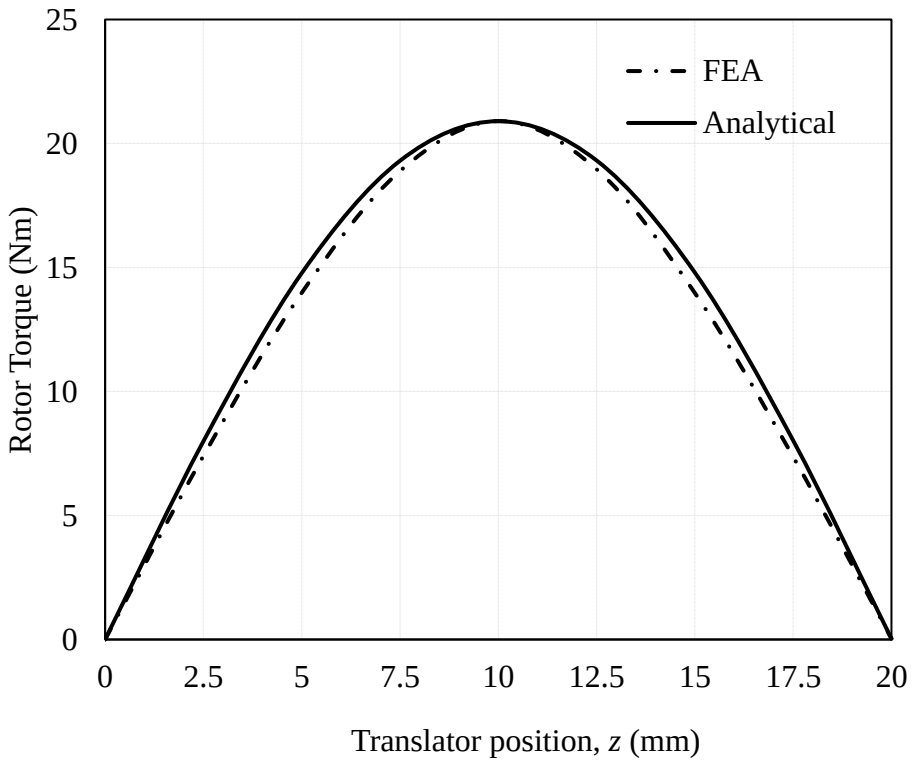

Figure 7. 3. Variations of rotor torque versus translator position at zero degree of rotor position, $\theta = 0$.

7.2.2 Oscillating prediction

A simple dynamic behavior of the magnetic gear is examined as an oscillatory rotational system by holding the translator stationary at position of $z(0) = 0$ (the magnets on the rotor and translator are aligned and the same the direction of polarisation), the rotor is manually twisted to a maximum torque position, $\theta(0) = -\pi/2$, and then the rotor is released to freely ascillate until it settles down to a stable equilibrium point. The rotor equation of motion can be descibed as

$$T_r = J_r\ddot{\theta} + C_r\dot{\theta} \tag{7.3}$$

Where J_r is the rotor moment of inertia and C_r is the damping coefficient associated with rotation of the rotor. Double upper dots indicates second time derivative and single dot indicates first time derivative. By substituting Eq. (7.1) into Eq. (7.3), is given

$$\ddot{\theta} + \frac{C_r}{J_r}\dot{\theta} + \frac{T_m}{J_r}\sin\theta = 0;\ \theta(0) = -\frac{\pi}{2};\ \dot{\theta}(0) = 0 \tag{7.4}$$

When the model of the proposed magnetic gear is linearised, the rotor's equation of motion will be transform to the following

$$\ddot{\theta} + \frac{C_r}{J_r}\dot{\theta} + \frac{T_m}{J_r}\theta = 0;\ \theta(0) = -\frac{\pi}{2};\ \dot{\theta}(0) = 0 \tag{7.5}$$

The close form solution for Eq. (7.5) can be obtained as

$$\theta(t) \cong \theta(0)e^{-\alpha_r t}\left(cos\beta_r t + \frac{C_r}{2J_r\beta_r}sin\beta_r t\right) \tag{7.6}$$

where

$$\alpha_r = \frac{B_r}{2J_r};\ \beta_r = \frac{1}{2}\sqrt{\frac{4T_m}{J_r} - \left(\frac{C_r}{J_r}\right)^2}$$

Therefore, the rotor torque can be expressed as

$$T_r(t) = -T_m\theta(t) \tag{7.7}$$

If damping is neglected, the solution in Eq. (7.6) can be rewritten as

$$\theta(t) \cong \theta(0) cos\omega_r t \tag{7.8}$$

Where $\omega_r = \sqrt{\frac{T_m}{J_r}}$ is the rotor's oscillation frequency.

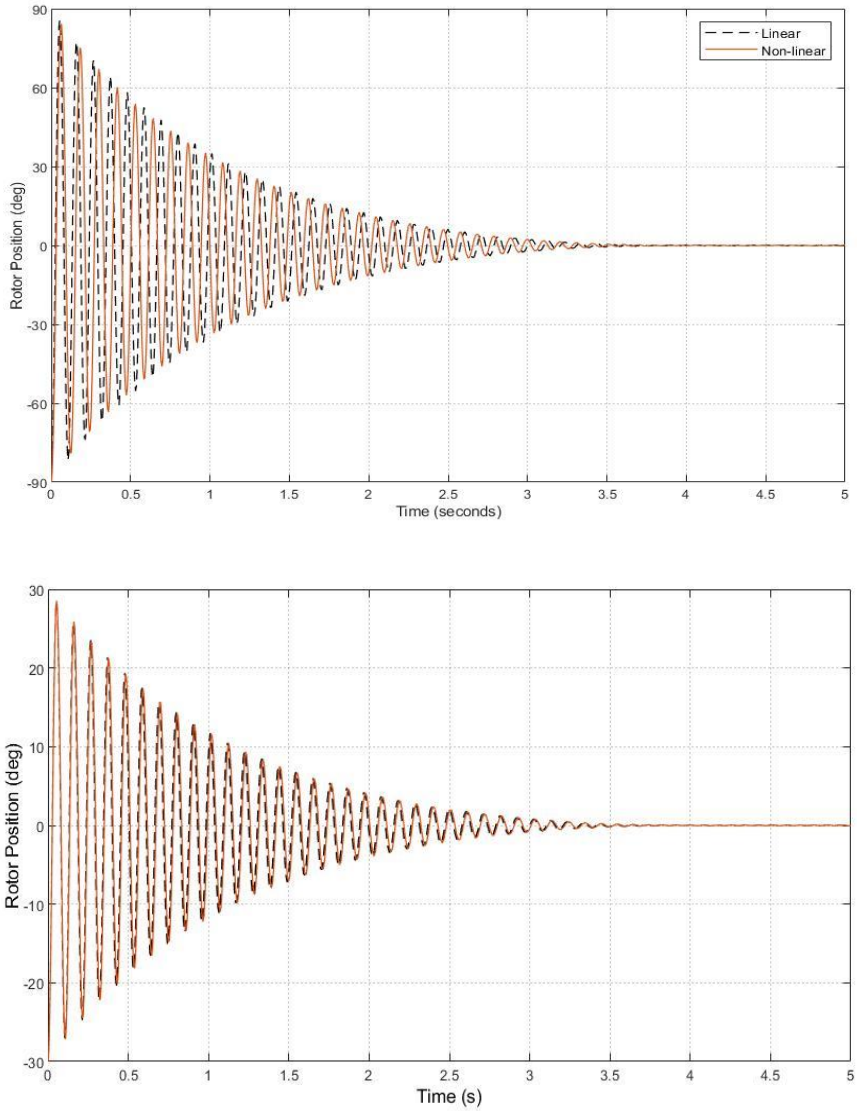

Figure 7. 4. Rotor position during a rotor oscillation test obtained from nonlinear and linearized analytical models: (a) rotor starting from -90 degrees, (b) rotor starting from -30 degrees.

7.2.3 Modelling of the proposed magnetic gear with an external excitation train

In this section, dynamic behavior of the magnetic gear is examined through an external force excitation that applies on translator, F_{ex}, and a load torque is applied on the rotor. A magnetic force due to the interactions between the rotor and translator is in the opposit direction to the external force. When the excitation force is higher than the magnetic force and momemt of inertia, the translator moves and the rotor rotates in the positive direction, i.e., $\omega > 0$.

$$F_{ex} + F_t = M\ddot{z} + C_t\dot{z} \tag{7.9-a}$$

$$T_r + T_L = J_r\ddot{\theta} + C_r\dot{\theta} \tag{7.9-b}$$

Where M is the total mass of the translating parts, C_r and C_t are damping coeficients associated with rotation and traslation, respectively. F_m and T_m denote magnetic force and the pull-out torque of the translator and rotor.

By substituting Eq. (7.1) into Eq. (7.9), the motion equation can be expressed as

$$F_{ex} - F_m sin\phi = M\ddot{z} + C_t\dot{z} \tag{7.10-a}$$

$$-T_m sin\phi + T_L = J_r\ddot{\theta} + C_r\dot{\theta} \tag{7.10-b}$$

The linearised dynamic models of the proposed magnetic gear can be written as

$$F_{ex} - GT_m(\theta + Gz) \cong M\ddot{z} + C_t\dot{z} \tag{7.11-a}$$

$$-T_m(\theta + Gz) + T_L \cong J_r\ddot{\theta} + C_r\dot{\theta} \tag{7.11-b}$$

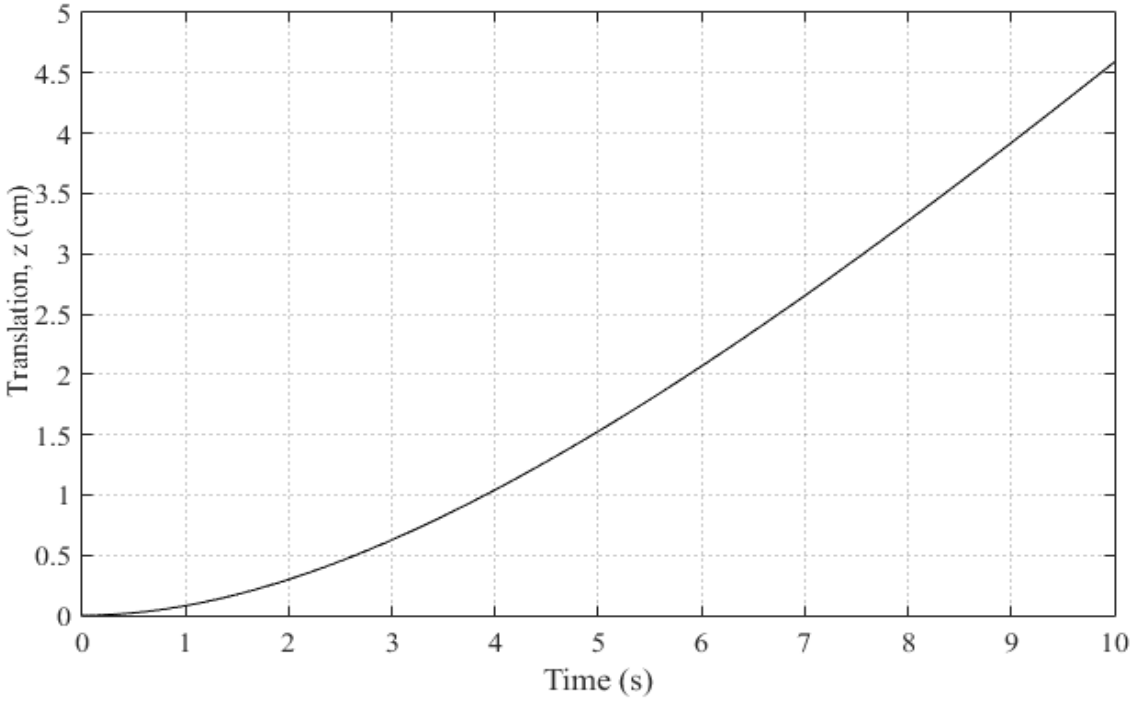
Translation, z (cm)
Time (s)
0
0.5
1
1.5
2
2.5
3
3.5
4
4.5
5
0
1
2
3
4
5
6
7
8
9
10

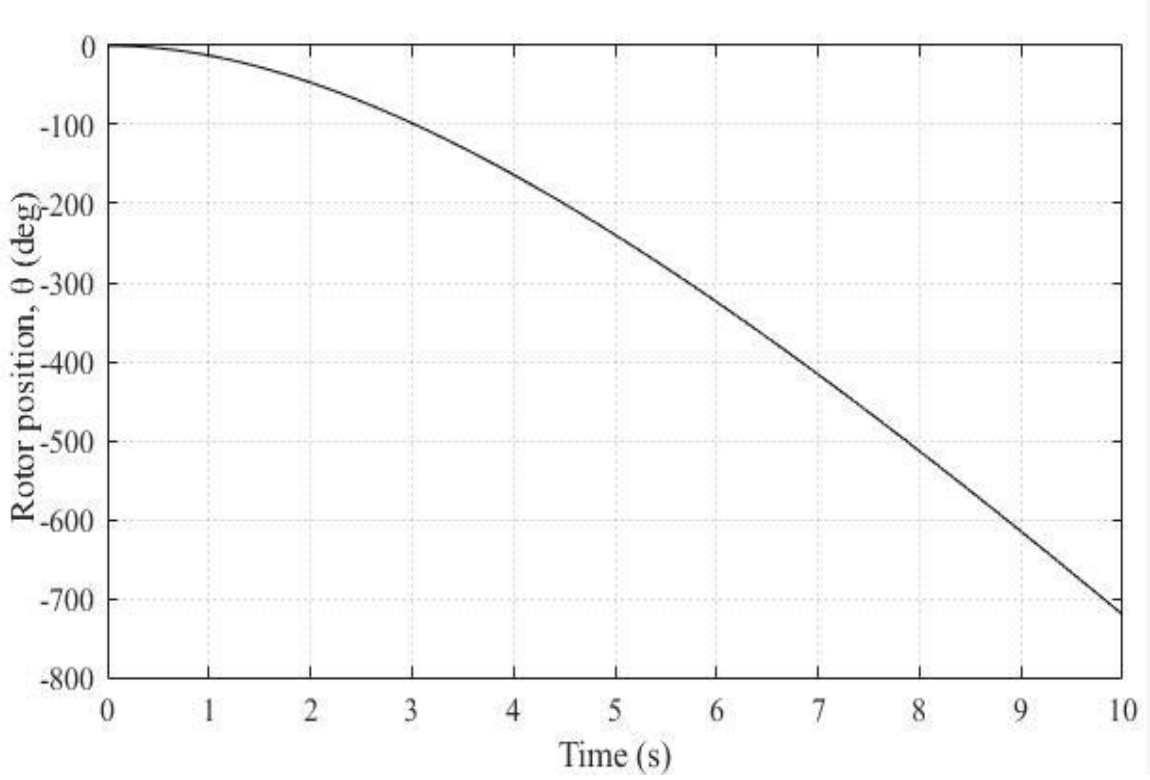
Rotor position, θ (deg)
Time (s)
0
-100
-200
-300
-400
-500
-600
-700
-800
0
1
2
3
4
5
6
7
8
9
10

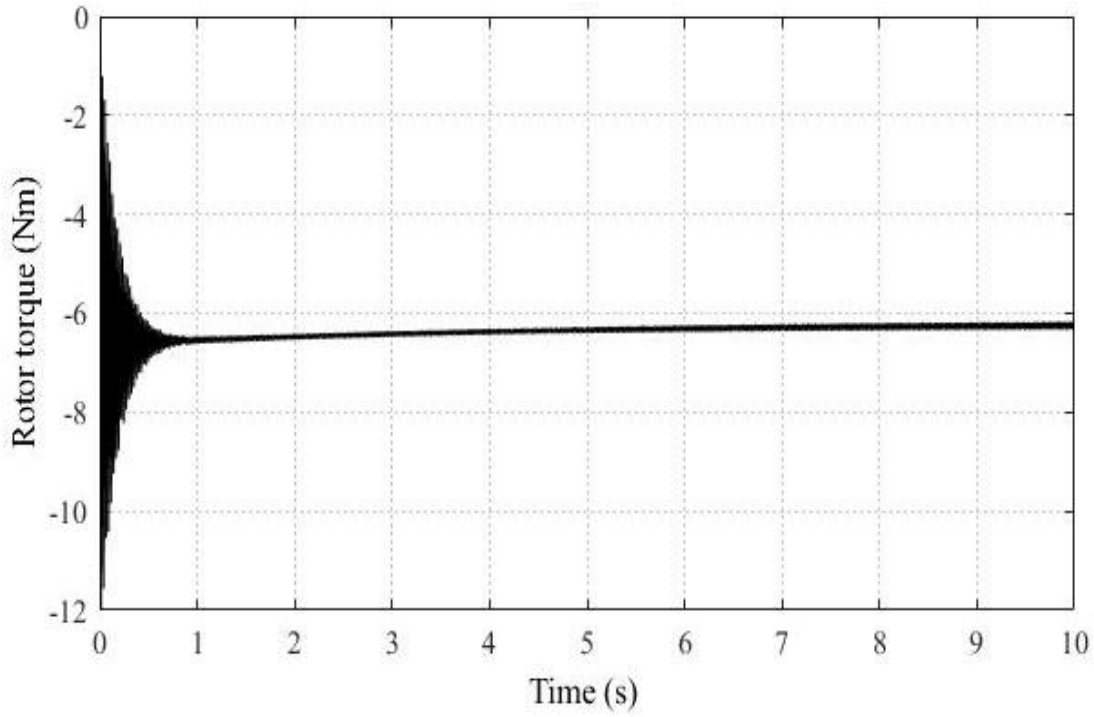

Figure 7. 5. Simulated response of the system when both z and θ variation

7.3 Dynamic model of the rotational harvester

In a rotational harvester, a suitable motion transmission system is used to convert low frequency linear motion to high frequency rotational one. In [82], a ball screw was employed in the vibration harvester, as shown in Figure 7.6. In this system, the base movement causes the mass to vibrate. The ball screw then converts the low frequency linear motion of the seismic mass to high-speed rotation.

The idea of this work is to replace the ball screw by a magnetic gear. In the ball screw system, the rotational parts rotate by an equivalent value when seismic mass translates (if the ball screw is ideal). In a magnetic gear, however, when the seismic mass moves, the rotor will not rotate until the magnetic force is equal to the working point, defined by an applied load to the rotor. This happene due to the magnetic force coupling between the rotor and translator. A zero rotor torque occurs at the equilibrium point and by changing either the translator or rotor positions, a maximum torque (pull-out torque) is obtained when the translator moves by half of the pole pitch or the rotor rotates byf 90 degrees. In other words,

the rotor will have a delayed response time in comparison with the seismic mass (or translator) if a load is applied to the rotor.

In [83] and [84], a helical magnetic gear was designed and used for the point-absorbing wave energy conversion systems. An analytical method was used to predict the dynamic operation of the harvesting system. However, the time delay between the translation and rotary parts was is ignored.

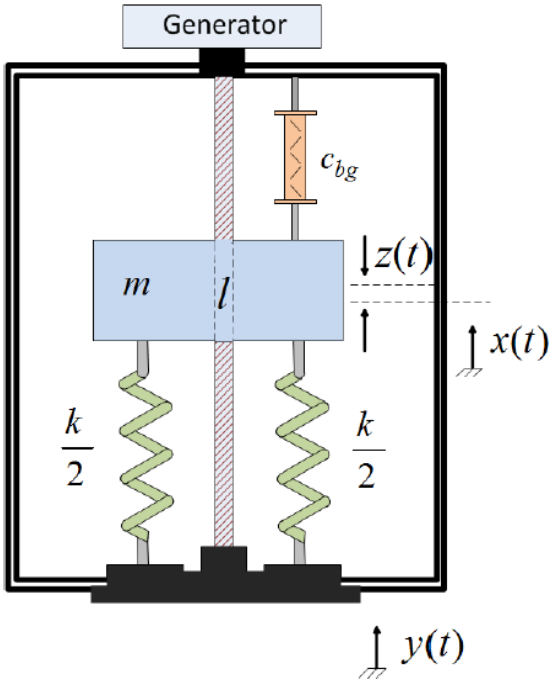

Figure 7. 6. Schematic diagram of an energy harvesting system consisting of a sprung mass coupled to a generator through a ball screw [75].

Consider J_M and C_{bg} being the moment of inertia and damping coefficient associated with the rotation of the magnetic gear's rotor and generator. $J_M G^2$ is the reflected moment of inertia of the magnetic gear and the generator. Then the sum of the seismic mass and reflected moment of inertia of rotational component is given by

$$M = m + J_M G^2$$

Let the relative displacement of the system be $z(t) = x(t) - y(t)$. If the base displacement is assumed to be sinusoidal $y(t) = Y_0 sin\omega$, then $z(t) = Zsin(\omega t + \phi)$ where Z is the maximum displacement of mass and ϕ is the phase angle between $y(t)$ and $z(t)$. It is more convenient to analyse the system in the frequency domain. Figure 5.7 shows a free body diagram of the system with a mass, *m*, mechanical damping, C_{bg}, overall spring stiffness, *k*, and the electrical torque of the generator, F_{EG}.

The electrical torque of the generator, $F_{EG} = 0$, If speed of the magnetic's rotor $\Omega = 0$, and $F_{EG} > 0$ if $\Omega > 0$. In reality, when the seismic mass departs from the balancing position, it will move a distance ($z > 0$) to reach a magnetic force to be able to against the moment of enertia of the magnetic's rotor and rotary parts (the generator' rotor…etc), then the magnetic's rotor rotates. The position of seismic mass is at the distance *z* that make the rotation of the rotor is called the working point. It can be deduced that when the translator moves backward, the distance of the seismic mass will be doubled to reach the working point state.

The governing differential equation of motion, with the magnetic gear, at the working point is written as

$$M\ddot{z} + C\dot{z} + kz = -m\ddot{y} + F_{EG} \tag{7.12}$$

where *C* is the reflected damping of the system is defined as

$$C = \left(C_{bg} + \frac{Ti^2}{R_l + R_i}\right)G^2 \tag{7.13}$$

and F_{EG} is defined as

$$F_{EG} = G\tau_G \tag{7.14}$$

where τ_G is the electrical torque due to the generation of an opposing magnetic field which causes current flowing through the generator coil as

$$\tau_G = -T_i i(t) \tag{7.15}$$

Here T_i is the generator torque constant and $i(t)$ is the current flowing through its coil. Ignoring the coil inductance, as it can be presented by adding a capacitor in series with generator, and defining R_i and R_l as the internal resistance of the rotational generator and the load resistance, respectively, the current flow based on the equivalent circuit of generator is related to the voltage produced across the idealized voltage source and is obtained from

$$i(t) = \frac{V_{emf}(t)}{R_l + R_i} = \frac{T_i v(t)}{R_l + R_i} \tag{7.16}$$

where $v(t)$ is the rotational speed of the magnetic gear's rotor coupled to the generator and is given by

$$v(t) = G\frac{d\big(x(t) - y(t)\big)}{dt} = G\frac{dz(t)}{dt} \tag{7.17}$$

Replacing Eq. (7.1), (7.3), (7.14) and (7.15) in (7.13), it can be rearranged as

$$M\ddot{z} + C\dot{z} + kz = -m\ddot{y} - GT_i i(t) \tag{7.18}$$

Applying the Fourier transform and linearized to (7.17), gives

$$Z(\omega)[k - M\omega^2 + jC\omega] = m\omega^2 Y(\omega) - GT_i I(\omega) \tag{7.19}$$

and substituting (7.15) into (7.16) and applying Fourier transform yields

$$I(\omega) = j\frac{\omega G T_i}{R_l + R_i} Z(\omega) \tag{7.20}$$

Substituting (7.19) into (7.18) and rearranging it results in

$$Z(\omega)\left(k - M\omega^2 + G^2 T_m + j\left(C + \frac{G^2 T_i^2}{R_l + R_i}\right)\omega\right) = m\omega^2 Y(\omega) \tag{7.21}$$

Therefore, the magnitude of Z is given by

$$Z = \frac{m\omega^2 Y_0}{\sqrt{(k - M\omega^2)^2 + \left(\left(C + \frac{G^2 T_i^2}{R_l + R_i}\right)\omega\right)^2}} \tag{7.22}$$

The power supplied to the load is inferred from the relative displacement and is derived as follows:

$$P_l(t) = R_l\left(\frac{V_{emf}(t)}{R_l + R_i}\right)^2 = \frac{R_l}{(R_l + R_i)^2} T_i^2 G^2 \omega^2 Z^2 cos^2(\omega t + \phi)$$

$$\Rightarrow P_{l-average} = \frac{1}{2} R_l i^2 = \frac{1}{2} R_l \left(\frac{V_{emf}}{R_l + R_i}\right)^2 \tag{7.23}$$

The average harvested power can be obtained by replacing (7.21) in (7.23) and is given by

$$P_{l-average} = \frac{1}{2}\frac{R_l}{(R_l + R_i)^2} T_i^2 G^2 \omega^2 x \left(\frac{(m\omega^2 Y_0)^2}{(k - M\omega^2)^2 + \left(\left(C + \frac{G^2 T_i^2}{R_l + R_i}\right)\omega\right)^2}\right) \tag{7.24}$$

Before going to the numerical calculation, a magnetic gear is designed for properly requirement of the harvesting system. Because all the parameters of the system in [85] is kept for a comparative assessment. A preliminary load can be calculated by the generator torque constant. Assuming velocity of the seismic mass is about 10 cm per second, by substituting Eq. (7.16) and (7.17) into (7.15) the electrical torque of the generator can be obtained by

$$\tau_G = \frac{{T_i}^2}{R_l + R_i} G \omega Z_0 \tag{7.25}$$

In [85], the seismic mass' displacement was constrained at certain value in order to calculate the optimal values of the load resistance and ball screw lead when the undamped natural frequency of system matches the oscillation frequency. In a constraint of seismic mass displacement of $Z_0 = 0.3$m, the optimal load resistance obtained was at 177.16 **Ω** and the corresponding ball screw lead was calculated to be 4 mm. If this value of ball screw lead

brings into a magnetic gear's lead, it becomes a disadvantage for a performance because its small pole pitch of magnets (2 mm) increases leakage between two adjacent magnets, as a result, a very small magnets' portion contribute to the characteristics. If a magnetic gear is designed for the gear ratio of G = 100π m^{-1} (corresponding to pole pitch of 10 mm), then the electrical torque of the generator is calculated by applying maximum power condition to derive the load resistance, R_l, and maximum displacement, Z_0, according to [85]. Furthermore, increasing pole pitch results in larger displacement of the seismic mass. To constrain the displacement of the seismic mass back to [85], weight of the seismic mass needs to be decreased. It proves that this solution is not properly because weight of the seismic mass depends on weight of the translator of the magnetic gear. Second solution can be used is that increasing the spring stiffness. This seems to be easier than the previous solution.

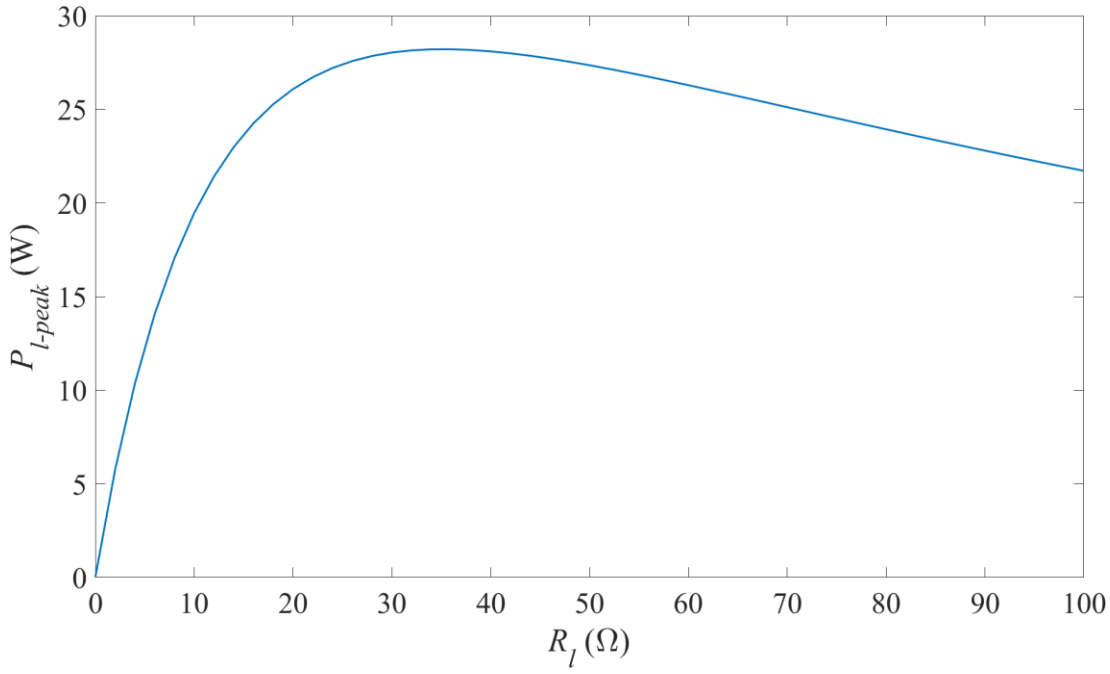

Figure 7. 7. Maximum power versus load resistance.

As discussion above, with the magnetic gear's lead of 20 mm (pole pitch is 10 mm), the maximum power can be obtained is about 28.2W, and the optimum load resistance for the system is 34 Ω, as seen in Figure 7.7. This result is nearly a half value in comparison with the maximum power that has obtained from [85] (it is about 62W). This happened dues to

the speed of the rotor is too low because of decreasing of the magnetic gear's lead (from 4mm of the ball screw to 20mm of the magnetic gear).

Appendix A

MATLAB-Simulink model

i) Simulink model of a magnetic gear

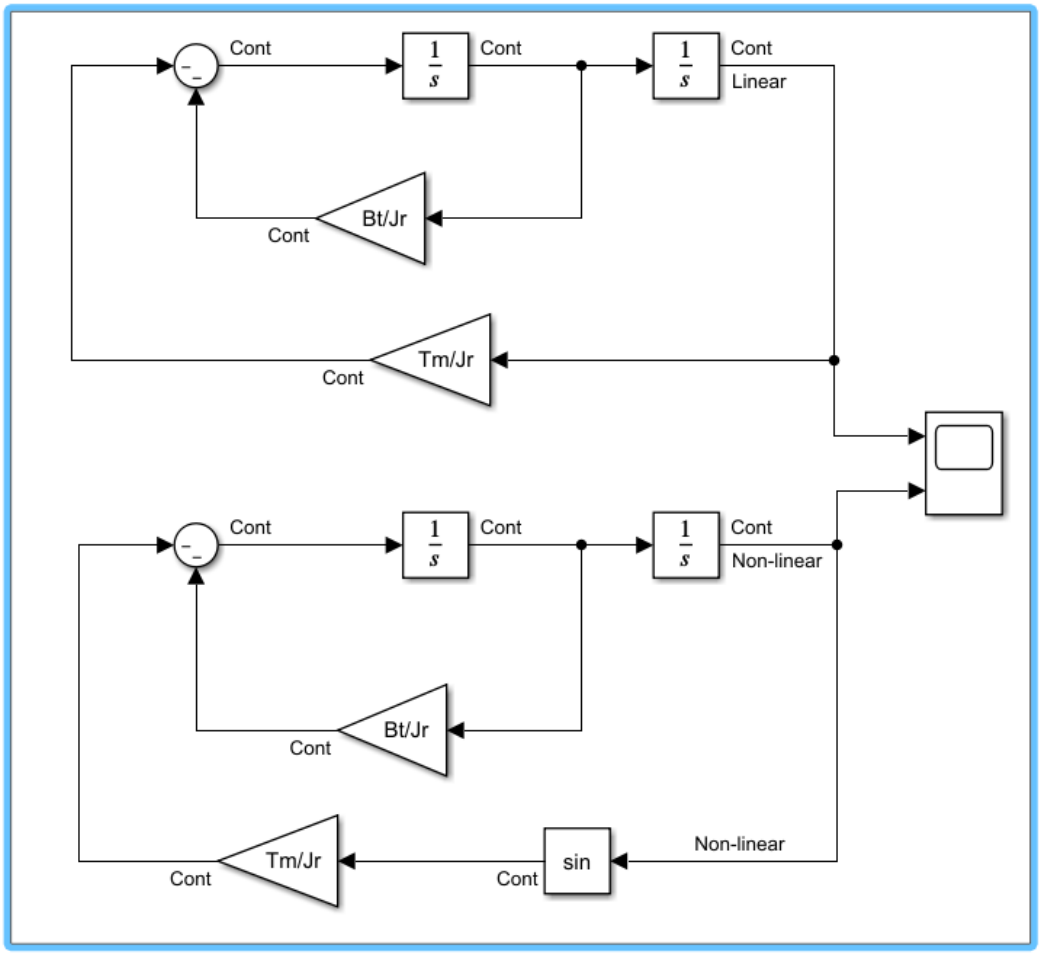

Figure A. 1. Simulink model of linear and non-linear oscillating magnetic gear.

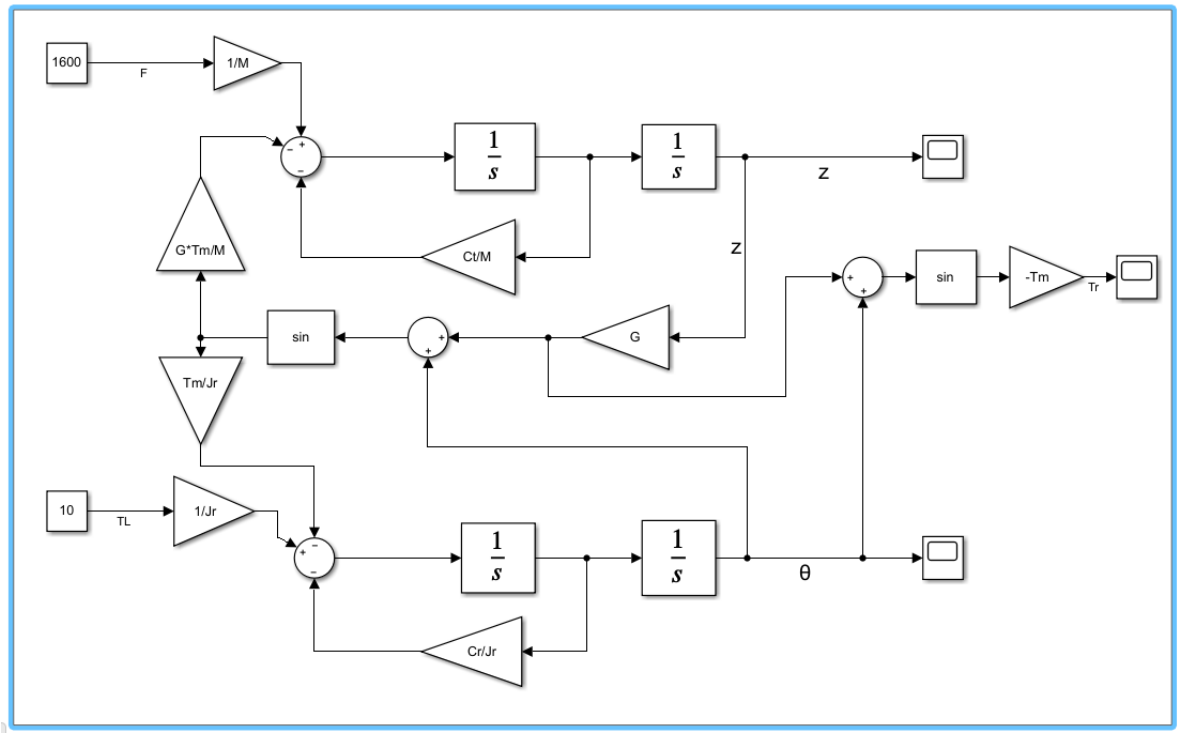

Figure A. 2. Simulink model of driven train system including a magnetic gear.

ii) MATLAB code for harvesting system

```
clear all;
clc;

% System parameters
Z0=0.3; %m
Y0=1;   %m
pi=3.14;
wd=pi;
Ri=16;  %Ohm
f=0.5;
kt=0.0764;  %V.s/rad
M=8;
w=2*pi*f;
Cmg=4.7e-6;
Cmb=3e-4;
Cbg=Cmb+Cmg;

i=0;
for RL=0:2:100;
   i=i+1;
   RT=RL+Ri;
   LL1=20e-3;
   RLL2(i)=RL;
   PP2(i)= RL*kt*kt*wd^4*M^2*Y0^2*LL1*LL1/((4*pi*pi)*(Cbg*RT+kt*kt)^2);
end

figure;
plot(RLL2,PP2, 'linewidth',1.5)
xlabel('{\itR_l }(\Omega)','FontName','Times New Roman','FontSize',24);
ylabel('{\itP_{l-peak}} (W)','FontName','Times New Roman','FontSize',24);
set(gca,'FontSize',24,'FontName','Times New Roman');
```

Appendix B

CAD Drawing of the demonstrator

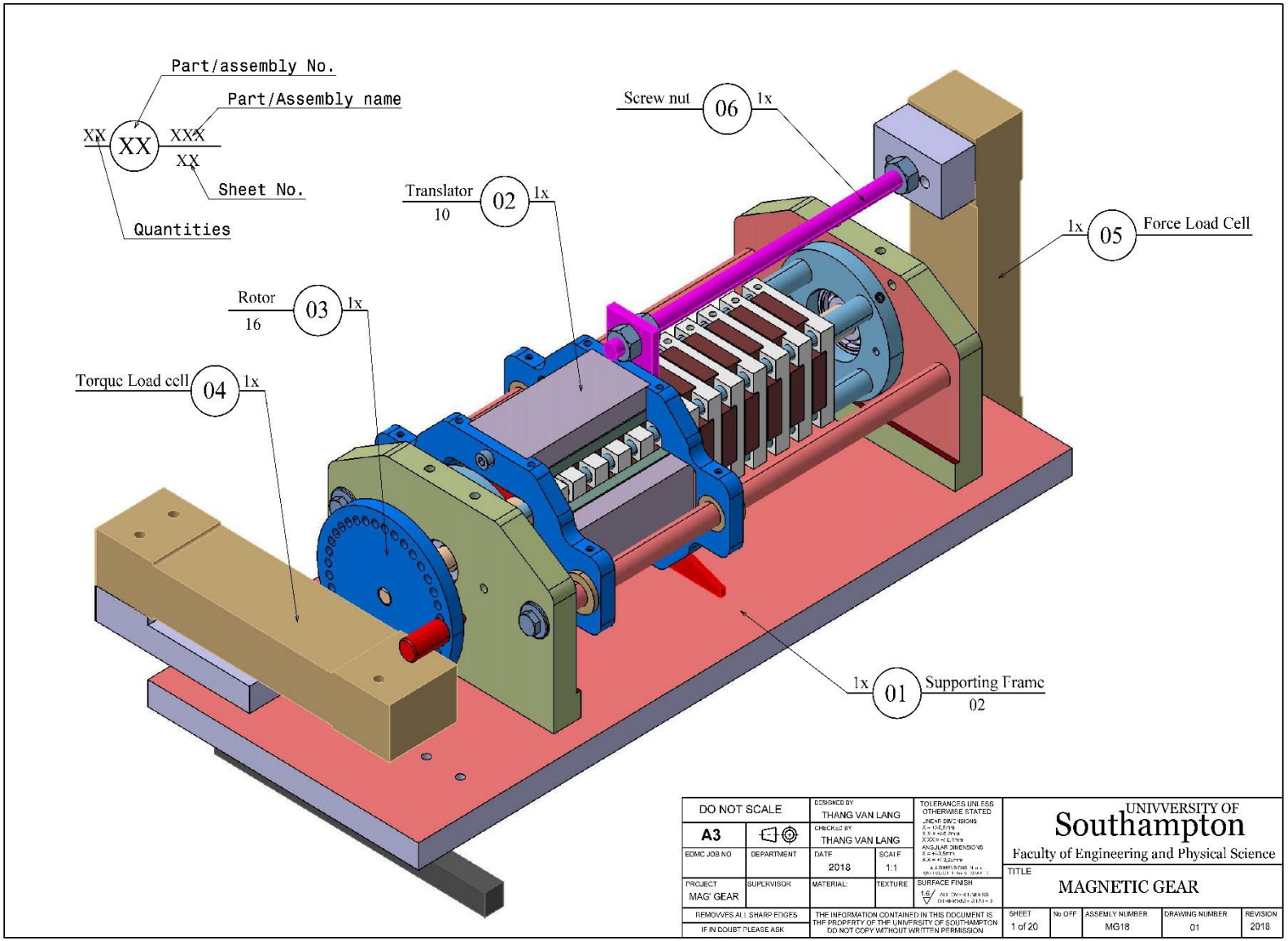
Part/assembly No.
Part/Assembly name
XX
XX
XXX
XX
Sheet No.
Quantities
Screw nut
06
1x
Translator
10
02
1x
1x
05
Force Load Cell
Rotor
16
03
1x
Torque Load cell
04
1x
1x
01
Supporting Frame
02
DO NOT SCALE
A3
DESIGNED BY
THANG VAN LANG
CHECKED BY
THANG VAN LANG
TOLERANCES UNLESS OTHERWISE STATED
LINEAR DIMENSIONS
ANGULAR DIMENSIONS
EDMC JOB NO
DEPARTMENT
DATE
2018
SCALE
1:1
PROJECT
MAG' GEAR
SUPERVISOR
MATERIAL:
TEXTURE
SURFACE FINISH
REMOVES ALL SHARP EDGES
IF IN DOUBT PLEASE ASK
THE INFORMATION CONTAINED IN THIS DOCUMENT IS THE PROPERTY OF THE UNIVERSITY OF SOUTHAMPTON DO NOT COPY WITHOUT WRITTEN PERMISSION
UNIVVERSITY OF
Southampton
Faculty of Engineering and Physical Science
TITLE
MAGNETIC GEAR
SHEET
1 of 20
No OFF
ASSEMLY NUMBER
MG18
DRAWING NUMBER
01
REVISION
2018

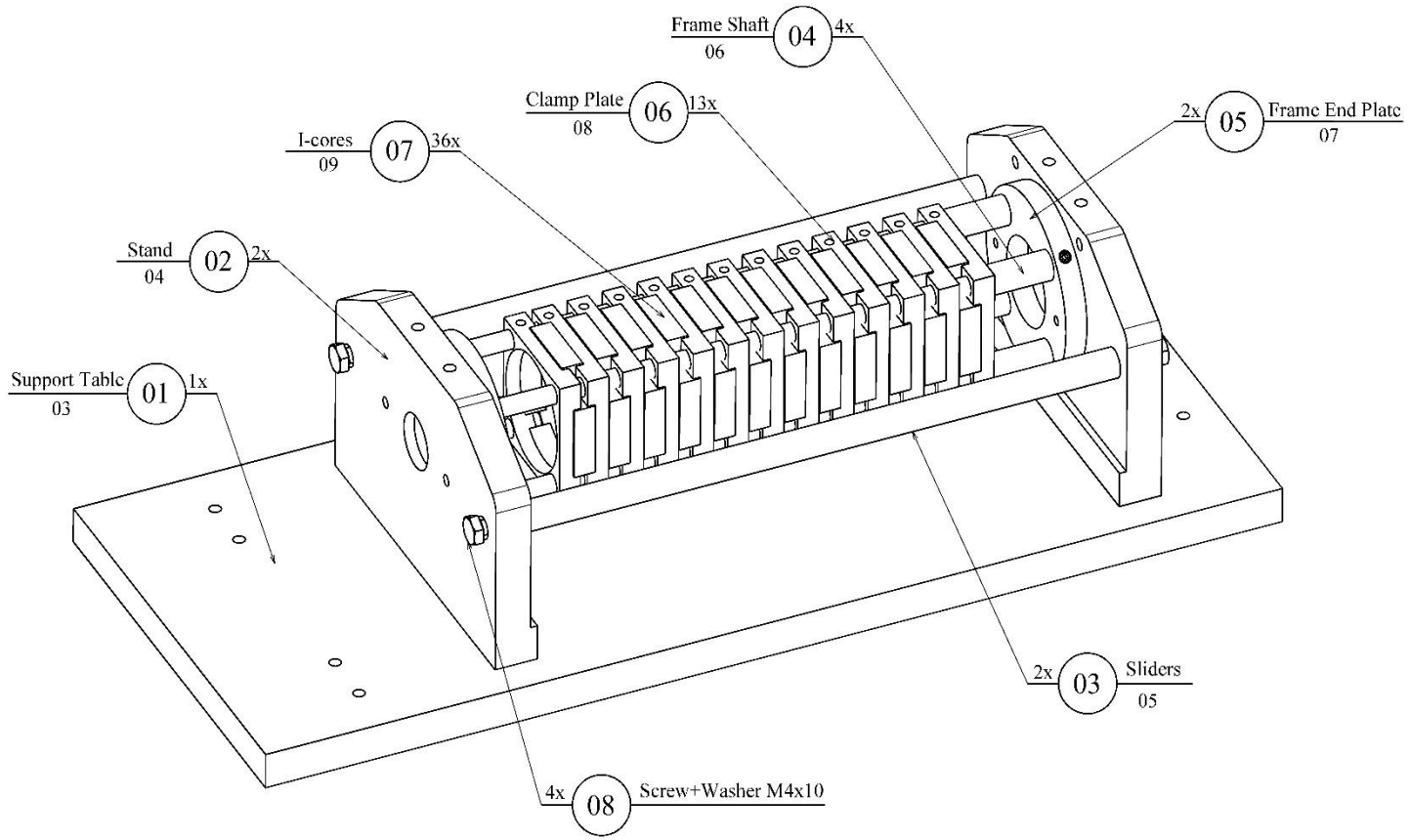

DO NOT SCALE		DESIGNED BY: THANG VAN LANG		TOLERANCES UNLESS OTHERWISE STATED	UNIVVERSITY OF Southampton
A3		CHECKED BY: THANG VAN LANG		LINEAR DIMENSIONS X = ±0.5mm X.X = ±0.2mm XXX = ±0.1mm ANGULAR DIMENSIONS X = ±0.5°m X.X = ±0.2°m ALL DIMENSIONS IN mm UNLESS OTHERWISE STATED	Faculty of Engineering and Physical Science
EDMC JOB NO	DEPARTMENT	DATE: 2018	SCALE: 1:1		TITLE: SUPPORTING FRAME
PROJECT: MAG' GEAR	SUPERVISOR	MATERIAL:	TEXTURE	SURFACE FINISH: 1.6 µm UNLESS OTHERWISE STATED	
REMOVES ALL SHARP EDGES		THE INFORMATION CONTAINED IN THIS DOCUMENT IS THE PROPERTY OF THE UNIVERSITY OF SOUTHAMPTON DO NOT COPY WITHOUT WRITTEN PERMISSION			
IF IN DOUBT PLEASE ASK					

SHEET	No OFF	ASSEMLY NUMBER	DRAWING NUMBER	REVISION
2 of 20		MG18-01	02	2018

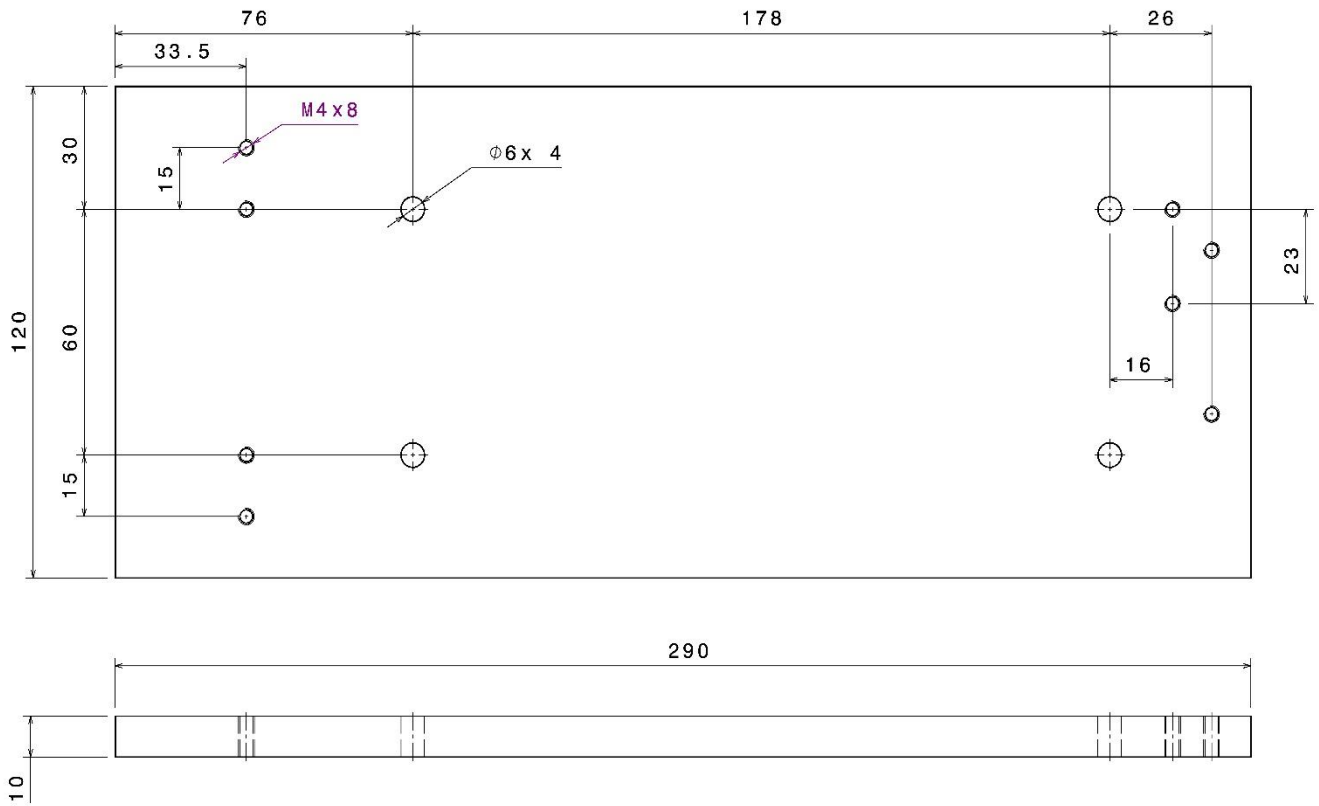

DO NOT SCALE		DESIGNED BY: THANG VAN LANG		TOLERANCES UNLESS OTHERWISE STATED: LINEAR DIMENSIONS X = ±0.5mm, XX = ±0.2mm, XXX = ±0.1mm; ANGULAR DIMENSIONS X = ±3.5mm, XX = ±2.0mm; ALL DIMENSIONS IN mm UNLESS STATED OTHERWISE	UNIVVERSITY OF Southampton Faculty of Engineering and Physical Science
A3		CHECKED BY: THANG VAN LANG			TITLE: SUPPORTING TABLE
EDMC JOB NO	DEPARTMENT	DATE: 2018	SCALE: 1:1		
PROJECT: MAG' GEAR	SUPERVISOR	MATERIAL: ALUMINIUM	TEXTURE	SURFACE FINISH: 1.6 ALL OTHER SURFACES 3.2	
REMOVES ALL SHARP EDGES		THE INFORMATION CONTAINED IN THIS DOCUMENT IS THE PROPERTY OF THE UNIVERSITY OF SOUTHAMPTON DO NOT COPY WITHOUT WRITTEN PERMISSION			SHEET: 3 of 20 / No OFF / ASSEMLY NUMBER: MG18-01 / DRAWING NUMBER: 03 / REVISION: 2018
IF IN DOUBT PLEASE ASK					

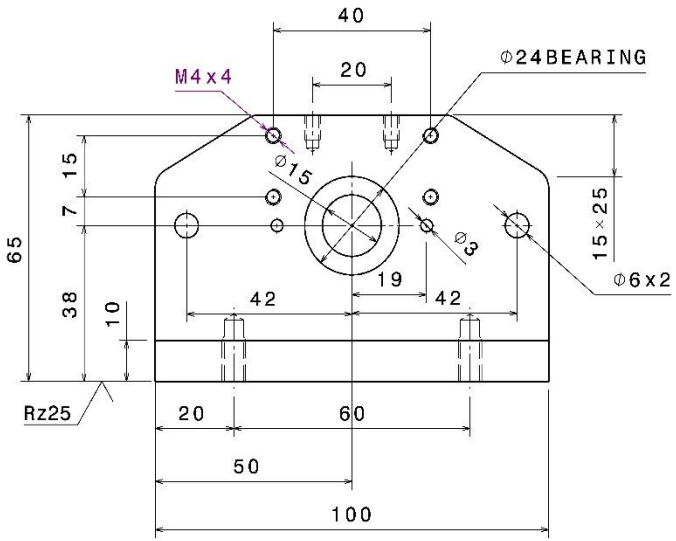

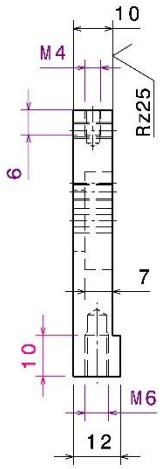

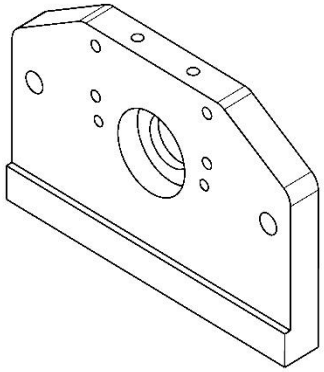

DO NOT SCALE		DESIGNED BY: THANG VAN LANG		TOLERANCES UNLESS OTHERWISE STATED	UNIVVERSITY OF Southampton
A3		CHECKED BY: THANG VAN LANG			Faculty of Engineering and Physical Science
EDMC JOB NO	DEPARTMENT	DATE: 2018	SCALE: 1:1		TITLE: SUPPORTING STAND
PROJECT: MAG' GEAR	SUPERVISOR	MATERIAL: ALUMINIUM	TEXTURE	SURFACE FINISH	
REMOVES ALL SHARP EDGES		THE INFORMATION CONTAINED IN THIS DOCUMENT IS THE PROPERTY OF THE UNIVERSITY OF SOUTHAMPTON DO NOT COPY WITHOUT WRITTEN PERMISSION			
IF IN DOUBT PLEASE ASK					

SHEET	No OFF	ASSEMLY NUMBER	DRAWING NUMBER	REVISION
4 of 20		MG18-01	04	2018

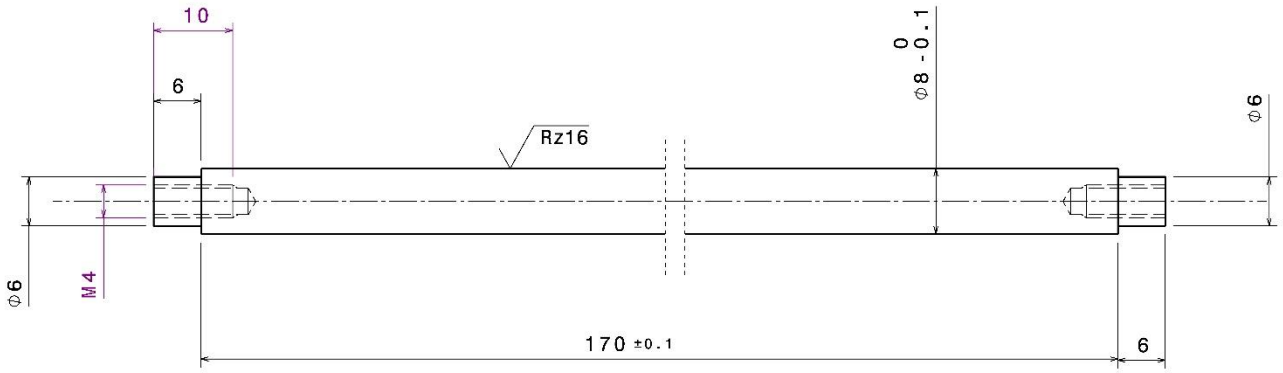

DO NOT SCALE		DESIGNED BY: THANG VAN LANG		TOLERANCES UNLESS OTHERWISE STATED: LINEAR DIMENSIONS X = ±0.5mm XX = ±0.2mm XXX = ±0.1mm ANGULAR DIMENSIONS X = ±0.5°m X.X = ±0.25°m ALL DIMENSIONS IN mm UNTOLERANCED SURFACES ARE 6.3	UNIVVERSITY OF Southampton Faculty of Engineering and Physical Science
A3		CHECKED BY: THANG VAN LANG			TITLE: TRANSLATOR SLIDER
EDMC JOB NO	DEPARTMENT	DATE: 2018	SCALE: 1:1		
PROJECT: MAG' GEAR	SUPERVISOR	MATERIAL: STEEL	TEXTURE	SURFACE FINISH: 1.6 √ (ALL UNLESS OTHERWISE STATED)	
REMOVES ALL SHARP EDGES		THE INFORMATION CONTAINED IN THIS DOCUMENT IS THE PROPERTY OF THE UNIVERSITY OF SOUTHAMPTON DO NOT COPY WITHOUT WRITTEN PERMISSION			
IF IN DOUBT PLEASE ASK					

SHEET	No OFF	ASSEMLY NUMBER	DRAWING NUMBER	REVISION
5 of 20		MG18-01	05	2018

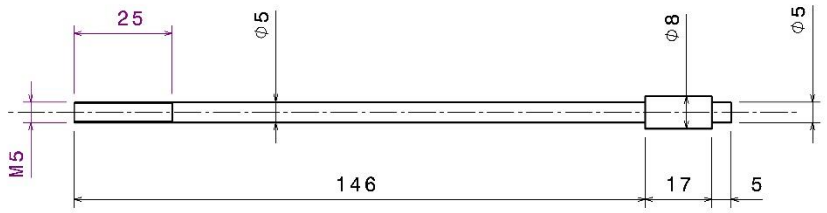

DO NOT SCALE		DESIGNED BY THANG VAN LANG		TOLERANCES UNLESS OTHERWISE STATED	UNIVVERSITY OF Southampton
A3		CHECKED BY THANG VAN LANG			Faculty of Engineering and Physical Science
EDMC JOB NO	DEPARTMENT	DATE 2018	SCALE 1:1		TITLE FRAME SHAFT
PROJECT MAG' GEAR	SUPERVISOR	MATERIAL STAINLESS STELL	TEXTURE	SURFACE FINISH	
REMOVVES ALL SHARP EDGES		THE INFORMATION CONTAINED IN THIS DOCUMENT IS THE PROPERTY OF THE UNIVERSITY OF SOUTHAMPTON DO NOT COPY WITHOUT WRITTEN PERMISSION		SHEET 6 of 20	NO OFF / ASSEMLY NUMBER MG18-01 / DRAWING NUMBER 06 / REVISION 2018
IF IN DOUBT PLEASE ASK					

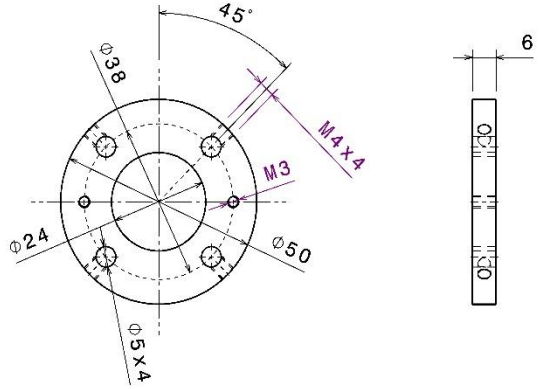

DO NOT SCALE		DESIGNED BY: THANG VAN LANG		TOLERANCES UNLESS OTHERWISE STATED	UNIVVERSITY OF Southampton
A3		CHECKED BY: THANG VAN LANG		UNDIMENSIONED X = ±0.5mm X.X = ±0.2mm X.XX = ±0.1mm ANGULAR DIMENSIONS ±1° FACE ±1mm X.X = ±0.25mm ALL DIMENSIONS in mm UNLESS OTHERWISE STATED	Faculty of Engineering and Physical Science
EDMC JOB NO	DEPARTMENT	DATE: 2018	SCALE: 1:1		TITLE: FRAME END PLATE
PROJECT: MAG' GEAR	SUPERVISOR	MATERIAL: ALUMINIUM	TEXTURE	SURFACE FINISH: 6.3 ALL OTHER UNLESS OTHERWISE STATED	
REMOVVES ALL SHARP EDGES		THE INFORMATION CONTAINED IN THIS DOCUMENT IS THE PROPERTY OF THE UNIVERSITY OF SOUTHAMPTON DO NOT COPY WITHOUT WRITTEN PERMISSION			
IF IN DOUBT PLEASE ASK					

SHEET	No OFF	ASSEMLY NUMBER	DRAWING NUMBER	REVISION
7 of 20		MG18-01	07	2018

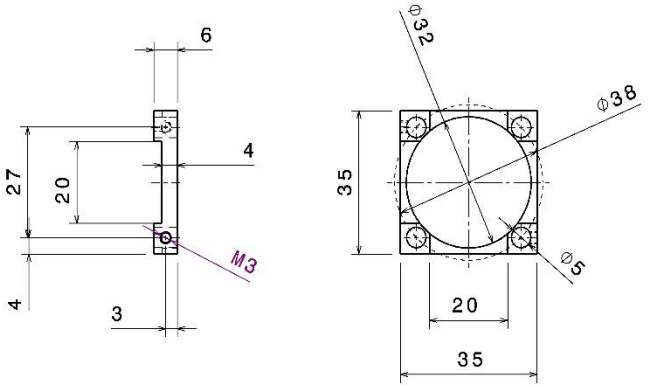

DO NOT SCALE		DESIGNED BY: THANG VAN LANG		TOLERANCES UNLESS OTHERWISE STATED	UNIVVERSITY OF Southampton
A3		CHECKED BY: THANG VAN LANG		LINEAR DIMENSIONS X = +/-0.5mm X.X = +/-0.2mm X.XX = +/-0.1mm ANGULAR DIMENSIONS X = +/-3.5mm X.X = +/-2.0mm X.XX = +/-1.0mm UNTOLERANCED RADII: 0.5 TO 1mm	Faculty of Engineering and Physical Science
EDMC JOB NO	DEPARTMENT	DATE: 2018	SCALE: 1:1		TITLE: CLAMPED PLATE
PROJECT: MAG' GEAR	SUPERVISOR	MATERIAL: ALUMINIUM	TEXTURE	SURFACE FINISH: 1.6 ALL OTHER MACHINED SURFACES TO BE 3.2 UNLESS OTHERWISE STATED	
REMOVES ALL SHARP EDGES		THE INFORMATION CONTAINED IN THIS DOCUMENT IS THE PROPERTY OF THE UNIVERSITY OF SOUTHAMPTON DO NOT COPY WITHOUT WRITTEN PERMISSION		SHEET: 8 of 20	No OFF:	ASSEMLY NUMBER: MG18-01	DRAWING NUMBER: 08	REVISION: 2018
IF IN DOUBT PLEASE ASK					

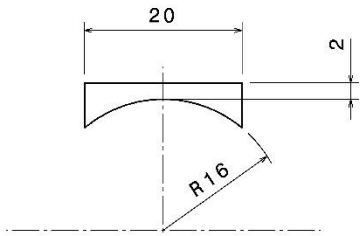

Thickness: 6 mm

DO NOT SCALE		DESIGNED BY: THANG VAN LANG		TOLERANCES UNLESS OTHERWISE STATED: LINEAR DIMENSIONS X = ±0.5mm XX = ±0.25mm XXX = ±0.1mm ANGULAR DIMENSIONS X = ±0.5deg XX = ±0.25deg ALL SURFACES TO BE FREE OF BURRS & SHARP EDGES	UNIVVERSITY OF Southampton Faculty of Engineering and Physical Science
A3		CHECKED BY: THANG VAN LANG			TITLE: I-CORES
EDMC JOB NO	DEPARTMENT	DATE: 2018	SCALE: 1:1		
PROJECT: MAG' GEAR	SUPERVISOR	MATERIAL: MILD STEEL	TEXTURE	SURFACE FINISH: ALL OTHER SURFACES TO BE FREE OF BURRS & SHARP EDGES	
REMOVES ALL SHARP EDGES IF IN DOUBT PLEASE ASK		THE INFORMATION CONTAINED IN THIS DOCUMENT IS THE PROPERTY OF THE UNIVERSITY OF SOUTHAMPTON DO NOT COPY WITHOUT WRITTEN PERMISSION			

SHEET	No OFF	ASSEMLY NUMBER	DRAWING NUMBER	REVISION
9 of 20		MG18-03	9	2018

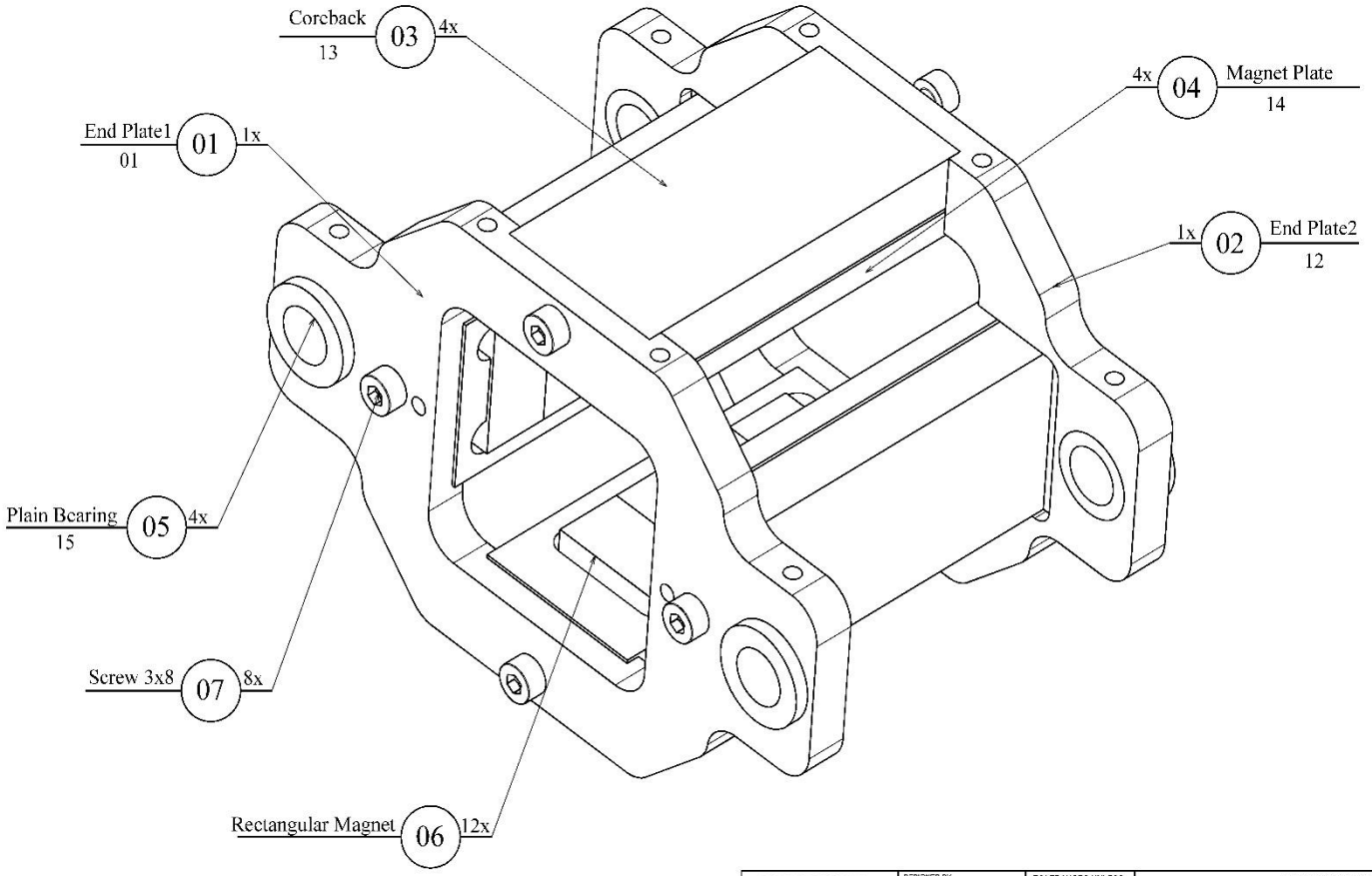

DO NOT SCALE		DESIGNED BY: THANG VAN LANG		TOLERANCES UNLESS OTHERWISE STATED	UNIVVERSITY OF Southampton
A3		CHECKED BY: THANG VAN LANG		LINEAR DIMENSIONS X = ±0.5mm XX = ±0.2mm XXX = ±0.1mm ANGULAR DIMENSIONS X = ±3.5mm X.X = ±2.0mm ALL DIMENSIONS IN mm UNLESS STATED OTHERWISE	Faculty of Engineering and Physical Science
EDMC JOB NO	DEPARTMENT	DATE: 2018	SCALE: 1:1		TITLE: TRANSLATOR
PROJECT: MAG' GEAR	SUPERVISOR	MATERIAL:	TEXTURE	SURFACE FINISH: 1.6 ALL OTHER SURFACES TO BE MACHINED ± 0.1	
REMOVVES ALL SHARP EDGES		THE INFORMATION CONTAINED IN THIS DOCUMENT IS THE PROPERTY OF THE UNIVERSITY OF SOUTHAMPTON DO NOT COPY WITHOUT WRITTEN PERMISSION		SHEET: 10 of 20	No OFF	ASSEMLY NUMBER: MG18	DRAWING NUMBER: 10	REVISION: 2018
IF IN DOUBT PLEASE ASK					

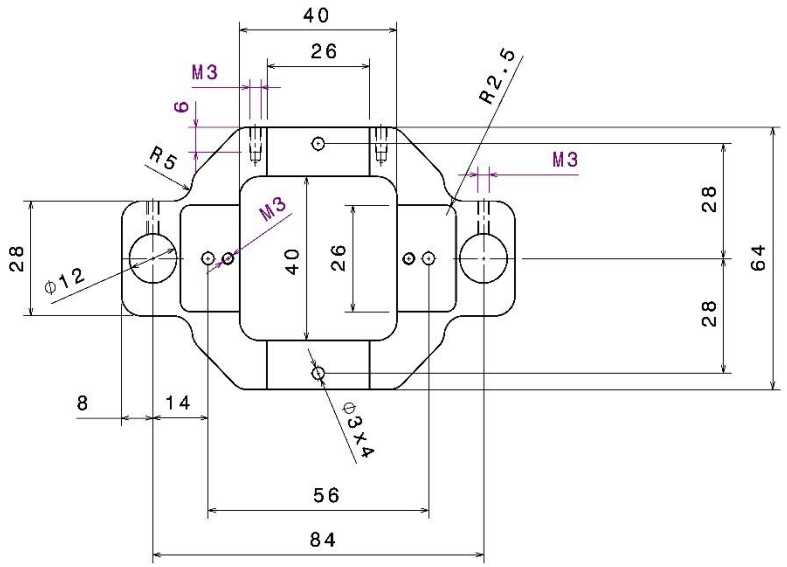

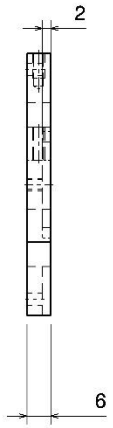

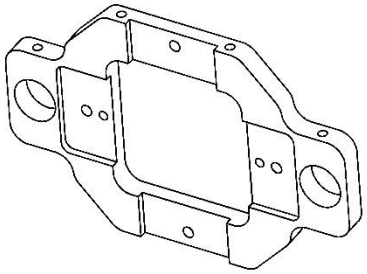

DO NOT SCALE		DESIGNED BY: THANG VAN LANG		TOLERANCES UNLESS OTHERWISE STATED	UNIVVERSITY OF Southampton
A3		CHECKED BY: THANG VAN LANG			Faculty of Engineering and Physical Science
EDMC JOB NO	DEPARTMENT	DATE: 2018	SCALE: 1:1		TITLE: END PLATE 1
PROJECT: MAG' GEAR	SUPERVISOR	MATERIAL: ALUMINIUM	TEXTURE	SURFACE FINISH	
REMOVES ALL SHARP EDGES		THE INFORMATION CONTAINED IN THIS DOCUMENT IS THE PROPERTY OF THE UNIVERSITY OF SOUTHAMPTON DO NOT COPY WITHOUT WRITTEN PERMISSION		SHEET: 11 of 20	No OFF:	ASSEMLY NUMBER: MG18-02	DRAWING NUMBER: 11	REVISION: 2018
IF IN DOUBT PLEASE ASK					

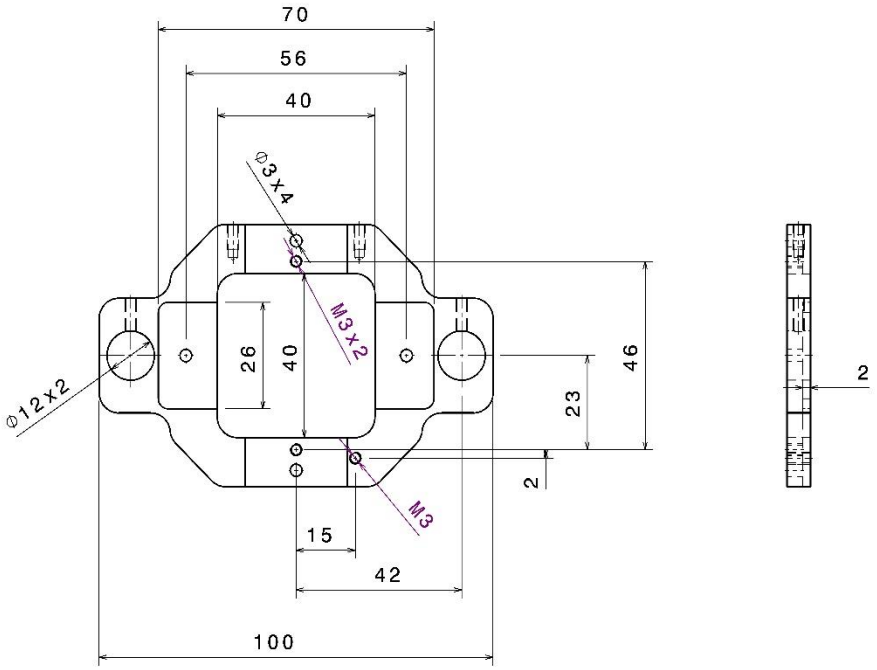

DO NOT SCALE		DESIGNED BY: THANG VAN LANG		TOLERANCES UNLESS OTHERWISE STATED: LINEAR DIMENSIONS X = ±0.5mm X.X = ±0.25mm X.XX = ±0.1mm ANGULAR DIMENSIONS X = ±0.5deg X.X = ±0.25deg ALL DIMENSIONS IN mm UNLESS STATED	UNIVVERSITY OF Southampton Faculty of Engineering and Physical Science
A3		CHECKED BY: THANG VAN LANG			TITLE: END PLATE 2
EDMC JOB NO	DEPARTMENT	DATE: 2018	SCALE: 1:1		
PROJECT: MAG' GEAR	SUPERVISOR	MATERIAL: ALUMINIUM	TEXTURE	SURFACE FINISH: 1.6 All Over Unless Otherwise Stated	
REMOVES ALL SHARP EDGES		THE INFORMATION CONTAINED IN THIS DOCUMENT IS THE PROPERTY OF THE UNIVERSITY OF SOUTHAMPTON DO NOT COPY WITHOUT WRITTEN PERMISSION			SHEET: 12 of 20 | No OFF | ASSEMLY NUMBER: MG18 | DRAWING NUMBER: 12 | REVISION: 2018
IF IN DOUBT PLEASE ASK					

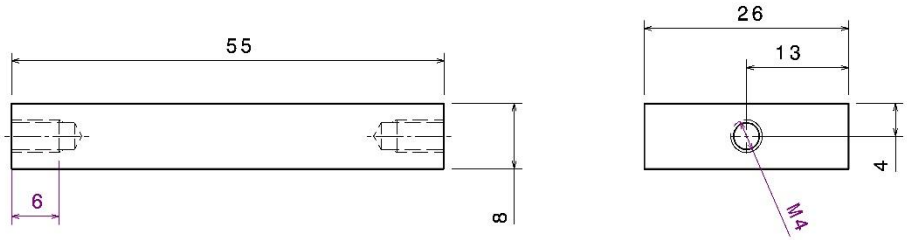

DO NOT SCALE		DESIGNED BY: THANG VAN LANG		TOLERANCES UNLESS OTHERWISE STATED	UNIVVERSITY OF Southampton
A3		CHECKED BY: THANG VAN LANG		LINEAR DIMENSIONS X = +/-0.5mm XX = +/-0.1mm XXX = +/-0.1mm ANGULAR DIMENSIONS X.X = +/-0.5° X.XX = +/-0.25° ALL DIMENSIONS ARE IN MILLIMETRES UNLESS STATED OTHERWISE	Faculty of Engineering and Physical Science
EDMC JOB NO	DEPARTMENT	DATE: 2018	SCALE: 1:1		TITLE: CORE-BACK
PROJECT: MAG' GEAR	SUPERVISOR	MATERIAL: MILD STEEL	TEXTURE	SURFACE FINISH: 1.6 ALL DIMENSIONS ARE IN MILLIMETRES UNLESS STATED OTHERWISE	
REMOVVES ALL SHARP EDGES IF IN DOUBT PLEASE ASK		THE INFORMATION CONTAINED IN THIS DOCUMENT IS THE PROPERTY OF THE UNIVERSITY OF SOUTHAMPTON DO NOT COPY WITHOUT WRITTEN PERMISSION			

SHEET	No OFF	ASSEMLY NUMBER	DRAWING NUMBER	REVISION
13 of 20		MG18-02	13	2018

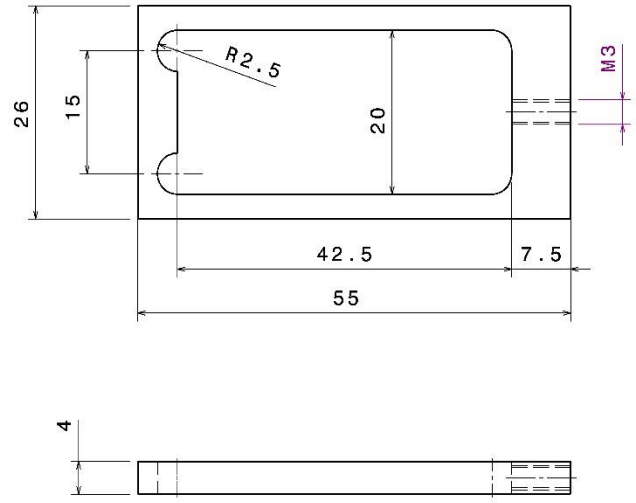

DO NOT SCALE		DESIGNED BY: THANG VAN LANG		TOLERANCES UNLESS OTHERWISE STATED	UNIVVERSITY OF Southampton
A3		CHECKED BY: THANG VAN LANG			Faculty of Engineering and Physical Science
EDMC JOB NO	DEPARTMENT	DATE: 2018	SCALE: 1:1		TITLE: MAGNET PLATE
PROJECT: MAG' GEAR	SUPERVISOR	MATERIAL: ALUMINIUM	TEXTURE	SURFACE FINISH	
REMOVES ALL SHARP EDGES		THE INFORMATION CONTAINED IN THIS DOCUMENT IS THE PROPERTY OF THE UNIVERSITY OF SOUTHAMPTON DO NOT COPY WITHOUT WRITTEN PERMISSION		SHEET: 14 of 20	No OFF:	ASSEMLY NUMBER: MG18-02	DRAWING NUMBER: 14	REVISION: 2018
IF IN DOUBT PLEASE ASK					

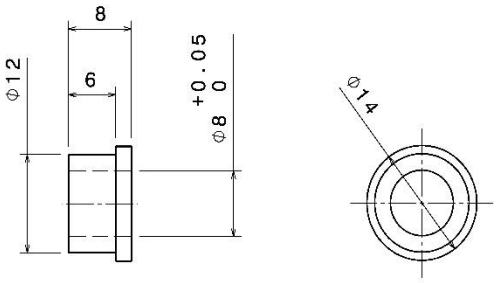

DO NOT SCALE		DESIGNED BY: THANG VAN LANG		TOLERANCES UNLESS OTHERWISE STATED	UNIVVERSITY OF Southampton
A3		CHECKED BY: THANG VAN LANG		LINEAR DIMENSIONS X = ±0.5mm X.X = ±0.2mm X.XX = ±0.1mm ANGULAR DIMENSIONS X = ±0.5° X.X = ±0.25° ALL DIMENSIONS IN mm UNLESS STATED OTHERWISE	Faculty of Engineering and Physical Science
EDMC JOB NO	DEPARTMENT	DATE: 2018	SCALE: 1:1		TITLE: PLAIN BEARING
PROJECT: MAG' GEAR	SUPERVISOR	MATERIAL: BRASS	TEXTURE	SURFACE FINISH: 1.6 ALL OTHER UNLESS OTHERWISE STATED	
REMOVVES ALL SHARP EDGES		THE INFORMATION CONTAINED IN THIS DOCUMENT IS THE PROPERTY OF THE UNIVERSITY OF SOUTHAMPTON DO NOT COPY WITHOUT WRITTEN PERMISSION			
IF IN DOUBT PLEASE ASK					

SHEET	No OFF	ASSEMLY NUMBER	DRAWING NUMBER	REVISION
15 of 20		MG18-02	15	2018

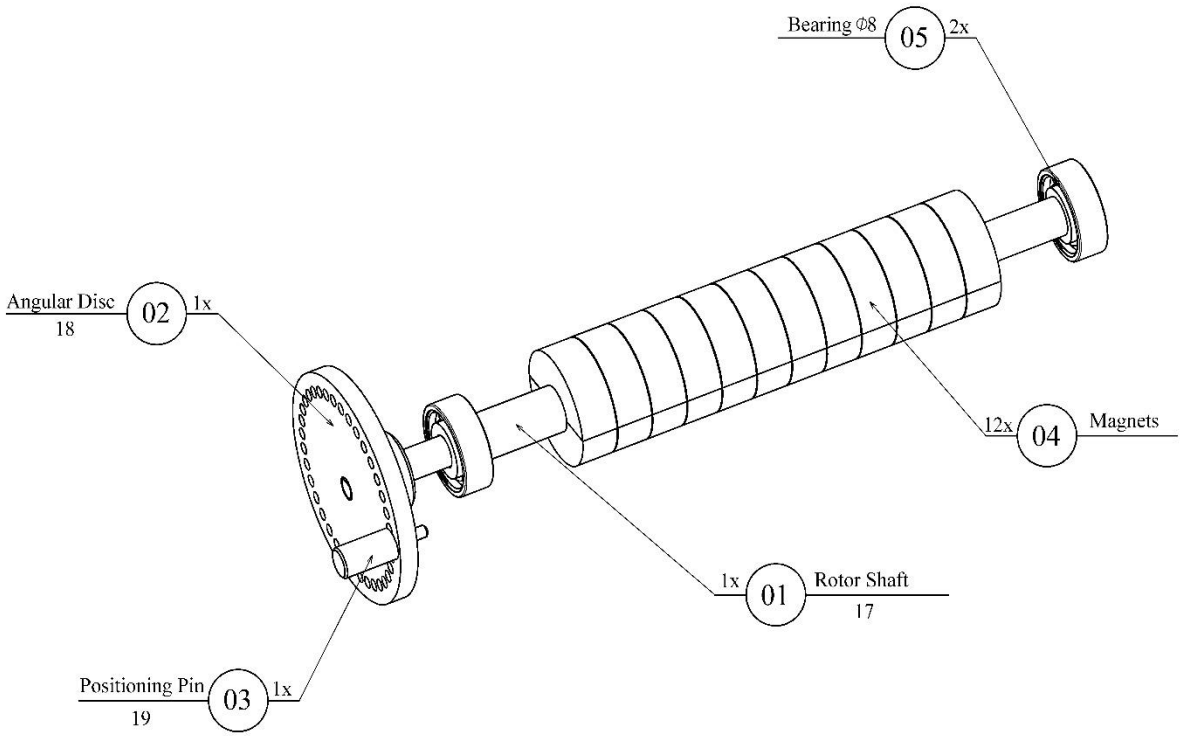

DO NOT SCALE		DESIGNED BY: THANG VAN LANG		TOLERANCES UNLESS OTHERWISE STATED	UNIVVERSITY OF Southampton
A3		CHECKED BY: THANG VAN LANG			Faculty of Engineering and Physical Science
EDMC JOB NO	DEPARTMENT	DATE: 2018	SCALE: 1:1		TITLE: ROTOR
PROJECT: MAG' GEAR	SUPERVISOR	MATERIAL:	TEXTURE	SURFACE FINISH	
REMOVES ALL SHARP EDGES		THE INFORMATION CONTAINED IN THIS DOCUMENT IS THE PROPERTY OF THE UNIVERSITY OF SOUTHAMPTON DO NOT COPY WITHOUT WRITTEN PERMISSION		SHEET: 16 of 20	No OFF:	ASSEMLY NUMBER: MG18-03	DRAWING NUMBER: 16	REVISION: 2018
IF IN DOUBT PLEASE ASK					

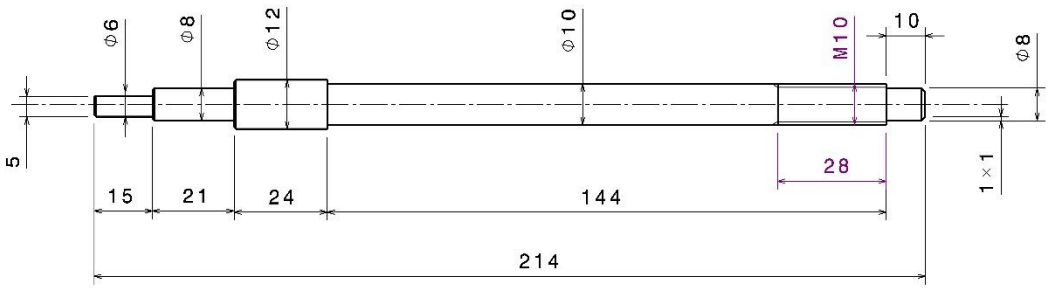

DO NOT SCALE		DESIGNED BY: THANG VAN LANG		TOLERANCES UNLESS OTHERWISE STATED LINEAR DIMENSIONS X = +/-0.5mm XX = +/-0.1mm XXX = +/-0.05mm ANGULAR DIVISIONS X = +/-0.5 deg XX = +/-0.25 deg	UNIVVERSITY OF Southampton Faculty of Engineering and Physical Science
A3		CHECKED BY: THANG VAN LANG			TITLE: ROTOR SHAFT
EDMC JOB NO	DEPARTMENT	DATE: 2018	SCALE: 1:1		
PROJECT: MAG' GEAR	SUPERVISOR	MATERIAL: MILD STEEL	TEXTURE	SURFACE FINISH: 6.3 / (all over unless otherwise stated)	
REMOVES ALL SHARP EDGES		THE INFORMATION CONTAINED IN THIS DOCUMENT IS THE PROPERTY OF THE UNIVERSITY OF SOUTHAMPTON DO NOT COPY WITHOUT WRITTEN PERMISSION			
IF IN DOUBT PLEASE ASK					

SHEET	No OFF	ASSEMLY NUMBER	DRAWING NUMBER	REVISION
17 of 20		MG18-03	17	2018

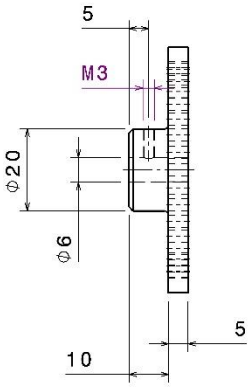

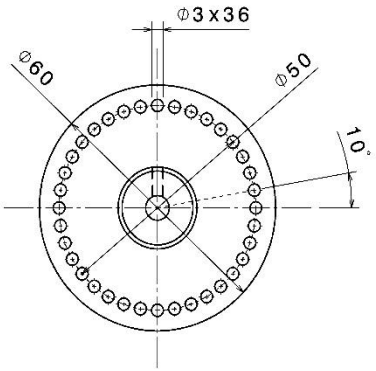

DO NOT SCALE		DESIGNED BY: THANG VAN LANG		TOLERANCES UNLESS OTHERWISE STATED	UNIVVERSITY OF Southampton
A3		CHECKED BY: THANG VAN LANG			Faculty of Engineering and Physical Science
EDMC JOB NO	DEPARTMENT	DATE: 2018	SCALE: 1:1		TITLE: ANGULAR DISC
PROJECT: MAG' GEAR	SUPERVISOR	MATERIAL: ALUMINIUM	TEXTURE	SURFACE FINISH	
REMOVES ALL SHARP EDGES		THE INFORMATION CONTAINED IN THIS DOCUMENT IS THE PROPERTY OF THE UNIVERSITY OF SOUTHAMPTON DO NOT COPY WITHOUT WRITTEN PERMISSION		SHEET: 18 of 20	No OFF:	ASSEMLY NUMBER: MG18-03	DRAWING NUMBER: 18	REVISION: 2018
IF IN DOUBT PLEASE ASK					

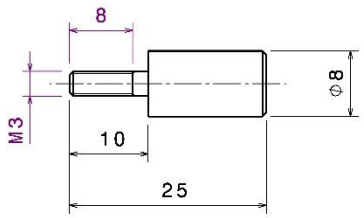

DO NOT SCALE		DESIGNED BY: THANG VAN LANG		TOLERANCES UNLESS OTHERWISE STATED: LINEAR DIMENSIONS X = ±0.5mm; XX = ±0.25mm; XXX = ±0.125mm; ANGULAR DIMENSIONS X = ±0.5deg; XX = ±0.25deg; ALL DIMENSIONS IN mm UNLESS OTHERWISE STATED	UNIVVERSITY OF Southampton Faculty of Engineering and Physical Science
A3		CHECKED BY: THANG VAN LANG			TITLE: POSITIONING PIN
EDMC JOB NO	DEPARTMENT	DATE: 2018	SCALE: 1:1		
PROJECT: MAG' GEAR	SUPERVISOR	MATERIAL: STEEL	TEXTURE	SURFACE FINISH: ALL OTHER FINISHES ∇∇∇	
REMOVES ALL SHARP EDGES		THE INFORMATION CONTAINED IN THIS DOCUMENT IS THE PROPERTY OF THE UNIVERSITY OF SOUTHAMPTON DO NOT COPY WITHOUT WRITTEN PERMISSION			
IF IN DOUBT PLEASE ASK					

SHEET	No OFF	ASSEMLY NUMBER	DRAWING NUMBER	REVISION
19 of 20		MG18-03	19	2018

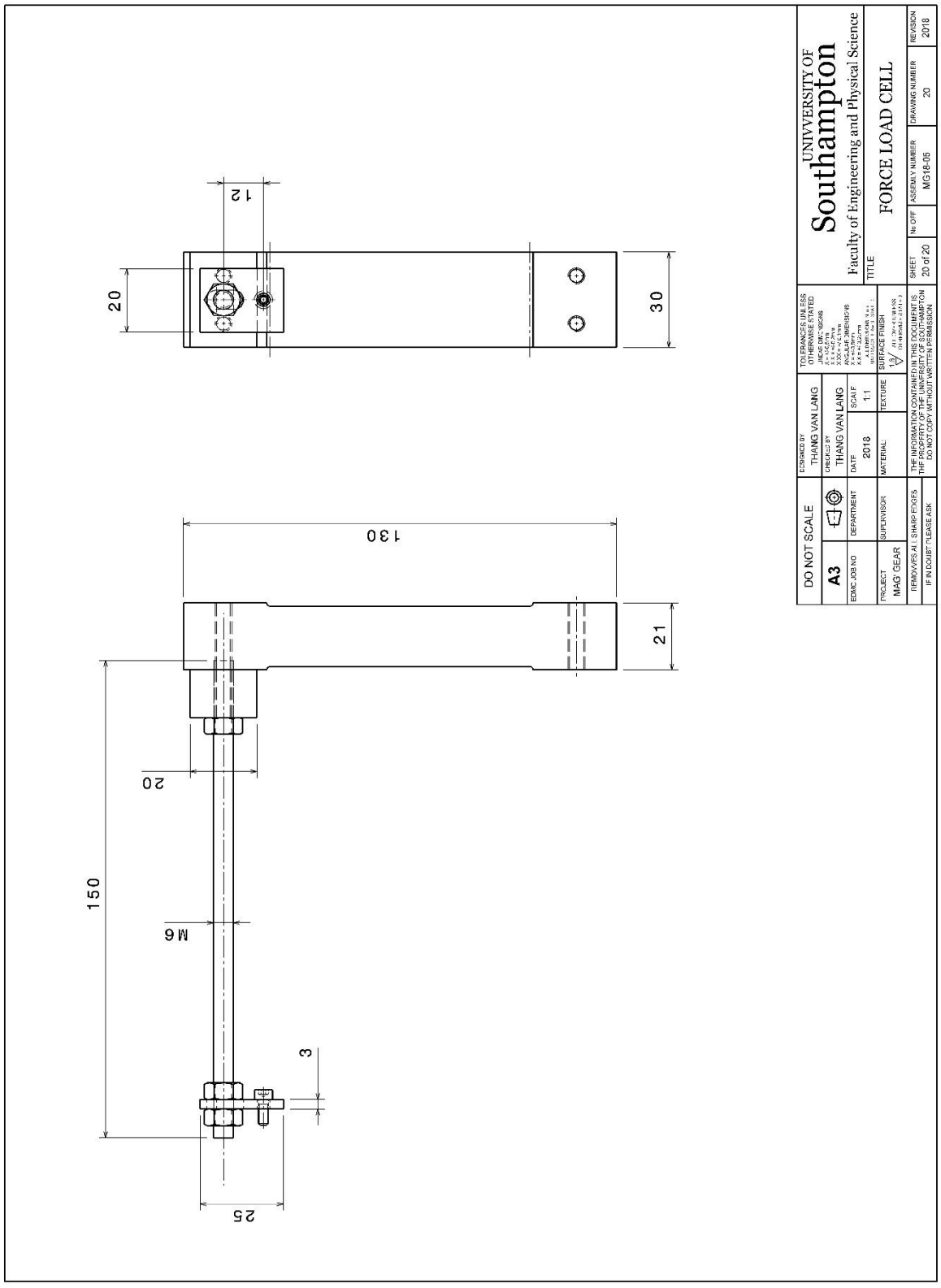
12
20
30
130
21
20
150
M6
3
25
DO NOT SCALE
A3
EDMC JOB NO
DEPARTMENT
PROJECT
MAG GEAR
SUPERVISOR
DESIGNED BY
THANG VAN LANG
CHECKED BY
THANG VAN LANG
DATE
2018
SCALE
1:1
MATERIAL
TEXTURE
SURFACE FINISH
TOLERANCES UNLESS OTHERWISE STATED
REMOVE ALL SHARP EDGES
IF IN DOUBT PLEASE ASK
THE INFORMATION CONTAINED IN THIS DOCUMENT IS THE PROPERTY OF THE UNIVERSITY OF SOUTHAMPTON
DO NOT COPY WITHOUT WRITTEN PERMISSION
UNIVERSITY OF Southampton
Faculty of Engineering and Physical Science
TITLE
FORCE LOAD CELL
SHEET
20 of 20
No. OFF
ASSEMLY NUMBER
MG18-05
DRAWING NUMBER
20
REVISION
2018

References

[1] The European Parliament and the Council of the European Union, "Directive EU 2018/2001 of the European Parliament and of the Council of 11 December 2018 on the promotion of the use of energy from renewable sources," *Official Journal of the European Union*, 2018.

[2] U.K. Government, "Renewable statistics," Renewable sources of energy: Chapter 6, Digest of United Kingdom Energy Statistics (DUKES), 2020.

[3] Taichi Matsuoka, Kenichiro Omata, Hiroyuki Kanda and Kenichiro Tachi, "A study of wave energy conversion systems using ball screws – comparison of output characteristics of the fixed type and the floating type," in *Conference of International Offshore and Polar Engineering* , Kitakyushu, Japan, 2002.

[4] M. Hendijanizadeh, "Design and optimisation of constrained electromagnetic energy harvesting devices," PhD Thesis, University of Southampton, 2014.

[5] M. Moshrefi-Torbati, T.V. Lang, M. Hendijanizadeh, T.B. Le, S.M. Sharkh, "A novel hybrid energy harvester with increased power density," *Procedia Engineering*, Volume 199, 2017, Pages 3498-3503, ISSN 1877-7058, https://doi.org/10.1016/j.proeng.2017.09.464.

[6] J. D. Kidd, "Magnetic gear system", US patent US20150263597A1, 2015.

[7] B. Andrews, "Magnet screw," US Pat. 1 562 730, 1925.

[8] R. J. A. Paul, "Magnetic rotary-linear or linear-rotary converter," IEE J. Elect. Power Appl., vol. 2, no. 4, pp. 135–138, Aug. 1979.

[9] J. R. Anglada, "Novel Electric Machines for Renewable Energy Applications", PhD Thesis, University of Southampton, 2015.

[10] X. Li, K. T. Chau, M. Cheng, and W. Hua, "Comparison of magnetic-geared permanent-magnet machines," *Progress In Electromagnetics Research*, Vol. 133, 177-198, 2013, doi:10.2528/PIER12080808.

[11] C. G. Armstrong, "Power transmitting device," US Pat. 687 292, 1901.

[12] H. T. Faus, “Magnet gearing,” US Pat. 2-243-555, 1941.

[13] P. M. Tlali, R. J. Wang and S. Gerber, "Magnetic gear technologies: A review," *2014 International Conference on Electrical Machines (ICEM)*, Berlin, 2014, pp. 544-550, doi: 10.1109/ICELMACH.2014.6960233.

[14] B. McGilton, M. Mueller and A. McDonald, "Review of magnetic gear technologies and their applications in marine energy," *5th IET International Conference on Renewable Power Generation (RPG) 2016*, London, 2016, pp. 1-6, doi: 10.1049/cp.2016.0535.

[15] Zhu, Z.Q.; Howe, D.: 'Halbach permanent magnet machines and applications: a review', *IEE Proceedings - Electric Power Applications*, 2001, 148, (4), p. 299-308, DOI: 10.1049/ip-epa:20010479

[16] K. Tsurumoto and S. Kikuchi, "A new magnetic gear using permanent magnet," in *IEEE Transactions on Magnetics*, vol. 23, no. 5, pp. 3622-3624, September 1987, doi: 10.1109/TMAG.1987.1065208.

[17] S. Kikuchi, K. Tsurumoto, “Design and characteristics of a new magnetic worm gear using permanent magnet,” *IEEE T-MAG*, 29(6):2923-2925, 1993.

[18] S. Kikuchi, K. Tsurumoto, “Trial construction of a new magnetic skew gear using permanent magnet,” *IEEE T-MAG*, 30(6):4767-4769, 1994.

[19] S. Rand, “Magnetic transmission system,” US Pat. 3 523 204, 1970.

[20] M. Hetzel, “Low friction miniature gear drive for transmitting small forces, and method of making same,” US Pat. 3 792 578, 1974.

[21] D. E. Hesmondhalgh and D. Tipping, “A multielement magnetic gear,” *IEE Proceedings*, Vol. 127, No. 3, 129-138, 1980.

[22] K. Ikuta, S. Makita and S. Arimoto, "Non-contact magnetic gear for micro transmission mechanism," *[1991] Proceedings. IEEE Micro Electro Mechanical Systems*, Nara, 1991, pp. 125-130.

[23] Y. D. Yao, D. R. Huang, C. M. Lee, S. J. Wang, D. Y. Chiang and T. F. Ying, "Magnetic coupling studies between radial magnetic gears," in *IEEE Transactions on Magnetics*, vol. 33, no. 5, pp. 4236-4238, Sept. 1997, doi: 10.1109/20.619721.

[24] F. T. Jorgensen, T. O. Andersen and P. O. Rasmussen, "Two dimensional model of a permanent magnet spur gear," *Fourtieth IAS Annual Meeting. Conference Record of the 2005 Industry Applications Conference, 2005.*, 2005, pp. 261-265 Vol. 1.

[25] E. P. Furlani, "A two-dimensional analysis for the coupling of magnetic gears," in *IEEE Transactions on Magnetics*, vol. 33, no. 3, pp. 2317-2321, May 1997, doi: 10.1109/20.573848.

[26] Y. Akcay, P. Giangrande and M. Galea, "A Novel Magnetic Coupling Configuration for Enhancing the Torque Density," *2020 23rd International Conference on Electrical Machines and Systems (ICEMS)*, Hamamatsu, Japan, 2020, pp. 228-233, doi: 10.23919/ICEMS50442.2020.9291073.

[27] J. Yonnet, "A new type of permanent magnet coupling," in *IEEE Transactions on Magnetics*, vol. 17, no. 6, pp. 2991-2993, November 1981, doi: 10.1109/TMAG.1981.1061486.

[28] E. P. Furlani, "Formulas for the force and torque of axial couplings," in *IEEE Transactions on Magnetics*, vol. 29, no. 5, pp. 2295-2301, Sept. 1993, doi: 10.1109/20.231636.

[29] R. Wang, E. P. Furlani and Z. J. Cendes, "Design and analysis of a permanent magnet axial coupling using 3D finite element field computations," in *IEEE Transactions on Magnetics*, vol. 30, no. 4, pp. 2292-2295, July 1994, doi: 10.1109/20.305733.

[30] Y. D. Yao, G. J. Chiou, D. R. Huang, and S. J. Wang, “Theoretical computations for the torque of magnetic coupling,” *IEEE Transactions on Magnetics*, Vol. 31, No. 3, 1881-1884, 1995, doi: 10.1109/20.376405.

[31] W. Wu, H. C. Lovatt, and J. B. Dunlop, “Analysis and design optimization of magnetic couplings using 3D finite element modeling,” *IEEE Transactions on Magnetics*, Vol. 33, No. 5, 4083-4085, 1997, doi: 10.1109/20.619670.

[32] P. Elies, and G. Lemarquand, “Analytical study of radial stability of permanent-magnet synchronous couplings,” *IEEE Transactions on Magnetics*, Vol. 35, No. 4, 2133-2136, 1999, doi: 10.1109/20.774183.

[33] C. Huang, M. Tsai and B. Lin, "Development of New Magnetic Planetary Gears for Transmission Systems," *INTERMAG 2006 - IEEE International Magnetics Conference*, San Diego, CA, 2006, pp. 225-225.

[34] C. Huang, M. Tsai, D. G. Dorrell and B. Lin, "Development of a Magnetic Planetary Gearbox," in *IEEE Transactions on Magnetics*, vol. 44, no. 3, pp. 403-412, March 2008, doi: 10.1109/TMAG.2007.914665.

[35] M. Tsai and C. Huang, "Development of a Variable-Inertia Device With a Magnetic Planetary Gearbox," in IEEE/ASME Transactions on Mechatronics, vol. 16, no. 6, pp. 1120-1128, Dec. 2011, doi: 10.1109/TMECH.2010.2077679.

[36] F. Kong, Y. Ge, X. Zhu, L. Qiao and L. Quan, "Optimizing Design of Magnetic Planetary Gearbox for Reduction of Cogging Torque," *2013 IEEE Vehicle Power and Propulsion Conference (VPPC)*, Beijing, 2013, pp. 1-5, doi: 10.1109/VPPC.2013.6671697.

[37] X. Li et al., “Comparison of magnetic-geared PM machines,” *Progress In Electromagn. Research*, 133:177-198, 2013, doi:10.2528/PIER12080808.

[38] Y. D. Yao, D. R. Huang, C. C. Hsieh, D. Y. Chiang, S. J. Wang, and T. F. Ying, “The radial magnetic coupling studies of perpendicular magnetic gears," *IEEE Transactions on Magnetics*, Vol. 32, No. 5, 5061-5063, 1996.

[39] G. Muruganandam, K. S. Jayakumar, Hariharan. S, and Joshua. E, “Torque analysis of perpendicular magnetic gear with high gear ratio,” *International Journal of Scientific & Engineering Research,*Volume 3, Issue 6, June-2012.

[40] K. Atallah and D. Howe, "A novel high-performance magnetic gear," in *IEEE Transactions on Magnetics*, vol. 37, no. 4, pp. 2844-2846, July 2001, doi: 10.1109/20.951324.

[41] K. Atallah, D. Howe, “Design, analysis and realisation of a high performance magnetic gear,” *IEE Proc. Electr. Power Appl*., 151(2):135-143, 2004, DOI: 10.1049/ip-epa:20040224.

[42] P. O. Rasmussen, T. O. Andersen, F. T. Joergensen and O. Nielsen, "Development of a high performance magnetic gear," *38th IAS Annual Meeting on Conference Record of the Industry Applications Conference, 2003.*, Salt Lake City, UT, USA, 2003, pp. 1696-1702 vol.3, doi: 10.1109/IAS.2003.1257784.

[43] S. Mezani, K. Atallah, and D. Howe, “A high-performance axial-field magnetic gear,” *J.of Appl. Phys*., 99(8):08R303-08R303-3, 2006, DOI: 10.1063/1.2158966.

[44] D. Zhu, F. Yang, Y. Du, F. Xiao, and Z. Ling, “An axial-field flux-modulated magnetic gear,” *IEEE Transactions on Applied Superconductivity*, vol. 26, no. 4, June 2016.

[45] L. Jian, K. T. Chau and J. Z. Jiang, "A Magnetic-Geared Outer-Rotor Permanent-Magnet Brushless Machine for Wind Power Generation," in *IEEE Transactions on Industry Applications*, vol. 45, no. 3, pp. 954-962, May-June 2009, doi: 10.1109/TIA.2009.2018974.

[46] L. N. Jian, K. T. Chau, D. Zhang, J. Z. Jiang and Z. Wang, "A Magnetic-Geared Outer-Rotor Permanent-Magnet Brushless Machine for Wind Power Generation," *2007 IEEE Industry Applications Annual Meeting*, New Orleans, LA, USA, 2007, pp. 573-580, doi: 10.1109/07IAS.2007.42.

[47] L. Jian, and K. Chau, “Design and analysis of a magnetic geared electronic continuously variable transmission system using finite element method,” *Progress In Electromagnetics Research*, Vol. 107, 47-61, 2010, doi:10.2528/PIER10062806.

[48] K. T. Chau, D. Zhang, J. Z. Jiang, C. Liu and Y. Zhang, "Design of a Magnetic-Geared Outer-Rotor Permanent-Magnet Brushless Motor for Electric Vehicles," in *IEEE Transactions on Magnetics*, vol. 43, no. 6, pp. 2504-2506, June 2007, doi: 10.1109/TMAG.2007.893714.

[49] Y. Fan, H. Jiang, M. Cheng, and Y. Wang, “An improved magnetic-geared permanent magnet in-wheel motor for electric vehicles,” *IEEE Vehicle Power and Propulsion Conference*, Lille, France, 2010, doi: 10.1109/VPPC.2010.5729245.

[50] K. Atallah, J. Wang, and D. Howe, “A high-performance linear magnetic gear,” *Journal of Applied Physics*, Vol. 97, 10N516-1-3, 2005.

[51] W. Li, K. T. Chau, and J. Z. Jiang, “Application of linear magnetic gears for pseudo-direct-drive oceanic wave energy harvesting,” *IEEE Transactions on Magnetics*, Vol. 47, No. 10, 2624-2627, 2011, doi: 10.1109/TMAG.2011.2146233.

[52] R. C. Holehouse, K. Atallah, and J.Wang, “Design and realization of a linear magnetic gear,” *IEEE Transactions* on *Magnetics*, vol. 47, no. 10, pp. 4171–4174, 2011, doi: 10.1109/TMAG.2011.2157101.

[53] J. Wang, K. Atallah, and W. Wang, “Analysis of a magnetic screw for high force density linear electromagnetic actuators,” *IEEE Transactions on Magnetics*, VOL. 47, NO. 10, 4477 – 4480, October 2011, doi: 10.1109/TMAG.2011.2157464.

[54] S. Pakdelian, N. W. Frank, and H. A. Toliyat, "Principles of the trans-rotary magnetic gear," *IEEE Trans Mag*., vol. 49, pp. 883-889, 2013, doi: 10.1109/TMAG.2012.2215046.

[55] S. Pakdelian, N. W. Frank, and H. A. Toliyat, “Magnetic design aspects of the trans-rotary magnetic gear,” *IEEE Trans. Energy Convers*., vol. 30, no. 1, pp. 41–50, Mar. 2015, doi: 10.1109/TEC.2014.2361289.

[56] R. K. Holm, N. I. Berg, M. Walkusch, P. O. Rasmussen and R. H. Hansen, "Design of a magnetic lead screw for wave energy conversion," *2012 XXth International Conference on Electrical Machines*, Marseille, 2012, pp. 618-626, doi: 10.1109/ICElMach.2012.6349934.

[57] L. Hua, J. Xu and Q. Xiaolong, "Research on the rotary-linear motion magnetic gear based on ANSYS," *2016 Chinese Control and Decision Conference (CCDC)*, Yinchuan, 2016, pp. 3259-3264, doi: 10.1109/CCDC.2016.7531545.

[58] M. B. Kouhshahi and J. Z. Bird, "Analysis of a magnetically geared lead screw," 2016 IEEE Energy Conversion Congress and Exposition (ECCE), Milwaukee, WI, 2016, pp. 1-5, doi: 10.1109/ECCE.2016.7854873.

[59] M. B. Kouhshahi, J. Z. Bird, A. Jannsen, J. Kadel and W. Williams, "A Magnetically Geared Lead Screw Without Translator Skewing," *2018 IEEE Energy Conversion Congress and Exposition (ECCE)*, Portland, OR, 2018, pp. 4994-4999, doi: 10.1109/ECCE.2018.8557751.

[60] M. B. Kouhshahi, J. Z. Bird, J. D. Kadel and W. B. Williams, "Designing and Experimentally Testing a Magnetically Geared Lead Screw," in *IEEE Transactions on Industry Applications*, vol. 54, no. 6, pp. 5736-5747, Nov.-Dec. 2018, doi: 10.1109/TIA.2018.2846651.

[61] V. Ostovic, "A Method for Evaluation of Transient and Steady State Performance in Saturated Squirrel Cage Induction Machines," in *IEEE Transactions on Energy Conversion*, vol. EC-1, no. 3, pp. 190-197, Sept. 1986, doi: 10.1109/TEC.1986.4765754.

[62] V. Ostovic, "Computation of Saturated Permanent-Magnet AC Motor Performance by Means of Magnetic Circuits," in *IEEE Transactions on Industry Applications*, vol. IA-23, no. 5, pp. 836-841, Sept. 1987, doi: 10.1109/TIA.1987.4504992.

[63] V. Ostovic, "A simplified approach to magnetic equivalent-circuit modeling of induction machines," in *IEEE Transactions on Industry Applications*, vol. 24, no. 2, pp. 308-316, March-April 1988, doi: 10.1109/28.2871.

[64] M. Amrhein and P. T. Krein, "3-D Magnetic Equivalent Circuit Framework for Modeling Electromechanical Devices," in *IEEE Transactions on Energy Conversion*, vol. 24, no. 2, pp. 397-405, June 2009, doi: 10.1109/TEC.2009.2016134.

[65] K. J. Bathe, Finite Element Procedures. Prentice Hall 1996.

[66] P. Silvester and M. V. K. Chari, "Finite Element Solution of Saturable Magnetic Field Problems," in *IEEE Transactions on Power Apparatus and Systems*, vol. PAS-89, no. 7, pp. 1642-1651, Sept. 1970, doi: 10.1109/TPAS.1970.292812.

[67] J. Kirtley, Electric Machines. Massachusetts Institute of Technology: Class Notes, 2003.

[68] H. H. Woodson and R. J. Melcher, Electromechanical Dynamics. John Wiley & Sons, 1968.

[69] C. T. McLyman, Transformer and Inductor Design Handbook, Taylor & Francis, 2011.

[70] G. H. Pajooman, Performance assessment and design optimisation of VRPM (transverse flux) machines by finite element computation. PhD Thesis, University of Southampton, 1997.

[71] M. R. Harris and B. C. Mecrow, "Variable reluctance permanent magnet motors for high specific output," in Sixth International Conference on Electrical Machines and Drives (Conf. Publ. No. 376), Oxford, UK, 1993.

[72] R. Blissenbach and I.-A. Viorel, “On the Single-Sided Transverse Flux Machine Design," Electric Power Components and Systems, vol. 31, pp. 109{128, Feb. 2003.

[73] E. M. Rashad, T. S. Radwan and M. A. Rahman, "A maximum torque per ampere vector control strategy for synchronous reluctance motors considering saturation and iron losses," *Conference Record of the 2004 IEEE Industry Applications Conference, 2004. 39th IAS Annual Meeting.*, 2004, pp. 2411-2417 vol.4, doi: 10.1109/IAS.2004.1348813.

[74] T. V. Lang, S. M. Sharkh, J. R. Anglada, M. Hendijanizadeh and M. Moshrefi-Torbati, "Low Cost Rotary-to-Linear Magnetic Gear," *2020 International Conference on Electrical Machines (ICEM)*, 2020, pp. 1923-1929, doi: 10.1109/ICEM49940.2020.9271021.

[75] Arlold magnetic Technology, “Sintered Neodymium-Iron-Boron Magnets,” https://www.arnoldmagnetics.com/products/neodymium-iron-boron-magnets/N35 access to 15 June 2018.

[76] R. G. Montague, C. M. Bingham and K. Atallah, "Magnetic gear dynamics for servo control," *Melecon 2010 - 2010 15th IEEE Mediterranean Electrotechnical Conference*, Valletta, 2010, pp. 1192-1197, doi: 10.1109/MELCON.2010.5475900.

[77] S. Pakdelian and H. A. Toliyat, "Dynamic modeling of the trans-rotary magnetic gear for the point-absorbing wave energy conversion systems," 2014 IEEE Energy Conversion Congress and Exposition (ECCE), Pittsburgh, PA, 2014, pp. 3163-3170, doi: 10.1109/ECCE.2014.6953830.

[78] S. Pakdelian, H. A. Hussain, M. Moosavi and H. A. Toliyat, "Control of an electric machine integrated with the trans-rotary magnetic gear in a motor drive train," *2015 IEEE International Electric Machines & Drives Conference (IEMDC)*, Coeur d'Alene, ID, 2015, pp. 662-668, doi: 10.1109/IEMDC.2015.7409130.

[79] M. C. Gardner and H. A. Toliyat, "Nonlinear Analysis of Magnetic Gear Dynamics Using Superposition and Conservation of Energy," *2019 IEEE International Electric Machines & Drives Conference (IEMDC)*, San Diego, CA, USA, 2019, pp. 210-217, doi: 10.1109/IEMDC.2019.8785356.

[80] M. Desvaux, R. Le Goff Latimier, B. Multon, S. Sire and H. Ben Ahmed, "Analysis of the dynamic behaviour of magnetic gear with nonlinear modelling for large wind turbines," *2016 XXII International Conference on Electrical Machines (ICEM)*, Lausanne, 2016, pp. 1332-1338, doi: 10.1109/ICELMACH.2016.7732697.

[81] R. G. Montague, C. M. Bingham and K. Atallah, "Dual-observer-based position-servo control of a magnetic gear," in *IET Electric Power Applications*, vol. 5, no. 9, pp. 708-714, November 2011, doi: 10.1049/iet-epa.2011.0046.

[82] M. Hendijanizadeh, S. M. Sharkh, S. J. Elliott and M. Moshrefi-Torbati, "Output power and efficiency of electromagnetic energy harvesting systems with constrained range of motion," Smart Materials and Structures, 22 (2013), p. 125009.

[83] R. K. Holm, N. I. Berg, M. Walkusch, P. O. Rasmussen and R. H. Hansen, "Design of a magnetic lead screw for wave energy conversion," 2012 XXth International Conference on Electrical Machines, Marseille, 2012, pp. 618-626, doi: 10.1109/ICElMach.2012.6349934.

[84] S. Pakdelian and H. A. Toliyat, "Dynamic modeling of the trans-rotary magnetic gear for the point-absorbing wave energy conversion systems," *2014 IEEE Energy Conversion Congress and Exposition (ECCE)*, Pittsburgh, PA, 2014, pp. 3163-3170, doi: 10.1109/ECCE.2014.6953830.

[85] Hendijanizadeh, M., Moshrefi-Torbati, M., and Sharkh, S. M. (November 20, 2013). "Constrained Design Optimization of Vibration Energy Harvesting Devices." ASME. *J. Vib. Acoust*. April 2014; 136(2): 021001. https://doi.org/10.1115/1.4025877.